HELIOPHYSICS V.
SPACE WEATHER AND SOCIETY
Early chapter collection V. July 7, 2014

v.

http://www.lmsal.com/∼schrijver/HSS5/HSS5_20140707.pdf

edited by
CAROLUS J. SCHRIJVER,
Lockheed Martin STAR Labs

FRANCES BAGENAL
University of Colorado

and
JAN J. SOJKA
Utah State University

Contents

Preface

Editors' notes

This volume is being developed over the course of several years of the Heliophysics Summer School, starting with the first chapter in 2012. Chapters are being added as they become available from the authors/lectureres over the period 2012-2015, after which this volume will be completed as the 5th in the Heliophysics series. We recommend that the reader occiasionally check the School's website (see below) for updates. Until the volume is complete, the numbering of chapters, figures, and tables is subject to change.

Additional resources

The texts were developed during a summer school series for heliophysics, taught at the facilities of the University Corporation for Atmospheric Research, in Boulder, Colorado, funded by the NASA Living With a Star program. Additional information, including text updates, lecture materials, (color) figures and movies, and teaching materials developed for the school can be found at http://www.vsp.ucar.edu/Heliophysics. Definitions of many solar-terrestrial terms can be found via the index of each of the first four volumes; a comprehensive list can be found at http://www.swpc.noaa.gov/info/glossary.htm.

Heliophysics

helio-, pref., on the Sun and environs, from the Greek helios.
physics, n., the science of matter and energy and their interactions.

Heliophysics is the

- *comprehensive new term for the science of the Sun - Solar System Connection.*
- *exploration, discovery, and understanding of our space environment.*
- *system science that unites all of the linked phenomena in the region of the cosmos influenced by a star like our Sun.*

Heliophysics concentrates on the Sun and its effects on Earth, the other planets of the solar system, and the changing conditions in space. Heliophysics studies the magnetosphere, ionosphere, thermosphere, mesosphere, and upper atmosphere of the Earth and other planets. Heliophysics combines the science of the Sun, corona, heliosphere and geospace. Heliophysics encompasses cosmic rays and particle acceleration, space weather and radiation, dust and magnetic reconnection, solar activity and stellar cycles, aeronomy and space plasmas, magnetic fields and global change, and the interactions of the solar system with our galaxy.

From NASA's "Heliophysics. The New Science of the Sun - Solar System Connection: Recommended Roadmap for Science and Technology 2005 - 2035."

1
Introduction

Carolus J. Schrijver, Frances Bagenal, and Jan J. Sojka

... [Not yet available] ...

For a collection of reading materials on space weather and its societal impacts, see http://www.lmsal.com/∼schryver/SWlibrary.html.

2

Space weather: impacts, mitigation, forecasting

Sten Odenwald

2.1 Introduction

Normal, terrestrial weather is a localized phenomenon that plays out within a volume of 4 billion cubic kilometers over scales from meters to thousands of kilometers, and times as diverse as seconds to days. Whether you use the most humble technology found in remote villages in Bangladesh, or the most sophisticated computer technology deployed in Downtown Manhattan, terrestrial weather can and does have dramatic impacts all across the human spectrum. During 2011 alone, annual severe weather events cost humanity 2000 lives and inflicted damages upwards of $37 billion dollars (Berkowitz, 2011). The public reaction to terrestrial weather is intense, and visceral, with armies of meteorologists reporting daily disturbances around the globe, and weather forecasting models that have decades of development behind them and that have improved in reliability over the years.

In contrast to terrestrial weather and to our methods of mitigating its impact, we have the arena of space weather, which occurs within a volume spanned by our entire solar system, over time scales from seconds to weeks and spatial scales from meters to billions of kilometers. Unlike the impacts caused by terrestrial weather, space weather events on the human scale are often much more subtle, and change with the particular technology being used. There are, for example, no known space weather events in the public literature that have directly led to the loss of human life. The public reaction to space weather events when announced, seldom if ever reaches the level of urgency of even an approaching, severe thunderstorm. Despite the fact that, since the 1990s, we have become more sophisticated about communicating to the public about the potential impacts of severe space weather, these alerts are still only

consumed and taken seriously by a very narrow segment of the population with technology at risk; satellite owners, power grid operators, airline pilots and the like. The historical record shows that in virtually all instances, space weather events have only led to nuisance impacts; disrupted radio communication; occasional short-term blackouts; and occasional satellite losses that were quickly replaced. Yet, when translated into the 21st Century, these same impacts would have a significantly larger impact in terms of the numbers of people affected. For instance, the Galaxy 4 satellite outage in 1998 deactivated 40 million pagers in North America for several hours. Pagers at that time were heavily used by physicians and patients for emergency surgeries, to name only one type of direct impact. Numerically, and in terms of function, we are substantially less tolerant of "outages" today than at any time in the history of space weather impacts.

In this chapter, I review the various technologies and systems that have historically-proven susceptibilities to space weather, why they are susceptible, methods being used to mitigate these risks, and how one might estimate their social impacts. I hope to demonstrate that, although we have a firm understanding of why technologies are at risk from basic physics considerations, we are still a long ways from making the case that extraordinary means need to be exerted to improve the reliability of present-day forecasts. One of the reasons for this is that we have been living through a relatively moderate period of solar activity spanning the majority of the Space Age. Without a major "Hurricane Katrina" equivalent in space weather, perhaps akin to the 1859 Carrington-Hodgson Superstorm, there is not much public outcry, commercial foresight, or political will, to significantly improve the current preparedness situation. Moreover, the progress of technology has been so rapid since the beginning of the Space Age in the late 1950s, that many of the technologies that were most susceptible to space weather, such as telegraphy, compass navigation, and short-wave communication, have largely vanished in the 21st Century, to be replaced by substantially more secure, albeit more inter-dependent, consumer technologies.

2.1.1 Open-air radio communication

Although telegraphic communication was the dominant victim of solar geomagnetic activity during the 1800s, by the mid-20th Century, virtually all telegraphic systems had been replaced by land lines carrying telephonic communications, and by the rapid rise of short-wave broadcasting and submarine cables for trans-continental communication (Odenwald, 2010). At its peak around 1989, over 130 million weekly listeners tuned-in to the BBC's World Service. Once the Cold War ended, short-wave broadcasting and listening de-

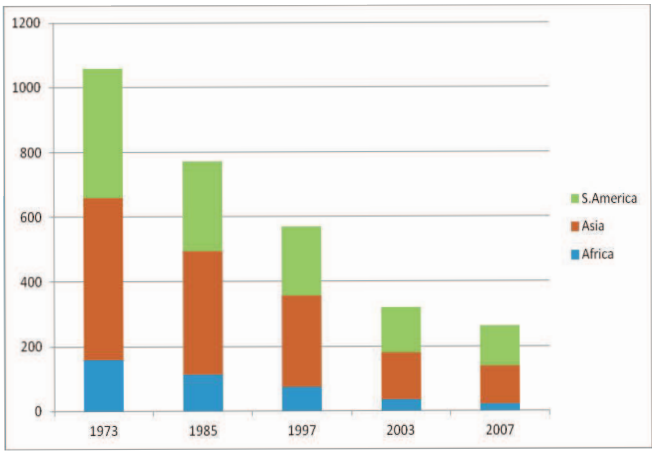

Fig. 2.1. The number of short wave stations (vertical axis) has dropped dramatically since the advent of the World Wide Web and other wireless media, which now provide the main source of news reporting in the 21st century. (Data courtesy Careless, 2010)

clined. As Figure 2.1 shows, less than one third of the stations on the air in 1970s are still operating. Compared to other forms of communication (such as web-based programming) shortwave is very expensive in terms of setting up a radio station and providing operating costs to purchase megawatts of broadcasting power. (Careless, 2010, 2011). Nevertheless, by December 2011 an estimated 33% of the human population had access to the Internet and its vast network of formal and informal "news" aggregators, including online counterparts of nearly all of the former shortwave broadcasting stations.

Although shortwave broadcasting is a ghost of its former self, there are still a number of functions that it continues to serve in the 21st Century. It is a back-up medium for ship-to-shore radio, delivering state-supported propaganda to remote audiences, time signals (at station WWV, the call sign of the U.S. NIST time signal), encrypted diplomatic messaging, rebel-controlled, clandestine stations, and the mysterious "Numbers Stations". There also continues to be a die-hard population of amateur radio "hams" who continue to thrill at DXing a dwindling number of remote, low-power stations around the world when the ionospheric conditions are optimal. Sometimes, these ham operators serve as the only communication resource for emergency operations. For example, during Hurricane Katrina in 2005, over 700 ham operators formed networks with local emergency services, and were the only medium for rapidly communicating life-saving messages. Despite the lack of public interest or awareness of the modern shortwave band, its disruption could leave many critical emergency services completely blind and unresponsive in a crisis.

Short wave (SW) broadcasting played such a key societal role during the first-half of the 20th century that millions of people were intimately familiar with its quality, program scheduling, and disruptions to this medium. Any disruption was carried as a Front Page story in even the most prestigious newspapers such as the New York Times. Although shortwave stations were routinely jammed by the then Soviet Union or Germany during World War II, these efforts paled in comparison to the havoc wreaked by even a minor solar storm. Known as the Dellinger Effect, a solar flare increases the ionization in the D and F Regions of the ionosphere on the dayside of Earth, spanning the full sun-facing hemisphere. This absorbs shortwave radiation but causes very low frequency (VLF) waves to be reflected. During the four solar cycles that spanned the "Short Wave Era" from 1920 to 1960, there were dozens of flares that delivered radio blackouts, which regularly interfered with trans-Atlantic communication, which was then a major news and espionage flyway for information between Europe and North America. Examples of events reported in the New York Times include:

- July 8, 1941 - Shortwave channels to Europe are affected (p. 10)
- September 19, 1941 - Major baseball game disrupted (p. 25)
- February 21, 1950 - Sun storm disrupts radio cable service (p. 5)
- August 20, 1950 - Radio messages about Korean War interrupted. (p. 5)
- April 18, 1957 - World radio signals fade (p. 25)
- February 11, 1958 - Radio blackout cuts US off from rest of world. (p. 62)

Although as we noted before, contemporary public contact with shortwave radio is nearly zero, today there are some places where SW is still in limited use, and where the public in those regions would be as conversant with SW fade-outs as the western world was around 1940. For instance, China is expanding its SW broadcasting to remote populations across its territory who do not as yet have access to other forms of communications networks. Even today, short wave outages still make the news:

On August 9, 2011 a major solar flare caused fade-outs in the SW broadcasts of Radio Netherlands World (RNW), but after an hour, broadcasting had returned to its normal clarity. Solar flare disrupts RNW short wave reception (RNP, 2011). This was the first major SW blackout in China since the X7.9-class flare on January 21, 2005, which affected Beijing and surrounding eastern population centers (Xinhuanet, 2005). On February 15, 2011 another large solar flare disrupted southern Chinese SW broadcasting. The China Meteorological Administration reported an X2.2-class flare at that time. (Xihuanet, 2011). The January 23, 2012 M9-class solar flare disrupted broadcasts on the 6 20 meters bands across North America, and severely affected the UHF and VHF bands for a period of a few hours (Shortwave America, 2012).

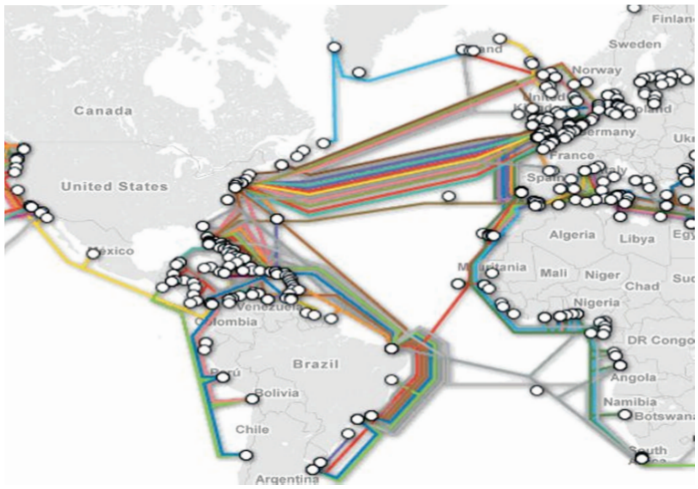

Fig. 2.2. A small portion of a map of the current locations of submarine fiber optic cables around 2011. (Courtesy TeleGeography, 2012)

2.1.2 Submarine telecommunications cables

The first copper-insulated, trans-Atlantic cable was deposited on the ocean floor in 1856 between Ireland and New Foundland, but because it was run at voltages that were too high, the insulation broke down and the cable failed within a few weeks. The first successful cable was laid in 1865 between Brest, France and Duxbury, Massachusetts and worked successfully for many years, passing telegraphic signals at a speed of 2 words per minute (≈0.01 bps!). The first copper-insulated, trans-Atlantic telephone cable was laid in 1956. By 1950, over 750,000 miles of copper-based undersea cable had been installed between all of the major continents (International Cable Protection Committee [ICPC], 2009). This was followed by the first fiber optic cable TAT-8 installed between Europe and North America in 1988. By 2009, some 500,000 miles of fiber optic cable has been deployed, and has largely replaced all copper cable traffic due to the much higher bandwidths approaching several terabytes/sec (see Fig. 2.2).

Because signals degrade in strength as they travel through thousands of miles of copper, devices called repeaters are added to the cable every 50 miles or so, and are powered by a current flowing through a separate HV power line that parallels the cable from end to end. Loss of power to a cable can cause immediate loss of signal, so all cables must be continuously powered through connection to the domestic power grid or back-up generators. These voltages can exceed 500 kV, and pose an electrocution hazard to fishing boats that accidentally snag them. Cables are typically broken through fishing accidents,

earthquakes and mechanical failure about 150 times a year, causing a loss of communication capacity that may last from days to weeks depending on the depth of the required repair (ICPC, 2009). Because the repair site may only be a meter or so in length, modern repair ships routinely use GPS to reach the proper location of the identified failed repeater, or cable damage. Also, GPS systems are used in deploying fiber optic cables along exact, preplanned routes that minimize cable waste.

There is no formal requirement for communications companies to log cable outage events, especially in a public archive. Consequently, outages only become public knowledge when they impact public telecommunications activities. For example, on February 25, 2012, The East African Marine System (TEAMS) data cable linking East Africa to the Middle East and Europe was severed off the coast of Kenya by a ship that illegally dropped anchor in a restricted area. This cable was already taking the traffic from three other fiber optic cables that had been damaged only 10 days before. It would take three weeks before this cable could be repaired, and data and e-commerce traffic restored to Kenya, Uganda, Rwanda, Burundi, Tanzania and Ethiopia. (Parnell, 2012).

Copper-based submarine cables are deployed in a manner similar to the old-style telegraph cables. For this reason they are subject to the same space weather impacts, though for different reasons, and perhaps not the ones you might initially consider. The original telegraphic systems and submarine cables of the 1800s were single conductors through which one-half of the battery was connected. The other half of the battery was grounded to the local Earth to complete the circuit! This works well when the naturally-occurring terrestrial ground current is stable in time, and over large geographic distances comparable to the telegraph network. However, both of these conditions are badly violated during a geomagnetic storm.

During a geomagnetic storm, a strong ionospheric current appears, called the electrojet. This current induces a secondary magnetic field that penetrates the local ground causing ground currents to flow that are called Geomagnetically-Induced Currents or GICs. Any single-wire telegraph system will immediately detect this GIC, which can be much greater than the original battery current, hence the frequent reports about mysterious high voltages and equipment burn out. The older trans-Atlantic cables were not immune from this because they, too, were patterned after the single-wire telegraph system and so GICs were a corresponding problem on these systems. For example, the geomagnetic storm that occurred on 2 August 1972 produced a voltage surge of 60 volts on AT&T's coaxial telephone cables between Chicago and Nebraska. The magnetic disturbance had a peak rate of change of 2200 nT/min., observed at the

Geological Survey of Canada's Meanook Magnetic Observatory, near Edmonton, and a rate of change of the magnetic field at the cable location estimated at 700 nT/min. The induced electric field at the cable was calculated to have been 7.4 V/km, exceeding the 6.5 V/km threshold at which the line would experience a high current shutdown (Space Weather Canada, 2011).

One might think that modern-day fiber optic cables are immune from this GIC effect because they involve a non-conductive optical fiber. High-voltage (HV)power is supplied to the cable at each end, with one end being at V^+ and the other at V^- potential. Just as for telegraph systems, one side of the HV supply is grounded to Earth, which provides a pathway for GICs. Repeaters for boosting the signal are connected in series along the cable axis and supplied by a coaxial power cable. GIC currents can temporarily overload the local power supply, causing repeaters to temporarily fail, and usually require resetting.

Have any incidents involving fiber optic cables ever been reported? We are mindful of the old adage that absence of evidence is not the same as evidence of absence. The fact that there is no impartial way to track outages on modern fiber optic telecommunications cables, and there are no federal regulations that require this reporting, means that reports are voluntary. When we search through public documents and find no cases of space weather-related cable outages, it only means that we cannot choose between two possible situations: Either they do occur and are not reported to save embarrassment, or the public records are unbiased and so lack of examples indicated lack of an impact. There are, however, some notable examples: At the time of the March 1989 storm, a new transatlantic telecommunications fiber-optic cable was in use. It did not experience a disruption, but large induced voltages were observed on the power supply cables (Space Weather Canada, 2011).

2.1.3 Ground-based computer systems

Solar storms can be a rich source of energetic particles via shock-produced Solar Proton Events (SPEs), galactic cosmic ray (GCR) enhancements during sunspot minimum, or events taking place within the magnetosphere during the violent magnetic reconnection events attending a geomagnetic storm. Although high-energy cosmic rays can penetrate to the ground and provide about 10% of our natural radiation background, secondary neutrons can be generated in air showers and penetrate at much higher fluxes to the ground. A number of monitoring stations, such as the Delaware Neutron Monitor, provide day-to-day measurements of the GCR secondary neutron background and detect ground-level enhancements (GLEs). At aviation altitudes, these high-energy neutrons can produce avionics upsets, which are easily corrected by error detection and correction (EDAC) algorithms or multiply-redundant avionics sys-

tems. On the ground, and ostensibly shielded by a thick atmosphere, computer systems and chip manufacturing processes have been allegedly affected by solar storm events (Tribble, 2010). Trying to identify even one case where such "computer glitches" were caused by GCR or space weather events remains problematical. Nevertheless, consumers and governments expect their computer systems to function reliably (computer virus attacks excepted), so even manufacturers such as Intel take this issue seriously. US patent 7,309,866, was assigned to Intel for their invention of "Cosmic ray detectors for integrated circuit chips" (Hannah, 2004): "Cosmic particles in the form of neutrons or protons can collide randomly with silicon nuclei in the chip and fragment some of them, producing alpha-particles and other secondary particles, including the recoiling nucleus. [...] Cosmic ray induced computer crashes have occurred and are expected to increase with frequency as devices (for example, transistors) decrease in size in chips. This problem is projected to become a major limiter of computer reliability in the next decade."

Bit-flip errors, in which the contents of a memory cell become switched from a "0" state to a "1" state or vice versa, are a pernicious form of Single Event Upset (SEU) that continues to plague ground based computer systems that use high-density VLSI (very large-scale integration) memory. The mechanism is that a high-energy neutron collides with a substrate or gate nucleus, producing a burst of secondary charged particles. These electrons and ions drift into a memory cell and increase the stored charge until a state threshold is achieved, at which point the cell indicates a high-Q state of "1" rather than a relatively empty, low-Q state of "0"; hence the bit-flip error. Extensive testing and research to identify the origin of these soft-memory errors led to alpha particle emission from naturally occurring radioisotopes in the solder and substrate materials themselves. Extensive re-tooling of the fabrication techniques, however, failed to completely eliminate SEUs. Currently, a system with 1 GB of RAM can expect one soft-memory error every week, and a 1 terabyte system can experience SEUs every few minutes. Error detection and correction (EDAC) algorithms cost power and speed, and do not handle multi-bit errors where the parity does not change (Tezzaron, 2003). According to Paul Dodd, manager for the radiation effects branch at Sandia National Labs: "It could be happening on everyone's PC, but instead everyone curses Microsoft. Software bugs probably cause a lot of those blue-screen problems, but you can trace some of them back to radiation effects" (Santarini, 2005).

Although there are no specific, documented examples of ground-based computer crashes due to specific solar storms, it is legitimate to consider what might be the societal consequences of space weather-induced computer glitches.

If they occur from time to time, it is instructive to consider the impact that other more prosaic glitches have produced:

- March 2, 2012 - Computer glitch hits Brazil's biggest airline. "Brazil's biggest airline says a computer glitch took down its check-in system in several airports across the country, causing long delays" (boston.com, 2012).
- November 5, 2011 - HSBC systems crash affects millions across UK. "HSBC was today hit by a nationwide systems crash thought to have affected millions of customers. The bank's cash machines, branches, debit cards, and internet banking services all stopped working at 2.45pm after a computer glitch" (Paxman, 2011).

2.1.4 Space-based computers

The first documented space weather event on a satellite occurred on Telstar-1 launched in July1963. By November, it had suddenly ceased to operate. By exposing the ground-based duplicate Telstar to various radiation backgrounds, Bell Telephone Laboratory engineers were able to trace the problem to the gate of a single transistor in the satellite's command decoder. Apparently, excess charge had built up on the gate, and by simply turning the satellite off for a few seconds, the problem disappeared. By January, 1963 the satellite was back in commercial operation relaying trans-Atlantic television programs between Europe and North America (Reid, 1963).

During the 1960s, a number of NASA reports carefully documented the scope and nature of space weather-induced satellite and spacecraft malfunctions. There was as yet no significant commercial investment in space, so NASA analyzed glitches to its own satellites and interplanetary spacecraft. Of course, military satellites of ever increasing complexity, cost, and political sensitivity were also deployed, but no unclassified documents were then, or are now, available to compare space weather impacts across many different satellite platforms. This leads to an important issue that is crucial to impact assessment and mitigation. How can we assess risks and prospective economic losses when so much of the required data is protected through national secrecy regulations and commercial confidentiality? Even among the "public domain" NASA satellites, data as to the number and severity of "glitches" is usually buried in the "housekeeping" data and rarely makes it out of the daily briefing room since it is irrelevant to the scientific data-gathering enterprise.

In a perfect world, we would like to have data for all of the 2000+ currently operational satellites that describes the numbers, dates and types of spacecraft anomalies that they experienced. From this we would be able to deduce how to mitigate the remaining radiation effects, identify especially sensitive satellites

and quantify their reliability, and to develop accurate models for forecasting when specific satellites will be most vulnerable. In reality, much of what we can learn is by "reading between the lines" in news reports, correlating these biased forms of information against the known space weather events, and hoping that a deterministic pattern emerges. Even this has been a daunting challenge when adjacent satellites in orbit can experience the same space weather conditions, but have very different anomalies, thereby making correlations between space weather conditions and satellite anomalies seem less certain.

2.1.4.1 How does it happen?

Satellite anomalies can be broadly defined to include any event in which some operating mode of a satellite differs from an expected or planned condition. In this context, the term "anomaly" is extremely broad, spanning a continuum of severities from trivial satellite state changes and inconsequential data corruption, to fatal conditions leading to satellite loss. Actual data from satellite-born sensors shows that these events can be quite numerous. For instance, SOHO data from a 2 GB onboard Solid State Recorder typically records over 1000 SEUs/day (Brecca et al, 2004). Only rarely, however, do SEUs actually lead to satellite conditions requiring operator attention a condition commonly termed an anomaly. For SOHO, only ≈60 anomalies during an 8-year period (≈8 anomalies/satellite/year) have required significant operator intervention, despite the literally millions of SEU events recorded during this time.

Anomalies need not be fatal to be economically problematical. On January 20, 1994, the Anik E1 and E2 satellites were severely affected by electrostatic discharges (ESDs). Although the satellites were not fatally damaged, they required up to $70 million in repair costs and lost revenue, and accrued $30 million for additional operating costs over their remaining life spans (Bedingfield et al., 1996). The Anik satellite problems were apparently the result of a single ESD event affecting each satellite (Stassinopoulos et al., 1996), suggesting that large numbers of anomalies are not required to 'take out' a satellite. If anomalies are frequent enough, however, the odds of a satellite failure must also increase, as will the work load to satellite operations. According to FUTRON (2003), satellite operators ordinarily spend up to 40 percent of their time on anomaly-related activities. Ferris (2001) has estimated the cost of dealing with satellite discrepancies (in which some system of the satellite and ground system does not operate as desired) as $4,300/event leading to overall operations impacts approaching $1 million/satellite/year under apparently routine space weather conditions. Anecdotal reports suggest that during major solar storms, far higher operator activity can occur. For example, the GOES-7 satellite experienced 36 anomalies on October 20, 1989, during a single, severe solar storm event (Wilkinson, 1994).

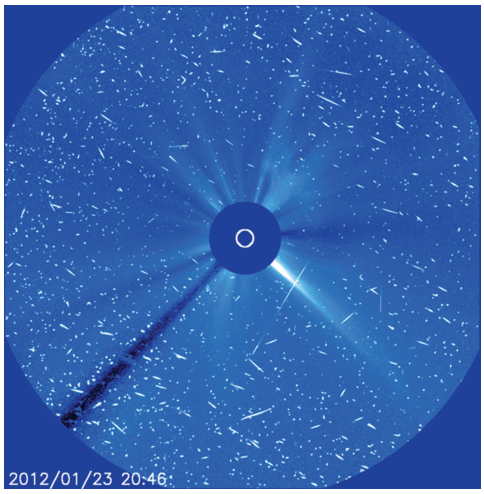

Fig. 2.3. This figure shows the effects of high-energy solar protons on an exposed imager on the Solar and Heliospheric Observatory during the January 23, 2012 solar storm. A greatly reduced flux of particles entering shielded satellite circuitry results in SEUs, many of which are harmless, but a few per year can result in serious operational anomalies.

Table 2.1. *Tabulation of statistics of satellite anomalies (see Sect. 2.1.4 for data and references).*

Rates:	study a: 1-10 /yr/sat study b: 3 /yr/sat for GEO, 2-3× more during enhanced space weather			
		study 1	study 2	study 3
Class:	1: mission failure	8%	6%	Class 1+2 comb.:
	2: interruption	7%	> 1 week 39%	0.019 ± 0.006 /yr/sat
	3: performance decr.	Class 3+4	2 h - 1 week 35%	
	4: inconsequential	comb.: 84%	<1 h 20%	
Cause:	ESD: 23-49%; SEU: 18-26%; Rad. damage: ∼ 5%			

The issue of "how bad can it get?" is an interesting one, especially given our dramatically increased reliance upon GEO satellite systems since ca 1980 that are economically baselined on the assumption of 100% reliability during a 10 to 15 year satellite service life span. The ≈250 GEO satellites now in operation produce an annual revenue of $80 billion (Ferster, 2005) so any space weather impact is potentially costly, and can involve more than one satellite at a time. Satellite designers use sophisticated tools to assess radiation

hazards under "worst case" conditions (e.g. the August 1972 and March 1991 events) however, recent studies of extreme space weather conditions suggest that the period since ca 1960 has not been typical of the historical record of severe storms during the last 500 years (McCracken et al., 2001; Townsend, 2003). Moreover, there is a large discrepancy between models that predict, for example, SEU events and actual satellite observations of them (e.g. Hoyos, Evans and Daly, 2004). Some recent studies have attempted to estimate the economic consequences to commercial GEO satellites for severe solar storm episodes (e.g. Odenwald and Green, 2007), but the studies were hampered by the lack of detailed knowledge of how the frequencies of satellite anomalies vary in severity with storm intensity. Consequently, the loss of a satellite during a severe space weather event could not be modeled realistically, nor its economic impact properly assessed. Most reported anomalies, broadly defined, are nuisances involving recoverable data corruption, easily-corrected phantom commands, or 'bit flips' often caught by onboard EDAC algorithms. These are not the kinds of anomalies that lead to significant economic consequences for a commercial satellite. Other less frequent anomalies cause sub-system failures, out-of-spec satellite operations, attitude and telemetry-lock errors and even outright satellite failures. These are most certainly the kinds of anomalies that have economic consequences. Some authors have also classified anomalies by satellite orbital location (e.g. LEO, MEO, GEO), recognizing that each environment has its own physical drivers for anomaly generation, but more often than not, these classes are aggregated together. Here is one possible scheme:

- Class 1 - Mission-Failure: The satellite ceases operation as a consequence of an unrecoverable system malfunction (e.g. Telstar-401).
- Class 2 - Mission interruption: Involves a recoverable damage to sub-systems. Only built-in redundancies, if available, are capable of mitigating some of these problems, where the satellite's safe mode may be enabled, or a back-up subsystem has to be activated (e.g. Anik-E1). These may take hours of effort to remedy, at a cost to satellite revenue and operator overhead charges.
- Class 3 - Performance decrease: Can include spacecraft pointing errors, attitude control system error, or a brief loss of data or telemetry usually corrected by a manual or automatic system reset.
- Class 4 - Inconsequential: Memory bit-flips and switching errors easily corrected using on-board EDAC software, or simple operator action. (e.g. TDRSS-1 telemetry; cosmic ray corruption of Hubble Space Telescope data).

One of the earliest, and most detailed, publically available studies of satellite anomalies and reliability is the work by Hecht and Hecht (1986: the Hecht

Report). The study was based on 2,593 anomaly reports for 300 satellites launched between ca 1960 and 1984. There were ≈350 satellites in operation by 1984, so the Hecht Report is relatively complete. This ground-breaking study analyzed the detailed reports provided by 96 satellite programs. A 'failure' was defined as "...the loss of operation of any function, part, component or subsystem, whether or not redundancy allowed the recovery of operation". Their study identified 213 Class 1 and 192 Class 2 anomalies out of a total collection of 2593 anomalies for a mission failure rate defined by our Class 1 of about 405/2593 or 1 in 6. No attempt was made to correlate the anomalies with space weather conditions.

One of the most widely used, recent starting points for anomaly studies is the archive assembled by Wilkinson and Allen (1997; National Geophysical Data Center, hereafter NGDC) which identifies most of the 259 satellites by name, or code, along with orbital location and/or altitude information. The date and type of anomaly is provided for many of the 5,033 events spanning the time period from 1970 to 1997, so that a proper assessment can be attempted of the various category-specific anomaly rates as a function of date and satellite type. There are 3,640 events that have been tagged according to type and system impact, including 647 SEU events and 848 ESD events. The NGDC archive contains 43 commercial GEO satellites included in the archive, accounting for a total of 480 anomalies spanning 20 years, and also appears to contain about 40% of all operating satellites during the sample time span, and is relatively complete for our purposes. The average annual anomaly rate of the GEO satellites was found to be about 3 anomalies/satellite/year, but can rise to twice or three times this rate during enhanced space weather conditions.

Robertson and Stoneking (2005: Goddard) examined 128 severe (Class 1 and 2) anomalies among 764 satellites. The data were culled from web-based satellite anomaly lists including the 'Airclaims Space Track' as well as NASA documents and the Aerospace Corporation 'Space Systems Engineering Database', and only included satellites from the US, Europe, Japan or Canada. The total number of satellites (military + commercial) operating during this interval is 827, so the sample contains about 92% of all possible operational systems during the 1990-2001 time period. A total of 35 anomalies were Class 1, which led to what was considered the total loss of the satellites. Four each anomaly in Class 1 there are three in Class 2. Their calculated anomaly rate was based on the number of anomalies recorded, divided by the number of satellites launched during a given year. Re-normalizing their mishap rates to, instead, reflect the annual operating satellites, the average mishap rate for Classes 1+2 is about 0.019 ± 0.006 anomalies/sat/year. The inverse of this rate is 166 which is sometimes called the mean time to failure (MTF). Clearly

for commercial satellites expected to last 10 to 15 years before replacement, a MTF of 166 years is good news! The correlation between these anomalies and space weather events was not studied.

The extensive studies by Belov et al. (2004) and Dorman et al. (2004) included satellite anomaly reports based on 300 satellites and ≈6,000 anomalies spanning the time period from 1971 to 1994. The data was drawn from NASA archives, the NGDC archive and unpublished reports from 49 Kosmos satellites (1971-1997). The term 'anomaly' was never precisely defined, but since the survey included the NGDC archive without distinction, we can assume that all Class 1-4 events were grouped together. The sample included 136 satellites in GEO orbits. They deduced that there were typically 1 to 10 anomalies/satellite/year. Specifically, the LEO Kosmos satellites experienced 1-7 anomalies/satellite/year, however some Kosmos satellites (Kosmos 1992 and 2056) reported ≈30 anomalies/satellite/year. Their statistical analysis indicated that anomalies occur during days when specific space weather parameters (electron/proton fluxes, Dst, Ap, etc) are disturbed. The largest increases coincide with times when electron and proton fluences are large, and can cause enhancements up to a factor of 50 in anomalies over quiet-time conditions. There appears to be a threshold of 1,000 pfu ($E > 10$ Mev) for proton fluxes, below which there are few anomalies reported. The anomalies continue to remain high for two days after the SPE event.

Koons et al. (1999) published "The Impact of the Space Environment on Space Systems", which investigated a sample of 326 anomaly 'records' collected from a diverse assortment of satellites culled from the NGDC 'Satellite Anomaly Manager', Orbital Data Acquisition Program (ODAP: Aerospace Corp.), NASA's Anomaly reports (Bedingfield et al. 1996, and Leach and Alexander, 1997), and the USAF Anomaly Database maintained by the 55th Space Weather Squadron. The specific number of satellites involved was not stated, however, the ODAP archive contains information from 15 USAF and 91 non-Air Force 'programs' no doubt drawn from LEO, MEO and GEO satellite populations. Although no information was provided as to the time period spanned by the study, the individual archives extend from 1970 to 1997. The definition of a record in terms of anomalies can vary enormously. Each record contained information for one class of anomalies for one 'vehicle'. Anomalies of a similar class were of the same functional type. Approximately 299 records out of 326 (92%) have causes diagnosed as 'space environment' but this does not necessarily correlate with a count based on anomaly frequencies. An example cited is that one record for the MARECS-A satellite included 617 anomalies. About 51 of 326 records were from commercial satellite systems and programs. In terms of the distribution of the records with anomaly

diagnosis, 162 (= 49%) were associated with Electrostatic Discharges, 85 (= 26%) with SEUs, and 16 (=5%) with 'total radiation damage'. Based on 173 reports of how quickly the anomalies were rectified, the Koons et al. (1999) study indicates that the number of mission failures represents 9/173 reports for a frequency rate of 1 in 19. The rates for the other classes are: Class 2 (More than 1 week) = 39%; Class 3 (1 hr to 1 week) = 35% and Class 4 (Less than 1 hour) = 20%.

Ferris (2001) analyzed 9,200 satellite operations discrepancy reports from 11 satellites between 1992-2001. A 'discrepancy' was defined as "the perception by a satellite operator that some portion of the space system had failed to operate as desired." The satellites were selected on the basis of which operators and owners were willing to divulge detailed anomaly logs for this study, which is a strong bias probably in favor of systems that had low absolute rates and few critical failures. Only three of the satellites were communications satellites; none were for civilian commercial use. This, of itself, is a problem since we cannot know to what extent these satellites are typical, or whether they are pathological. This is often the case when working with studies in which the satellite identities are not publically revealed. Of the discrepancies catalogued, only 13% involved the satellites themselves. The vast majority, 48%, involved issues with the ground segment, and specifically, most were discrepancies generated by software issues (≈61% of total discrepancies). Typical discrepancy rates involving 1,200 events imply ≈13 discrepancies/satellite/year. There were, however, higher rates recorded in 1996 involving 160 events for 4 satellites for a rate of 40 discrepancies/satellite/year or about one every 9 days. The study was the first one published in the open literature that also provided an assessment of the cost of rectifying these anomalies. Routine problems that require no more than 10 minutes to resolve by a team of 8 people cost $800 per event. More significant problems requiring 3-8 hours and more people cost $4,300 per event. The estimate only included labor hours and an average of the resolution times for the logged events, and not the cost of equipment or materials. In the latter case an 'event' may include the replacement of part of the ground station, processors or other mechanical items.

Cho and Nozaki (2005) investigated the frequency of ESDs on the solar panels of five LANL satellites between 1993-2003. During this period, LANL 1989-046 experienced 6038 ESDs/year while LANL-92A recorded 290 ESDs each year. Although the cumulative lifetime ESD rates on solar panels can exceed 6,000 events/kW over 15 years, the chances of a catastrophic satellite failure involving substantial loss of satellite power, remains small, though not negligible. For example, in 1973, the DSCS-9431 satellite failed as a result of an ESD event. More recently, the Tempo-2 (1998) and ADEOS-2 (2003)

satellites were also similarly lost. Koons et al. (1991, 2000) and Dorman et al. (2005) have shown that ESDs appear to be ultimately responsible for half of all mission failures (e.g. Class 1 anomalies) and correlated with space weather events.

Wahlund et al. (1999) have studied 291 ESD events on the Freja satellite (MEO orbit) and have found that the number of ESDs increases with increasing Kp. A similar relationship between increasing Kp and anomaly frequency was found by Fennell et al (2000) for the SCATHA satellite (near-GEO orbit). These results are consistent with earlier GOES-4 and 5 satellite studies by Farthing et al. (1982) and by Mullen et al. (1986). In addition to Kp, Fennell et al. (2000) and Wrenn, Rogers and Ryden (2002) identified a correlation between 300 keV electron fluxes and the probability of internal ESDs from the SCATHA satellite. The probability increases dramatically for electron fluxes in excess of 100,000ṗfu. A similar result was found a number of years earlier by Vampola (1987). At daily total fluences of $\approx 10^{12}$ electrons/cm^2 the probability of an ESD occurring on a satellite exponentially reaches 100% (e.g. Baker, 2000).

2.1.4.2 That was then – this is now

During the 23rd Sunspot Cycle (1996-2008) there were dozens of satellite malfunctions and failures noted soon after a major solar storm event, beginning with Telstar-401 (1996) and ending with the Japanese research satellite ASCA on October 29, 2003. The 24th Cycle had its own satellite outages and malfunctions of note.

On August 25, 2011, South Africa's $13 million LEO satellite SumbandilaSat failed. The explicit cause was stated publically to be 'damage from a recent solar storm', which caused the satellite's onboard computer to stop responding to commands from the ground station. This was not, however, the first time this satellite was damaged by radiation. Shortly after its launch in September 2009, radiation caused a power distribution failure that rendered the Z-axis and Y-axis wheel permanently inoperable, meaning that the craft tumbles as it orbits and has lost the ability to capture imagery from the green, blue and xantrophyll spectral bands. The reason given for the lack of proper radiation hardening was that there was not enough money to do this properly, and the satellite was built from commercial off-the-shelf (COTS) equipment. Moreover, SumbandilaSat was intended only as a technology demonstrator (Martin, 2012).

The case of the Anik F2 'technical anomaly' on October 6, 2011 is a replay of similar stories during the 23rd Sunspot Cycle. The satellite entered a Safe Mode that caused it to stop functioning and turn away from Earth. The Boeing satellite was launched in 2004 and was expected to function for 15

years. The owner of the satellite, Telsat, indicated in public news articles that they did not believe the problem had to do with the arrival of a CME that reached Earth early the same morning, but was caused by some other unspecified internal issue with the satellite itself. It is the first serious anomaly of its kind since the satellite was launched in 2004. What the news reports failed to mention was that the Sun has been relatively quiet for the majority of this 7 year period (Mack, 2011).

The temporary outage of Anik F2 caused a number of problems that impacted millions of people covered by this satellite service. WildBlue satellite ISP in the United States uses Anik F2 to provide broadband services to about a third of its customers. A total of more than 420,000 subscribing households mostly in parts of rural America lost service for several days, along with ATM service. Canadian Broadcasting Corporation indicated that 39 rural communities, and 7,800 people lost long-distance phone service. The satellite is also used for air traffic control, causing the grounding of 48 First Air flights, and 1000 passengers, in northern Canada. Communities in the North West Territories were instructed to activate their emergency response committees, and start using their Iridium phones (Mack, 2012; CBS News, 2012; Marowits, 2011).

On April 5, 2010, Galaxy-15 experienced an electrostatic discharge that caused a severe malfunction, rendering the satellite capable of re-transmitting any received signal at full-power, but not able to receive new commanding de Shelding, 2011). Reports cited a space weather event on April 5 as the probable cause of the electrostatic discharge that was the likely triggering event, however although Intelsat acknowledged the ESD origin, they categorically refuted the space weather cause in the April 5 solar event, preferring to declare that the orgin of the ESD was unknown. A consequence of this type of satellite failure is that Galaxy-15 was potentially able to interfere with other GEO satellites as it came within 0.5 degrees of their orbital slots. Thanks to careful, and complex, maneuvering of the satellites to maximize their distance from this satellite as it entered their orbital slots, AMC-11, Galaxy-13, Galaxy-18, Galaxy-23 and SatMex-6 and Anik F3 were able to reduce or eliminate interference, and no impacts to broadcasting were reported or acknowledged. "The fact that you haven't heard about channels lost or interference is the proof that we have been able to avoid issues operationally," said Nick Mitsis, an Intelsat spokesperson. "I don't want to underplay that" (Clark, 2010). In January 2011 commanding of the satellite resumed and its "zombisat" moniker has been changed to "phoenix".

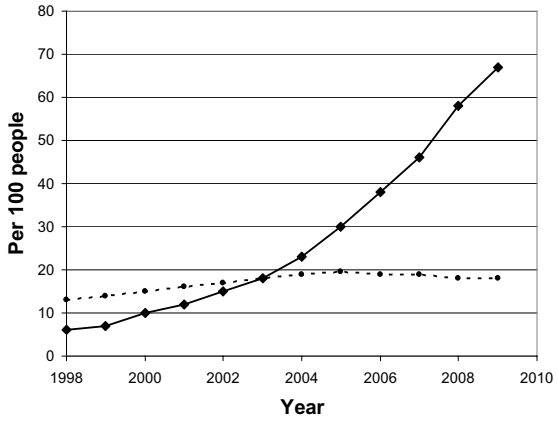

Fig. 2.4. A new report from the International Telecommunications Union finds that at the end of 2009, 67 percent of all people on Earth were cell phone subscribers (solid line). The number of land line subscribers is now in decline (dotted line) having reached a maximum of 19% of world inhabitants in 2005 (Duncan, 2010).

2.1.5 Cellular and satellite telephones

Although telephone calls by land lines are among the safest communication technology, and the most resistant to space weather effects, they have also been in rapid decline thanks to the wide spread adoption of cellular and mobile phones, especially among the under-30 population. According to an article in The Economist (2009) customers are discontinuing landline subscriptions at a rate of 700,000 per month, and that by 2025 this technology will have gone the way of telegraphy. Between 2005 and 2009, the number of households with cell phone-only subscriptions rose from 7% to 20%. In terms of space weather vulnerability, there is one important caveat. Without an electrical power grid, conventional land-lines fail, and cell phones may not be recharged even though the cell towers may have emergency back up power capability. An example of this vulnerability occurs whenever natural disasters strike and cell towers are unavailable, or the crushing load of cell traffic renders the local tower network unusable. Moreover, one does not have to wait for power grid failure to have an impact on cell phone access during episodes of solar activity.

A seminal paper by Lanzerotti et al. (2005) demonstrates that solar radio bursts, which occur rather often in an active photosphere, can cause enhanced noise at the frequencies used by cellphones (900 MHz to 1900 MHz), when the observer's angle between the cell tower and the Sun is small. This interference effect shows up in the Dropped-Call statistic for east-facing receivers at sunrise

or west-facing receivers at sunset. For a given cell phone and cell tower in the optimal line-of-sight geometry with respect to the Sun on the horizon, dropped calls occur about once every 3 days during solar maximum, and every 18 days during solar minimum. The article notes that the detailed, direct, evidence for solar-burst influence on cell phones remains a proprietary issue not openly available for investigation. The authors note that "solar bursts exceeding about 1000 sfu (solar flux units, 1 sfu = $10^{-22}\,\mathrm{W\,m^2\,Hz^{-1}}$) can potentially cause significant interference when the Sun is within the base-station antenna beam, which can happen for east- or west-facing antennas during sunrise and sunset at certain times of the year." Because base stations are only vulnerable for about two hours each day during sunrise and sunset, a typical station might be affected about one day out of 42 for solar maximum, and one day in 222 during solar minimum.

2.1.6 GPS-based systems

Navigation by satellite is not a new technology. It was first introduced by the US Navy in 1960 with the orbiting of five Transit satellites. This system was replaced by the NAVSTAR-GPS system in the 1970s. The first commercial use of satellite-based global positioning systems came less than 1 year after the next generation, 24-satellite 'Block I-GPS' constellation had been deployed in 1994, when Oldsmobile offered the GuideStar navigation system for its high-end automobiles. The GPS satellites provided an L1 channel at 1575 MHz capable of 10-meter-scale precision, that in 1990 was 'selectively degraded' to 100-meter precision. In 1999, President Clinton ordered that selective availability be turned off, and on May 1, 2000 the modern era of non-military GPS was ushered-in. Since 2000, the commercial applications of GPS have enormously expanded to include, not only car navigation aids, but oil extraction, fiber optic cable deployment, civilian aviation, emergency services, and even expanding public cellphone services, called apps, to locate nearby stores, restaurants and even parking spaces in downtown Manhattan! A report by Berg Insight (2011) indicates that GPS-enabled mobile phones reached 300 million units in 2011, and is expected to reach nearly 1 billion units by 2015.

Although the GPS constellation is stationed in polar orbits that frequently pass through the van Allen radiation belts in MEO, they are well-shielded and are upgraded every 5-10 years through replacement satellites such as the Block-II and Block-IIII systems. Although the details of the frequency of satellite anomalies is highly classified, it can be surmised that a legacy of 40 years of space operations has left the GPS system with a broad assortment of mitigation strategies for essentially eliminating outages. Nevertheless, there is one aspect of GPS system operation that cannot be so easily eliminated.

GPS signals must be delivered to ground stations by passage through the ionosphere. Because radio propagation through an ionized medium causes signal delays, and accurate timing signals are important in locating a receiver in 3-dimensional space, any changes in ionospheric electron content along the propagation path will cause position errors in the final solution (see Ch. 5). Space weather events, especially X-ray flares, cause increased ionization and introduce time-dependent propagation delays that can last for many hours until the excess ionospheric charge is dissipated through recombination. This also causes amplitude and phase variations called scintillation, which causes GPS receivers to loose lock on a satellite. Since a minimum of 4 satellites are required to determine a position, excess scintillation can result not just in a bad position solution, but can cause a loss-of-lock so that not enough satellites are available for various locations at various times during the event.

When civilian, single-frequency GPS systems using the L1 frequency are used, the anomalous propagation problem has to be mitigated by reference to a 'GPS Ionospheric Broadcast Model' and making the appropriate corrections. The resulting accuracy is about 5 meters. But this correction can only work for a limited period of time and so the path-delay problem is only partially solved. The result is that most civilian GPS systems can be easily disturbed by solar activity. Dual-frequency GPS systems that operate at L1 (1575 MHz) and L2 (1228 MHz) can measure the differential propagation of the satellite signal in real-time, and by relating this to the plasma dispersion equation, calculate the instantaneous total electron content (TEC) along a path, and then use this to make the requisite on-the-spot timing correction. In fact, this method can be turned around by using networks of GPS receivers to actually map out the changing ionospheric structure over many geographic locations. Figure 2.5 shows one such 'TEC' calculation for April 20, 2012 for 19:00 UT developed by JPL. The black spots are the GPS receivers in the network. Green indicates a TEC of about 50×10^{16} electrons/m^2 while red indicates 80×10^{16} electrons/m^2. Generally, a TEC of 6×10^{16} electrons/m^2 corresponds to an uncorrected position error of about 1 meter. The figure displays potential position errors as high as 13 meters over Chile.

Although the L1 carrier signal can be received without special instrumentation, the L2 timing information is coded and not accessible to non-military receivers. However, by using a technique called differential GPS, civilian GPS systems now rival, or even exceed, military precision in those areas where the requisite DGPS ground reference stations are available. If you are navigating in a large city, DGPS is probably available to you, but if you are 'in the middle of nowhere' chances are you only have single-frequency GPS to guide you.

We have already discussed this briefly in the context of GPS signal propa-

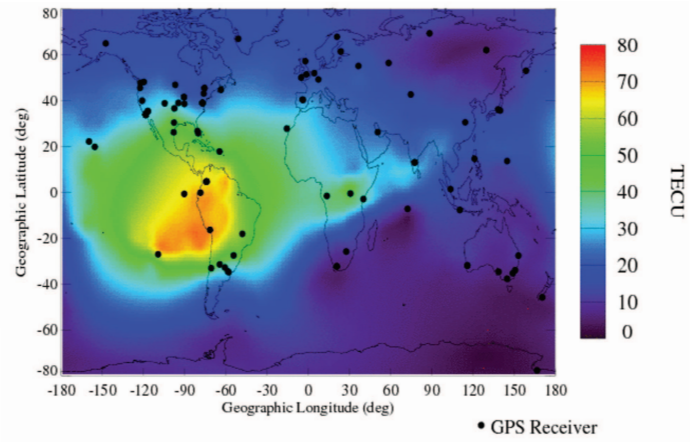

Fig. 2.5. Total electron content (TEC) calculation for April 20, 2012 for 19:00 UT developed by JPL.

gation and ionospheric scintillation. Because many space weather phenomena couple efficiently to the ionosphere, it is unsurprising that space weather issues have always been foremost in the discussion of GPS accuracy and reliability even apart from the fact that the GPS satellites themselves are frequently located in one of the most 'radio-active' regions of the magnetosphere. One of the first unclassified studies to quantitatively assess GPS behavior under solar storm conditions was conducted, inadvertently, by NOAA in 2001. They had set up a network of 70 GPS receivers from Alaska to Florida to test a new weather observation and climate monitoring system called the GPS-MET Demonstration Network. A major geomagnetic storm between March 30 and 31 caused significant changes in the GPS formal error, and was correlated with the published Kp index during the course of the event (NOAA, 2001). Since then, a variety of anomalous changes in GPS precision have been definitively traced to, and found to be correlated with, geomagnetic storms and solar flare events. This also means that systems that rely on GPS for high-precision positioning have almost routinely reported operational upsets of one kind or another. For example (NOAA, 2004):

- On October 29, 2003, the FAA's GPS-based Wide Area Augmentation System (WAAS) was severely affected. The ionosphere was so disturbed that the vertical error limit was exceeded, rendering WAAS unusable. The drillship GSF C.R. Luigs encountered significant differential GPS (DGPS) interruptions because of solar activity. These interruptions made the DGPS solutions unreliable. The drillship ended up using its acoustic array at the

seabed as the primary solution for positioning when the DGPS solutions were affected by space weather.

- On December 6, 2006, the largest solar radio burst ever recorded affected GPS receivers over the entire sunlit side of the Earth. There was a widespread loss of GPS in the mountain states region, specifically around the four corners region of New Mexico and Colorado. Several aircraft reported losing lock on GPS. This event was the first of its kind to be detected on the FAA, WAAS network.

Apart from changes in ionospheric propagation, we have the problem that, if the GPS signal cannot be detected by the ground station, and the minimum of 4 satellites is not detected, a position solution will not be available at any accuracy. This situation can arise if the GPS signal is actively blocked or jammed, or if the natural background radio noise level at the L1 and L2 frequencies is too high. This can easily happen during radio outbursts that accompany solar flare events. This happened the day after the December 5, 2006, solar flare, and was intensively studied by Kintner at Cornell, and presented at the Space Weather Enterprise Forum in Washington, DC on April 4, 2007 (NOAA, 2007).

2.1.7 Electrical power grids

The issue of space weather impacts to the electrical power grid is covered more extensively in Chapter 4, we review the main points of this vulnerability, provide concrete examples, and review briefly the impacts and consequences of future large geomagnetic storms.

It has been well known for decades that geomagnetic storms causes changes in the terrestrial ground current. The most dramatic examples of this effect are in the many reports of telegraph system failures during the 1800s. So long as a system requires an 'earth ground', its circuit is vulnerable to the intrusion of geomagnetically-induced currents (GICs). For the electric power grid, these DC currents do not need to exceed much above 100 amperes in order to do damage (Odenwald,1999, Kappenmann, 2010).

When GICs enter a transformer, the added DC current causes the relationship between the AC voltage and current to change. It only takes a hundred amperes of GIC current or less to cause a transformer to overload during one-half of its 60-cycle operation. As the transformer switches 120 times a second between being saturated and unsaturated, the normal hum of a transformer becomes a raucous, crackling whine physicists call magnetostriction. Magnetostriction generates hot spots inside the transformer where temperatures can increase very rapidly to hundreds of degrees in only a few minutes, and last

for many hours at a time. During the March 1989 storm, a transformer at a nuclear plant in New Jersey was damaged beyond repair as its insulation gave way after years of cumulative GIC damage. During the 1972 storm, Allegheny Power detected transformer temperature of more than 340 F (171 C). Other transformers have reached temperatures as high as 750 F (400 C). Insulation damage is a cumulative process over the course of many GICs, and it is easy to see how cumulative solar storm and geomagnetic effects were overlooked in the past.

Outright transformer failures are much more frequent in geographic regions where GICs are common. The Northeastern US with the highest rate of detected geomagnetic activity led the pack with 60% more failures. Not only that, but the average working lifetimes of transformers is also shorter in regions with greater geomagnetic storm activity. The rise and fall of these transformer failures even follows a solar activity pattern of roughly 11 years.

The connection between space weather events and terrestrial electrical systems has been documented a number of times. Some of these examples are legendary (1989, 2003) while others are obscure (1903, 1921). Given the great number of geomagnetic storms that have occurred during the last 100 years, and the infrequency of major power outages, this suggests that blackouts following a major geomagnetic storm are actually quite rare events. Consider the following historical cases:

- November 1, 1903: The first public mention that electrical power systems could be disrupted by solar storms appeared in the New York Times, November 2, 1903 "Electric Phenomena in Parts of Europe". The article described the, by now, usual details of how communication channels in France were badly affected by the magnetic storm, but the article then mentions how in Geneva Switzerland (New York Times, 1903). "All the electrical streetcars were brought to a sudden standstill, and the unexpected cessation of the electrical current caused consternation at the generating works where all efforts to discover the cause were fruitless".
- May 15, 1921: The entire signal and switching system of the New York Central Railroad below 125th street was put out of operation, followed by a fire in the control tower at 57th Street and Park Avenue. The cause of the outage was later ascribed to a "ground current" that had invaded the electrical system. Brewster New York, railroad officials formally assigned blame for a fire destroyed the Central New England Railroad station, to the aurora (New York Times, 1921).
- August 2, 1972: The Bureau of Reclamation power station in Watertown, South Dakota experienced 25,000-volt swings in its power lines. Similar disruptions were reported by Wisconsin Power and Light, Madison Gas and

Electric, and Wisconsin Public Service Corporation. The calamity from this one storm didn't end in Wisconsin. In Newfoundland, induced ground currents activated protective relays at the Bowater Power Company. A 230,000-volt transformer at the British Columbia Hydro and Power Authority actually exploded. The Manitoba Hydro Company recorded 120-megawatt power drops in a matter of a few minutes in the power it was supplying to Minnesota.

- March 13, 1989: The Quebec Blackout Storm - Most newspapers that reported this event considered the spectacular aurora to be the most newsworthy aspect of the storm. Seen as far south as Florida and Cuba, the vast majority of people in the Northern Hemisphere had never seen such a spectacle in recent memory. At 2:45 AM on March 13, electrical ground currents created by the magnetic storm found their way into the power grid of the Hydro-Quebec Power Authority. Network regulation failed within a few seconds as automatic protective systems took them off-line one by one. The entire 9,500 megawatt output from Hydro-Quebec's La Grande Hydroelectric Complex found itself without proper regulation. Power swings tripped the supply lines from the 2000 megawatt Churchill Falls generation complex, and 18 seconds later, the entire Quebec power grid collapsed. Six million people were affected as they woke to find no electricity to see them through a cold Quebec wintry night. People were trapped in darkened office buildings and elevators, stumbling around to find their way out. Traffic lights stopped working, Engineers from the major North American power companies were worried too. Some would later conclude that this could easily have been a $6 billion catastrophe affecting most US East Coast cities. All that prevented the cascade from affecting the United States were a few dozen capacitors on the Allegheny Network (Odenwald, 1999).
- October 30, 2003: Malmö, Sweden, population 50,000 lost electrical power for 50 minutes (Pulkkinen et al., 2005). The blackout was caused by the tripping of a 130 kV line. It resulted from the operation of a relay that had a higher sensitivity to the third harmonic (=150 Hz) than to the fundamental frequency (=50 Hz). The excessive amount of the third harmonics in the system has been concluded to have resulted from transformer saturation caused by GIC. Currents as high as 330 Amperes were recorded on the Simpevarp-1 transformer (Wik et al., 2009).
- October, 2003: South Africa Transformer Damage. The ESKOM Network reported that 15 transformers were damaged by high GIC currents.

Extensive studies have already been conducted on the most cost-effective means for reducing or eliminating GICs in electric power grid components (Kappenman, 2010). The strategies generally include adding individual ca-

pacitors to each of the transformer HV lines, or adding a blocking resistor or capacitor to the ground lines in all transformers. Blocking capacitors were, for example, installed on the entire Hydro-Quebec power grid following the March 1989 blackout, as well as the WECC region in the western US. Although this strategy seemed to be successful in reducing GICS and reactive power on some of the lines, the impact was deemed only modest, 12% to 20% for the WECC network with 50% penetration, given the cost expended. Adding blocking capacitors to the transformer neutral ground connector is the simplest and most direct method for achieving a 100% reduction in DC GICs from transformer primaries, but this method is known to alter the impedance of the network in unpredictable ways as the devices are selectively deployed rather than universally adopted.

The next most direct, and also the most cost-effective method is by adding a low-ohmage and low-voltage resistor to the neutral ground of each 3-phase transformer (see red boxes in figure). Preliminary studies (Kappenman, 2010) suggest that this method could achieve a 60% reduction in GIC amperages to transformer primaries. The cost would be at most $100,000 per transformer in the US power grid, which contains some 5000 transformers, for a total cost of about $500 million. A simulation of the Hydro-Quebec power grid during the 1989 failure, but with neutral ground resistors installed reveals a dramatic reduction in the GICs to which the 45 transformers in the 735 kV grid were subjected, with hypothetical 10-ohm blocking resistors reducing the GICs from 550 amps to only about 75 amps.

The maximum storm time disturbance was about 450 nT/min., but even with proper mitigation, the US grid may not be immune from the largest known geomagnetic events, although the severity of the impact could be reduced by 60% from the case where no such mitigation is implemented. During the 1921 storm, a disturbance field of 4800 nT/min. was estimated. Without mitigation, over 500 transformers would be damaged, but with mitigation only about 40 would be damaged according to these simulations (Kappenman, 2010). This tenfold reduction is not inconsequential.

It is also worth mentioning that, although blackouts are a dramatic consequence of severe GICs caused by space weather, economic consequences also flow from the on-going stresses to the power grid during non-black out conditions. For example, Forbes and St. Cyr (2004) note that the constant impacts of minor space weather events over a long period of time disrupts the system that transmits the power from where it is generated to where it is distributed to customers. In examining the determinants of the real-time electricity market price over the period June 1, 2000, through December 31, 2001, they concluded that solar storms (over this period) increased the wholesale price of

electricity by approximately 3.7 percent or approximately $500 million. Kappenmann (2012) has recently shown that in the months following the March 1989 Quebec event, a statistically significant number of transformers in the United States had to be prematurely replaced, with the greater number of replacements found in proximity to the Quebec power grid.

Of course, not all electrical power blackouts have anything to do with space weather. Most of us have experienced at least on "outage", and in some regions like Washington, DC, it is typical to have 3-5 outages every year lasting from hours to days. Hamachi-LaCommare and Eto (2004) have studied the economic costs of annual power outages and power "sags" and have found that they cost as much as $130 billion annually to the GDP. We are accustomed to electrical blackouts and quietly absorb them into our economy, with some grumbling about lost food and time. The long term trends for normal blackouts also points to the progressive failures inherent to an ageing domestic power grid (Karn, 2007). The over use of this resource is highlighted by the dramatic growth in bulk power transactions on, for example, the Tennessee Valley Authority system which exploded from less than 20,000 such transactions in 1996 to more than 250,000 by the end of 2001 (Dept. of Energy, 2005).

Increased bulk power transactions have led to a substantial drop in capacity margin, which provides little room either for growth or to maneuver in times of crisis. By some accounts (Patterson, 2010) there were 41 blackouts nationwide between 1991-1995, and 92 between 2001-2005. In 2011 alone, there were 109 affecting communities of 50,000 or more people. The Eaton Corporation, an agrigator of news and industry reports of blackouts across the US states, finds that between 2009 and 2011, the number of power outages rose from 2,169 to 3,041 and the number of people impacted climbed from 26 million to 42 million (Eaton Corporation, 2011).

A "typical" person comes into contact with the following technologies each day: cell phones, portable computing, credit card verification (ATM), navigation (GPS), electrical utilities (water pumps, gasoline pumps, hospital facilities, home lighting, city electrification, cell-phone recharging). All of these "essential" systems rely on electricity either at the point of creation (satellite GPS and ATM verification) or at the point of delivery (cell phone, gas pump, water, etc). All are expected to be ready when needed with 100% reliability. In recent human history, we have been successful in delivering these services even in the face of a number of space weather events. The lynchpin technology is, of course the electric power grid which citizens use to "tap into" essential communication and utility resources. It is unlikely that even a Superstorm event will dramatically impact the number of satellites operational,

and backup transponders are readily available in case of emergencies. The ubiquitous cell phone would not fail if satellites failed, but satellites do carry the bulk of financial transactions, GPS and military CCC (command, control, and communications) traffic. The loss of key satellites, or a critical number, would render these services reduced in capability.en made of the cascading problems involved in "re-booting" such a large grid, especially in the event of component failures and burn-outs which would necessitate replacement, not on a local scale, but quite possibly on a global scale, with only a few key manufacturers able to service these needs.

2.1.8 Airline travel

Generally, the known routes for space weather impacts to aviation are through passenger safety (radiation), flight avionics (computer/system glitches), communications (radio interference) and scheduling (delays, route changes). Historically there have been anecdotal instances of each of these being identified. For example, July 19, 1947 - Sunspots delay planes (New York Times, July 18, 1947 p. 15).

Although earlier flight navigation methods involved compass bearings and LORAN-C, which in principle could be affected by geomagnetic storms and shortwave interference, there are actually no known instances where space weather events caused significant disruptions to these navigation technologies. Today, however, the airline industry is adopting GPS navigation as the new standard, and its implementation in the Wide-Area Augmentation System (WAAS). WAAS is a combination of GPS and local, ground based metrology reference stations that provides 1-meter lateral and 1.5-meter vertical position resolution every 6 seconds for aircraft flying over the continental US, Canada and Alaska. There are also several satellites, such as Galaxy-15 that are involved in the WAAS system as part of its space-leg. Because its uses GPS satellites, the WAAS system is not immune to space weather effects that impact the ionosphere. Consequently during a severe storm event, WAAS may not be available for several minutes, or even hours, in some regions of the normal coverage area (Doherty, 2011). Studies have shown that approaches with vertical guidance (APV) are restricted during times of geomagnetic activity in terms of the APV coverage with Dst during the period from July 2003 to March 2004. For airports in which APV coverage is not available, flights must revert to IFR or VFR landing regulations within a vertical distance of 200 meters of the runway.

A number of national and international studies have been conducted to assess the radiation load on passengers during active space weather conditions and under otherwise normal circumstances. Normal background radiation

doses are typically 0.3 microSv/hr or 3 mSv/year. For passengers and flight crews, the actual cabin exposure varies with the geographic latitude of the flight, the altitude of the flight, and the combined GCR and solar fluxes of particles. For example, Bottollier-Depois et al. (2000) determined from direct measurements at maximum solar activity in 1991-1992 and at minimum activity in 1996-1998. The lowest mean dose rate measured was 3 microSv/hr during a Paris-Buenos Aires flight in 1991. The highest rates were 6.6 microSv/hr during a Paris-Tokyo flight on a Siberian route and 9.7 microSv/hr on Concorde in 1996-1997. A number of similar studies since then have supported the idea that there is in fact some additional passenger and flight crew radiation exposure caused by space weather. However, the levels are cumulatively very low for the vast majority of passengers who travel infrequently during the year.

Nevertheless, some airlines that fly polar routes, such as United Airlines, are sensitive to solar storm events, not necessarily for the added radiation load, but for the disruption of emergency high-frequency communications with ground controller, which violates FAA safety regulations. For example, on January 20, 2005 a severe solar storm event caused 26 United Airlines flights to be detoured to lower altitudes and latitudes. The steady increase in the number of polar routes suggests a larger number of people will be affected by such events as time goes on. As Figure 2.6 indicates, currently, 1.7 million passengers travel these routes each year (Murtagh, 2010).

The most recent, well publicized event where airlines were diverted to other routes came with the powerful January 23, 2012, solar flare and CME. Hailed as the biggest solar storm since 2003, Delta Airlines chose to divert its flights to more southerly routes, while American Airlines took no operational action (Waugh, 2012). Despite the impacts to airline communications and flight safety, there are no instances where space weather has affected passengers or airline flight crews, so in some sense, the issue of flight safety and space weather presents a very modest health risk, but ironically a significant cost in flight time and fuel to airline companies that choose to apply mitigation.

2.2 Forecasting strategies

The specific components of the space weather environment that are known to cause human impacts are solar x-ray flares, coronal mass ejections, solar proton events, geomagnetic storms, galactic cosmic rays, electrostatic discharges, and energetic particles in the magnetosphere. X-ray flares cause ionospheric changes and upper atmosphere heating, which cause problems for LEO satellites and GPS-based systems. During the impulsive phase of a CME, shocks also form that lead to the acceleration of particles and solar proton events.

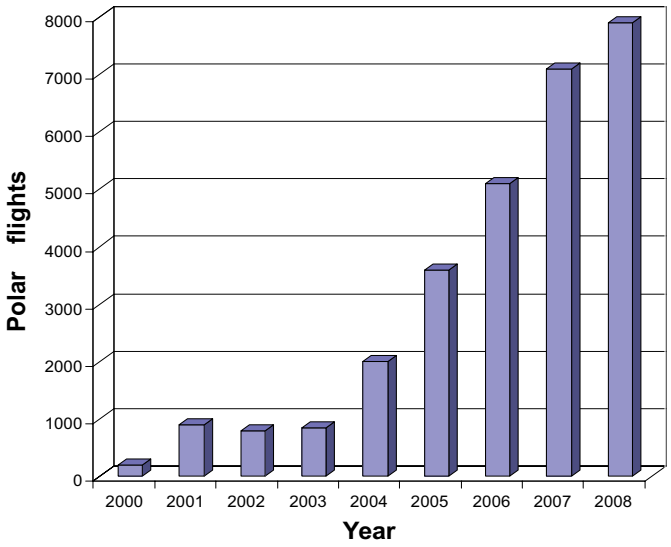

Fig. 2.6. The number of passengers flying "polar routes" continues to sharply increase each year to a current level of nearly 1.7 million passengers each year (Murtagh, 2010).

Some of these energetic particles can also arise from the site of the solar flare itself. Solar proton events and galactic cosmic rays can have energies of 10s of MeV, which lead to SEUs in computer circuitry, or to enhanced radiation exposure by airline passengers and astronauts.

The complexity of the space weather environment, and the many ways in which it can invade our technology to cause problems, almost precludes that we will ever be able to start from an initial set of solar or geophysical data and use this to determine whether a specific transformer or satellite system will fail. Consider that a satellite can be rendered inoperable if a single energetic particle causes a permanent failure of a critical gate, and the vast number of these particles that pass through a satellite's volume during its operational lifetime. In quantum electrodynamics, arguably the most precise physical theory known, precisions of 1 part per 10 billion are routine, but in terms of that fatal energetic particle, we would need a predictive algorithm of nearly the same caliber, otherwise we are forced to always deal in probabilities.

We also know that, in the space sector with over 2000 operating satellites, it is a rare event for satellites to actually fail during solar storms. How is it that, in the most recent Galaxy-15 or Anik-F6 outages, other satellites nearby were not similarly disturbed? We see this curious paradox again and again

in reports of satellite outages related to space weather events. The industrial response is that satellite failures have much less to do with external space weather events, which reasonably should have affected more than one satellite simultaneously, than with manufacturing or software problems internal to the satellite itself such as tin wisker growth (e.g. Galaxy-7 in about 2000), solar panels designs (e.g. Tempo-2 around 1997), or software errors (e.g. Galaxy-15 around 2010). This raises another important issue that has been a much-discussed topic among space weather forecasters. How can you predict which space weather events will be important if the various industries that control the vulnerable assets are not transparent with their anomaly data?

For most types of space weather events, by the time they are detected it is already too late to mitigate. This is the case for all of the events that flow from solar or cosmic energetic particles, or solar X-ray flares. Phenomena such as CMEs, on the other hand, provide us with 1 to 3 days notice of arrival near earth once they are spotted leaving the solar vicinity. To keep forecasting costs low, what we would like to do is to come up with a small number of inexpensive measurement indices of the solar and geophysical environment, and through some yet to be developed algorithm, convert these into a statement about whether a particular resource or asset is in eminent danger and what the nature of that danger might be so that industry can take action. We also want to minimize the number of false alarms which can be costly and result in progressive lack of confidence in the forecasts themselves.

2.2.1 Solar storms: flares and CMEs

The simplest correlations we can search for involve solar flares, CMEs, SPEs and the sunspot cycle, because sunspots can be inexpensively counted and studied with ground-based instrumentation. We are reasonably certain that solar flares and magnetic reconnection events require concentrated photospheric magnetic fields, which manifest themselves as sunspots, so we expect more of these events during times of sunspot maximum than sunspot minimum. Yet even during sunspot minimum the number of significant flare events is not zero as for example the M6.4 flare on February 7, 2010, or the X2.6 flare on July 9, 1996. So if you are operating a GPS system or a WAAS system and require 100% coverage for safety, you will need a back up plan even during sunspot minimum. What about coronal mass ejections and the effect they can have on electric power grids?

According to an analysis of 314 halo CMEs during the 23rd cycle by Tripathi and Mishra (2005), about 3 occurred during sunspot minimum (1996) and 61 during sunspot maximum (2001), yet fewer than 1 in 6 halo CMEs led to significant geomagnetic storms.

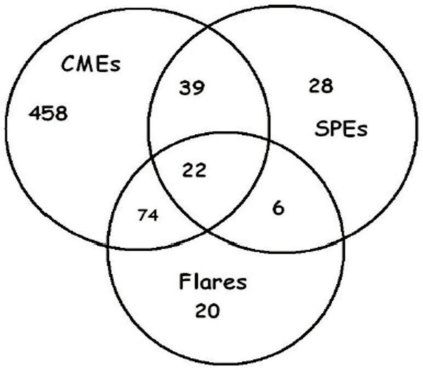

Fig. 2.7. A simple Venn diagram showing the frequency of halo CMEs, X-class flares and Solar Proton Events during Cycle 23. There were a total of 598 Earth-directed CMEs, 95 Solar Proton Events, and 122 X-class flares. It is clear from the intersection statistics that the vast majority of CMEs do not result in SPEs, or are associated with X-class flare events. However, it is also true that the majority of X-class flares are associated with CMEs, and that the majority of SPEs are associated with CMEs as well.

Odenwald (2007) created a combined data base of X-class flares, halo CMEs and Solar Proton Events (SPE) for the period January-1996 to June-2006, during a time in which SOHO/LASCO detected 11,031 coronal mass ejections. Of these, 1186 were nominally 'halo' events including back-side ejections, however, only 598 were actually directed towards Earth. During the same period of time, 95 solar proton events were recorded by the GOES satellite network orbiting Earth. Of these SPEs, 61 coincided with halo CME events. Solar flares were also recorded by the GOES satellites. During this time period, 21,886 flares were detected, of which 122 were X-class flares. Of the X-class flares, 96 coincided with halo CMEs, and 22 X-class flares also coincided with 22 combined SPE+halo CME events. There were 6 X-flares associated with SPEs but not associated with halo CMEs. A total of 28 SPEs were not associated with either halo CMEs or with X-class solar flares. The result can be summarized in the Venn diagram shown in Figure 2.7.

What this simple statistical exercise shows is that many of X-class flares (20 of 122), halo CMEs (458 of 598) and SPEs (28 of 95) are maveric events not associated in general with the other two types of phenomena. One cannot use halo CMEs to predict if an SPE will result (only (39+22)/598 = 10% of the time). One cannot use X-class flares to determine whether an SPE will result (28/122 = 23% of the time), or using halo CMEs to predict X-class flares,

(96/598 = 16% of the time), but if an X-class flare is seen, then you have a (96/122 =) 79% chance that a halo CME results, or a (28/95 =) 29% chance that an SPE results. These statistical results demonstrate that the path to any sensible form of space weather prediction will probably always be fraught with the shear uniqueness of each and every space weather event, and the way that it is then "transduced" by a myriad of technological platforms whose properties and succeptabilities are often out of the public domain. This is far less like the tornado that rumbles through a state and wreaks havoc than a lightning storm whose strike points are utterly random on the landscape and damage or death is literally a matter of bad luck. This may well be the situation for global forecasting, but at the individual active region-scale, the situation is fortunately much more optimistic.

2.2.2 Reliability of X-class forecasts

Solar flares and CMEs are the most dramatic precursors of transient changes in space weather conditions, and considerable effort has been expended in developing predictive schemes for them (for a review see Forbes, 2010). In all cases, the ability to predict whether a flare or a CME will occur depends on the quality of the data gathered through the deployment of sophisticated, and expensive equipment. CMEs cannot be studied without space-based chronographic equipment (e.g. SOHO/LASCO), sensitive photometers that detect scattered light from them in transit (STEREO), or in-situ particle and field measurements made at L1 (e.g. ACE). There are no ground-based techniques for studying CMEs that could lead to significant cost savings over using space-based assets that need to be replaced every 10 years or so. Similarly for solar flares and the solar X-ray emission, only space-based sensors provide the data required to detect and quantify their severity, with no ground-based analogues to the X-ray technology. The good news is that both CMEs and X-ray flares produce distinctive "Type-II" bursts of radio-wavelength radiation that ground-based radio telescopes can profitably detect (e.g. Gopalswamy et al., 2005). By combining ground-based and space-based data over the last 20 years, considerable progress has been made in developing reliable forecasting algorithms which can provide nearly 100% certainty over the next 24-hour period for significant CME or flare activity. Most rely on a description of the topology and morphology of sunspots and their pre-cursor magnetic fields.

Solar flares have been studied extensively since the 1930s since they are historically known to cause shortwave outages. It has been understood for some time that sunspots with complex field topologies are prime candidates for flaring activity (Hudson, 2010). Modern-day analyses that incorporate precursor information about changes in sunspot field topology such as rotation

and shear, and past time history of activity (Nunez et al, 2005), the McIntosh classification of the sunspot group (Gallagher et al., 2002) lead to forecasts of X-class flares in the next 24-hour period that are more than 90% reliable with few false-positives. More recently, Colak and Oahwaji (2007) use a neural network approach to achieve prediction accuracies of 92% for occurrence and 88% for classification (M or X-class). None of these statistical methods actually employ any physics-based knowledge of the underlying flaring process, but merely search for correlations among a diverse ensemble of parameters available in various data bases and archives.

Detailed measurements of the 3-d shape of active region, surface magnetic fields and their classification (e.g the Wilson classifications), has led to most of the advances in flare forecasting during the previous sunspot cycle. The legacy of this surface-field approach is best shown in the research by Steward et al. (2011) who used data from the National Solar Observatory's, Global Oscillation Network Group (GONG) to investigate strong-gradient polarity inversion lines, and neutral lines in maps of solar magnetic fields near active regions. By classifying each active region seen in 2003 according to a 5-parameter scheme (e.g., field gradient strength, curvature, neutral line length), they statistically compared 44 combinations of these 5 indices and found an optimal set that maximized the accuracy of predicting a flaring event. The resulting, optimized algorithm, called FlareCast, can predict a flare with 88% confidence within a 24-hour period, with a 10% false-positive rate (i.e. 1 prediction out of 10 will turn out not to occur).

But events transpire so rapidly that, by the time surface fields start to become twisted into the pre-flare state, it is already too late to prepare Earth-based systems for the resulting burst of X-rays and energetic particles, which arrive in less than an hour. During the first decade of the 21st century, a steadily accumulating archive of sub-surface active region images from the GONG program, has allowed changes in the plasma flows some 65,000 km below the surface to be studied at a 10-minute cadence, for over 1,000 active regions. In a path-breaking paper by Reinard et al. (2010), reoccurring sequences of magnetic topology change were discovered that presaged surface flaring events, with a lead time of 2 to 3 days before the surface eruption occurred. A vorticity-based index allows active regions to be classified in terms of its future activity, and can discriminate between regions producing C, M and X-class flares. The study supports the idea that rotational kinetic energy twists sub-surface fields into unstable configurations, which are then involved in explosive magnetic reconnection at the surface.

Coronal mass ejections have a shorter history in the space weather community since their role in the dynamics of the geomagnetic field was only deduced

in the 1980s, and actual space weather effects were not observed until the Quebec Blackout in 1989. X-class flares have been studied as precursors for CMEs (Wang et al., 2002) as have sigmoidal features revealed in soft X-ray imaging of the corona (Sterling, 2000; Canfield et al., 1999), and vector magnetogram studies of the length of the "strong-field, strong-shear" main neutral line in sunspot groups (Falconer, 2001). Actual predictive schemes remain lacking due to the failure to bridge the gap between the changes in the small-scale surface fields near measurable active regions, and the often hidden large-scale magnetic field rearrangements that occur before the CME is launched.

Once evidence is available for a CME launch, the arrival time at Earth and the geoeffectivness become important predictive issues. Some progress has been made in this area. It has been known for several decades that the most efficient energy transfer into the geomagnetic field occurs for "south directed" CME field orientations. This can currently only be determined by in situ measurements made by satellites at L1 such as ACE. Also, the speed of the CME and the quantity of entrained plasma determine the ram pressure of the arriving CME at the magnetosphere boundary. The effect of aerodynamic drag by the interplanetary medium has also been studied (Song, 2010), and the results provide significantly improved determinations of the initial CME speed, its speed at 1 AU, and the transit time. The advent of STEREO spacecraft imaging of CMEs at large angles from the sun-earth axis have verified the deceleration of fast-moving CMEs in the interplanetary medium, and that CMEs need to be tracked at least 30 degrees from the Sun in order to obtain arrival time accuracies less than about 6 hours.

Solar proton events, often associated with shock acceleration in the initial stages of CME ejection, have also entered the domain of forecasting through the same statistical studies that proved successful with X-ray forecasting. For instance, Chin (2005) used an archive of 28 SPE between 1997-2000 and compared these events with solar radio bursts recorded between 245 MHz and 15,400 MHz to find a strong correlation between Type-III radio bursts at 245 MHz and the appearance of an SPE observed some 1-2 days later.

2.3 Modeling the economic and societal impacts

Cycle 23 will be seen by historians, no doubt, as a watershed moment in space weather history. Prior to Cycle 23, there was little or no public discussion about space weather vulnerability during the Space Age, although our grandparents surely knew all about the practical consequences of space weather and the insufferable short wave outages. With Cycle 23, we had SOHO providing

the public with dazzling and ominous movies of solar storms, and many popularizers, including myself, who went on the stump to sort out for the public all the ways in which we could be affected. Then, just before the famous Halloween Storm of 2003, we had the first high-profile Congressional hearing about space weather in the context of why NOAAs Space Environment Center (SEC) budget should not be halved. Once Homeland Security became involved, we then had a new round of hearings about our infrastructure ulnerability to space weather events. The Space Weather Forum was held in Washington, DC on Capitol Hill in June 2008 to educate Capitol Hill about space weather issues. Meanwhile, researchers began the difficult task of trying to quantify what these impacts could cost us and the social disruption that might follow.

Kappenmann (1997) has an extensive record of modeling the US power grid with increasingly more sophisticated models of the electrodynamics of GICs and exhaustive studies of the North American electric grid network at the component level. Currently, his efforts use historical geomagnetic storms (e.g. 1921 event) and their impact on the contemporary electric power grid. Among the forecasts are for year-long recovery periods costing over $1 trillion in GDP.

Teisberg and Weiher (2000) estimated that the economic benefits of providing reliable warnings of geomagnetic storms to the electric power industry (alone) would be approximately $450 million over three years (note that this does not include any other impacted industries). This is well above the $100 million cost of a new operational satellite that would provide such warnings (ACE, Triana)

Odenwald and Green (2007) modeled the economic losses to commercial satellites in LEO, MEO and GEO orbits and deduced that an 1859-scale "superstorm" arriving near sunspot maximum could cost $50 billion in lost revenue and assets.

In August 1988, Oak Ridge National Laboratory and the NRC published "Evaluation of the Reliability for the Offsite Power Supply as a Contributor to the Risk of Nuclear Plants". This set the stage for considering the impact of space weather-related GICs on the reliability and safety of nuclear power plants (Kirby et al., 1988).

In April 1989, Northwest Power Coordinating Council (NPCC) approved the document "Procedures for Solar Magnetic Disturbances Which Affect Electric Power Systems" which has been updated several time.(NPCC, 1989) October 2003 What is Space weather and who should forecast it? Congressional Hearing on Space Weather held before the Subcommittee on Environment, Technology, and Standards, Committee on Science, House of Representatives,

One Hundred Eighth Congress, first session, October 30, 2003, (Congress, 2003)

In December 2005, Idaho National Laboratory and NRC published "Reevaluation of Station Blackout Risk at Nuclear Power Plants–Analysis of Station Blackout Risk." The executive summary from this report reads in part: The availability of alternating current (ac) power is essential for safe operations and accident recovery at commercial nuclear power plants. (INL, 2005)

April 2008 saw the publication of the "Report of the Commission to Assess the Threat to the United States from Electromagnetic Pulse (EMP) Attack: Critical Infrastructures". The US Congress funded a vulnerability assessment research under the National Defense Authorization Act to evaluate the impact of an electromagnetic pulse (EMP) from a high altitude nuclear detonation by a terrorist event on the nation's critical infrastructure including the electric grid. The same study also discussed geomagnetically-induced currents. (EMP Commission, 2008)

In 2008 "Severe Space Weather EventsUnderstanding Societal and Economic Impacts Workshop Report". The National Academy of Sciences determined that severe geomagnetic storms have the potential to cause long-duration outages to widespread areas of the North American grid. (NAS, 2008)

In June 2010, the report entitled "High-Impact, Low-Frequency Event Risk to the North American Bulk Power System" was published, jointly sponsored by NERC and the Department of Energy. NERC now concedes that the North American power grids have significant reliability issues in regard to High-Impact, Low-Frequency events such as severe space weather. The NERC report explains commercial grid vulnerability to space weather (NERC, 2010)

In October 2010 a report entitled "Electromagnetic Pulse: Effects on the U.S. Power Grid" appeared. In relation to that, Oak Ridge National Laboratory released a series of comprehensive technical reports for the Federal Energy Regulatory Commission (FERC) in joint sponsorship with the Department of Energy and the Department of Homeland Security. These reports disclose that the commercial power grids in two large areas of the continental United States are vulnerable to severe space weather. The reports conclude that solar activity and resulting large earthbound CME, occurring on average once every one hundred years, would induce a geomagnetic disturbance and cause probable collapse of the commercial grid in these vulnerable areas. The replacement lead time for extra high voltage transformers is approximately 1-2 years. As a result, about two-thirds of nuclear power plants and their associated spent fuel pools would likely be without commercial grid power for a period of 1-2 years. (Oak Ridge Labs, 2010)

Armed with all this bad news, and with the storms of Cycle 24 now begin-

ning, it has become commonplace for Reporters to quote these studies and offer titles such as "A big solar storm could cost $2 trillion, could be a global Katrina" or "Solar storm buffets Earth: How protected is the US power grid?"'. The danger is that, through constant repetition of this Doomsday theme, the public will become inured to the message in the face of the inevitable false alarms such as the January 2012 storm. While it is certainly important to keep the preparation message alive given the consequences to our infrastructure, as scientists and space weather forecasters, we need to be more careful with delivering this complex message to a public increasingly eager for a simple "yes or no" answer to their safety.

3

Commercial space weather in response to societal needs

W. Kent Tobiska

3.1 The history of commercial space weather

3.1.1 Space weathers challenge to our society

On Monday evening September 30, 2013 the U.S. Government began to close numerous facilities at the beginning of the Government shutdown. Included in the shutdown was the computer system that runs the Nowcast of Atmospheric Ionizing Radiation System (NAIRAS†) (Mertens et al., 2009, 2010, 2012, 2013) at NASAs Langley Research Center (LaRC). This system provides real-time data-driven climatology of the aviation radiation environment and Figure 3.1 shows the last report before the shutdown. The source radiation was from both Galactic Cosmic Rays (GCRs) and Solar Energetic Particles (SEPs). Coincidentally, the Government shutdown occurred just as a moderate solar radiation storm was peaking that had started a day earlier. The SEPs from a September 29 small X-ray solar flare coupled with the Earths magnetosphere to produce a 27-hour moderate S2 radiation storm on the NOAA scale‡ with a peak at 20 UT on September 30.

Since this type of radiation storm exposes passengers and crew in aircraft flying at high latitudes or high altitudes to elevated radiation risks, questions immediately arose: what were the risks for passengers and crew on commercial aircraft flights during the September 30–October 1, 2013 S2 radiation event? What was the peak effective dose rate at commercial aviation altitudes during the radiation event? What guidelines exist for flight crews, frequent flyers, and pregnant mothers to estimate their radiation risks?

This is the context in which the present-day commercial space weather sector

† http://sol.spacenvironment.net/~nairas
‡ http://www.swpc.noaa.gov/NOAAscales

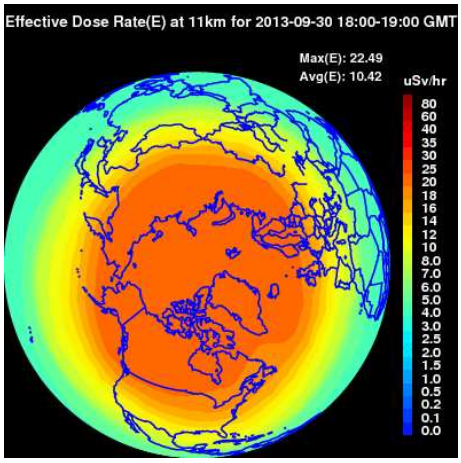

Fig. 3.1. NAIRAS effective dose rate at the time of the U.S. Government shutdown of NASA LaRC computers and prior to the 20:05 UT peak of the radiation storm on September 30, 2013. Courtesy of Space Environment Technologies and NASA Langley Research Center NAIRAS project.

has arisen. As technology has developed into this second decade of the 21st Century, it has become clear there are impacts from space weather on not only the near-Earth space environment but on the technology we come to rely upon, including conditions related to personal health and well-being.

This chapter explores the impact of space weather on society and the expanding management of those risks using capabilities developed by the Space Weather Enterprise. We highlight the role of commercial space weather, necessarily emphasizing the U.S. commercial sector since that domain is the most developed (though not the only) commercial space weather sector. Notably, European and South Korean commercial organizations also exist but are not described here.

3.1.2 What is space weather?

Space weather, i.e., the predominant but not exclusive dynamic and variable transfer of energy from the Sun to the Earth via photons, particles, and fields that vary on multiple time and spatial scales, affects our near Earth space environment as well as our societys technology. Components of our critical technological infrastructure, including satellites, communications, navigation, transportation, electric power, aviation, defense, information, banking/finance, energy exploration, health, construction/surveying, emergency services, government services, water, and data storage (called key industrial sectors in this chapter), all are key elements of the U.S. economy. These eco-

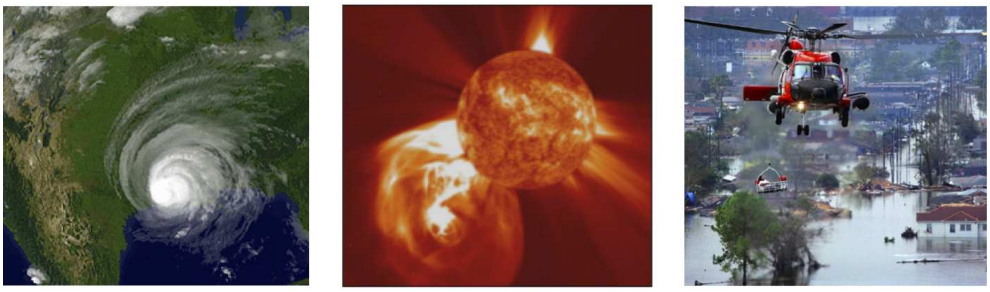

Fig. 3.2. (a) Hurricane Katrina hit New Orleans August 29, 2005 (left picture), (b) the X17 flare occurred on September 7, 2005 (center picture surrogate image), and (c) the helicopter recovery efforts (right picture) were without command center communications for several hours. Sources: (a) GOES satellite image, (b) NASA SOHO composite image, (c) AFP/Getty Images/James Nielsen

nomic engines, just to name a few, have capabilities that are reliant on space or ground systems with a susceptibility to the impacts of space weather.

The predominant source for severe space weather is the large solar flare above Class M5 (Tobiska et al., 2013), which, at times, can be associated with coronal mass ejections (CMEs). However, even without associated CMEs, large flares can threaten our technology and render it degraded or even useless. One example is the September 7, 2005 X17 flare, the fourth largest on record, during the Hurricane Katrina recovery period; the effects of this flare eliminated emergency high frequency (HF) radio communications between ships, helicopters, and ground-based emergency responders for several hours (private communication Rene Stiegler, ShipCom, LLC, Figure 3.2).

The great risks associated with severe space weather are based on our inability to predict both the timing and magnitude of large solar flares or the magnetospheric coupling of solar ejecta that traverses the solar wind to arrive at Earth and causes service degradations, equipment failures, and sometime catastrophic asset loss. Outside the solar system, variable GCRs (high energy, high Z charged particles) also affect our technology and the near-Earth space environment. That environment includes the Earths magnetosphere, radiation belts, neutral atmosphere, and ionosphere and it is this environment that requires specification of its conditions at the current epoch as well as forecasts for some future time.

3.1.3 What are societal impacts of space weather?

As our society has emerged into the 21st Century and become more reliant on space-based systems, we have found that a variety of technologies are impacted by space weather (National Academies Press, 2008; Tobiska, 2008, 2009). The

affected technologies are found in all key industrial sectors. Examples of those impacted technologies, the source events for space weather effects, their symptoms, and the relevant NOAA R (Radio blackouts), G (Geomagnetic), and S (Solar radiation) space weather scales (1=minor impact and 5=extreme impact) are listed in Table 3.1.

It should be noted that this list is certainly incomplete when compared across discipline areas. However, it does reflect the major force behind the evolution of the U.S. commercial sector from a funding and operational implementation perspective. This driver is specifically the USAF interest in both the ionosphere and the neutral atmosphere. As such, there is a U.S.-centric bias in these examples that is even more weighted towards activities with major funding to support DoD services. Other phenomena, such as GIC monitoring, is clearly important but has not received the operational funding in any country at the level compared to USAF ionosphere and neutral atmosphere specification.

Classic examples of impacts from space weather on our technology that have led to game-changing innovations include the following events:

(i) March 13, 1989 Hydro-Quebec transformer saturation from geomagnetically induced currents (GIC) that caused its power grid to go off line for 9 hours (Czech et al., 1992); this same storm caused GOES weather satellite communications to be interrupted with lost weather images, led to NASA's TDRS-1 communication satellite reporting over 250 anomalies, and induced unusually high pressure readings in a hydrogen fuel cell on the Space Shuttle Discovery; this storm spurred the current development of risk management efforts under the umbrellas of Federal Energy Regulatory Commission (FERC) and North American Electric Reliability Corporation (NERC) to warn the power industry of impending GIC surges, which are analogous to terrorism threats (National Academies Press, 2008, 2012a);

(ii) March 23–24, 1991 tracking loss of a significant number of satellites in the NORAD catalog (Bedingfield, et al., 1996) due to atmospheric drag caused by large solar flares and geomagnetic storms; these events led directly to the USAF Space Commands initiative to improve operational thermospheric density uncertainty to much less than 10% with the creation of the High Accuracy Satellite Drag Model (HASDM) and the Jacchia-Bowman 2008 (JB2008) model (Bowman, et al., 2008a,b; Tobiska, et al., 2008);

(iii) September 7, 2005 Hurricane Katrina recovery effort where an X17 solar flare caused HF radio communications between emergency responder helicopters and off-shore support ships to be lost for several hours (pri-

Table 3.1. *Example technologies affected by space weather, its effects, and NOAA scale (R – Radio blackout , G – Geomagnetic disturbance, and S – Solar energetic-particle radiation).*

Technology	Cause	Effect	Scale
Aviation communication (commercial, business jet, and general aviation)	Solar flares & CMEs	Loss of high frequency radio signal for communications	R & G
Aviation health and safety (commercial, business, and high altitude jet)	SEPs	Increased radiation dose for human tissue and avionics	S
Aviation navigation (commercial, business jet, and general aviation)	Solar flares & CMEs	Loss of GNSS position accuracy for plane en-route and loss of WAAS landing aid	R & G
Cell phones (connectivity)	Radio bursts	Interference with cell phone signals due to high energy solar radio bursts	–
Institutional facilities (hospitals, government, large data centers, banking, ERS)	CMEs	Power loss from electric grid outages	G
Oil & gas exploration (field ops)	CMEs	Drill bit misalignment using magnetic field; oil pipeline damage from GIC	G
Power grid (regional networks)	CMEs	Transformer loss from GIC surges	G
Radio communications (DoD, corporate fleet, Hams, ERS)	Solar flares, CMEs, & scintillation	Loss of HF/UHF/L-band radio signal for communications; D-region absorption	R & G
Satellite operations (LEO, MEO, GEO)	SEPs, solar flares & CMEs	LEO orbit error from drag; GEO spacecraft charging; SEUs and latch-up	S & G
Surveying (mega sites, roadways, field operations)	CMEs	Loss of GNSS position accuracy	G
Transportation navigation (shipping, corporate fleet, ocean, rail)	Solar flares, CMEs, & scintillation	Loss of GNSS position accuracy	R & G

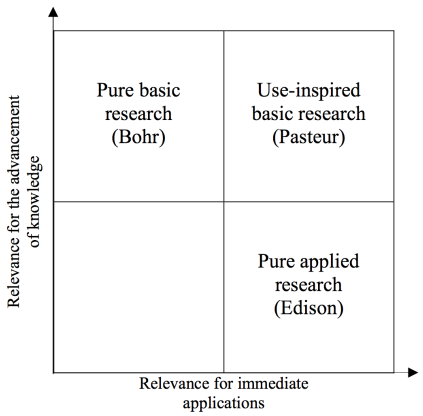

Fig. 3.3. Pasteurs Quadrant from Stokes (1997).

vate communication R. Stiegler, ShipCom, LLC.); this communication failure led to the Space Environment Technologies (SET) and Space Environment Corporation (SEC) Communication Alert and Prediction System (CAPS†) for improving HF communication signal strength availability. CAPS was followed by the establishment of the Utah State University (USU) Space Weather Center (SWC‡) with Utahs Federal ARRA funds, leading to its commercial spinoff, Q-up§ for leveraging USUs GAIM ionosphere for commercial applications;

(iv) December 6, 2006 solar radio burst that was 10 times more intense ($> 10^6$ sfu) than any previously recorded, affecting L-band GPS accuracies and cell phone reception; this led to the improvement of GPS sensors for scintillation and resulted in ASTRAs CASES instrument; and

(v) November 10, 2008 NigComSat1, the commercial Nigerian communication satellite, failed due to > 300 keV elevated energetic electron flux levels at Geosynchronous Earth Orbit (GEO) with a daily fluence of 2×10^{12} electrons cm^{-2} day^{-1} †; this event led to the establishment of SETs real-time GEO Alert and Prediction System (GAPS) for specifying the real-time and forecast surface and internal charging environment at GEO‡ while utilizing data-driven statistical models from SCATHA legacy studies.

† http://sol.spacenvironment.net/∼ionops/index_ionops_caps.html
‡ http://spaceweather.usu.edu
§ http://q-upnow.com
† http://www.cgwic.com/In-OrbitDelivery/CommunicationsSatellite/Program/NigComSat-1.html
‡ http://terra1.spacenvironment.net/∼gapops/

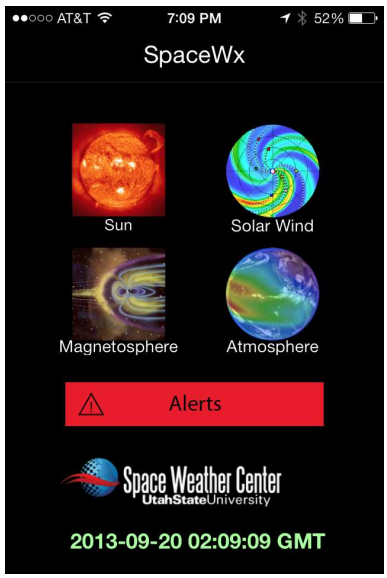

Fig. 3.4. SpaceWeather iPhone app for displaying real-time 24/7 space weather data. Courtesy of Utah State University Space Weather Center and Space Environment Technologies.

3.1.4 Emergence of three pillars in the U.S. space weather enterprise

Before the mid-1990s, when space weather was first recognized as a serious threat to our technological infrastructure (National Space Weather Program, 1995, 1997, 2000, 2006, 2010), there were a number of clues that not only foretold the importance of specifying and forecasting space weather but also showed its dramatic power, giving insight to its underlying physics. After the mid-1990s space weather came into its own as a discipline embodying Pasteurs Quadrant (Stokes, 1997), i.e., use, demand, and interest intersect to find basic answers (Figure 3.3). Highlights in the timeline of theoretical (T), experimental (E), programmatic (P), operational (O), and commercial (C) development of the space weather enterprise include the list below.

E 1859: Carrington and Hodgson identified a white light solar flare event that later came to be identified as one of the largest solar events affecting human technology;

T 1882: A conducting region in Earths upper atmosphere was speculated by Kelvin and Stewart in connection with daily magnetic variations;

E 1901: Marconi performed his wireless radio experiment from Cornwall to Newfoundland;

T 1902: Kennelly and Heaviside independently postulated that the radio waves

were reflected from an ionized layer (E region) to explain Marconis communication;

T 1912: Eccles provided a rudimentary theory for the ionosphere;

T 1926: Watson-Watt coined the term ionosphere;

T 1936: Saha theorized excess irradiances (EUV and X-rays) were needed above the solar blackbody spectrum to give the observed ionization levels;

E 1946: the first NRL upper atmosphere rocket, a captured German V-2, detected excess solar EUV irradiances above the blackbody spectrum;

T 1950s: One-dimensional upper atmosphere models were developed by Chapman, Bates, and Nicolet;

E 1965: USAF OV1-1 satellite observed electron density, magnetic fields, proton concentration;

T 1970s: Schunk (USU) developed first ionospheric, coupled 3-ion, model;

T 1980s: Roble (NCAR) achieved a 3D model of the thermosphere and ionosphere;

T 1990s: Schunk and Sojka (SEC) developed mid- and high-latitude ionosphere descriptions for the USAF PRISM model and the Ionospheric Forecast Model (IFM);

P 1995: First National Space Weather Program Strategic Plan published;

P 1997: First National Space Weather Program Implementation Plan published;

C 1998: Tascione (Sterling Software) introduced the commercial application of the Magnetospheric Specification Model (MSM) for NOAA via a CRADA;

E 1998: the first GAIM data assimilative ionospheric systems using physics-based models were developed through the ONR MURI program with USU and JPL/USC;

C 2000: Tobiska (SET) provided first commercial operational real-time and forecast solar irradiances for NOAA via a CRADA;

P 2000: Second National Space Weather Program Implementation Plan published;

O 2002: U.S. AFSPC HASDM system declared operational, reducing NORAD catalog error to less $< 10\%$;

C 2004: First ISO International Standard published for space environment on GCRs;

O 2005: AFRL and NRL validated USU GAIM as the gold standard for operational use by AFWA; 2006 ops implementation;

P 2006: National Space Weather Program Assessment Committee Report published;

O 2007: Fry (EXPI) provided first operational solar wind data using HAFv2 to AFWA;

E 2008: U.S. AFSPC and SET released the JB2008 thermospheric density model providing the most significant advance for satellite orbit accuracy in 40 years;

C 2008: SET and SEC released first real-time and forecast Communication Alert and Prediction System (CAPS) commercial operational ionosphere via Google Earth;

C 2009: USU SWC and SET released the first smartphone app (SpaceWx or SpaceWeather) (Figure 3.4) with 165 real-time data streams from 15 participating institutions;

C 2010: USU SWC initiated first commercial GAIM operational ionosphere system;

P 2010: Second National Space Weather Program Strategic Plan published;

E 2011: Mertens (NASA LaRC) and SET released first real-time global aviation radiation environment with NAIRAS;

O 2012: Tobiska (SET) demonstrated first operational Dst forecasts up to 6 days with 1 hour granularity using the solar data-driven Anemomilos algorithm;

O 2012: Crowley (ASTRA) achieved first commercial data streams for Alaska scintillation with CASES sensor;

P 2012: the National Research Council Decadal Survey published; and

E 2013: SET demonstrated first real-time downlink of aviation radiation dose and dose-rate, integrated into NAIRAS, and redistributed to the world via app with 15-minute latency.

From the combination of these events, three pillars (government agencies, academia, and industry) emerged to first understand, then characterize, and finally begin managing the risks associated with severe space weather. These pillars jointly form the backbone of the U.S. space weather enterprise and include: i) Government agencies (e.g., DOC/NOAA, DOD/USAF and USN, NASA, DOI/USGS, NSF, DOE, DHS/FEMA, DOS/OES, and DOT/FAA organized through the interagency Committee for Space Weather); ii) academic programmatic activities (e.g., GAIM MURI (USU and USC), CISM (BU), NADIR MURI (UCB), and SWC (USU USTAR)); and iii) commercial businesses (e.g. the American Commercial Space Weather Association (ACSWA†) 18 members of Atmospheric and Environmental Research (AER), Atmospheric and Space Technology Research Associates (ASTRA), Carmel Research Center (CRC), Computational Physics Inc. (CPI), Exploration Physics International (EXPI), Flare Forecast, GeoOptics, Geosynergy, PlanetIQ, Predictive Science (PSI), Propagation Research Associates (PRA), Q-up, Space Environment

† http://www.acswa.us

Corporation (SEC), Space Environment Technologies (SET), Scientific Solutions (SSI), Space Services Holdings, Inc. (SSH), Storm Analysis Consultants (SAC), and Space Weather For Today and Tomorrow (SWFTT)). Companies that have contributed a significant role to developing the commercial space weather enterprise outside of ACSWA include RPSI (DynaCast HF and data-driven VOACAP), Sterling Software (MSM), North West Research Associates (WBMOD), and Metatech (GIC information services).

3.1.5 The influence of professional societies and community meetings

Three professional societies have been particularly important in the development of the U.S. space weather enterprise. The American Geophysical Union (AGU), the American Meteorological Society (AMS), and the American Institute for Aeronautics and Astronautics (AIAA) have each provided a unique, different forum in which space weather sponsors, researchers, and implementers/users have been able to exchange ideas and move the enterprise forward.

The AGU holds its annual meeting every year (Fall) that highlights new, detailed topic area research in the Space Physics disciplines of Aeronomy (SA), Solar and Heliospheric Physics (SH), and Magnetospheric Physics (SM); AGU also hosts Chapman Conferences as a forum for the detailed study of space sciences. The AMS hosts the Space Weather Symposium at its annual meeting every year (Winter), which has become a forum for the three pillars to present their latest interdisciplinary results. AMS hosts roundtables and commissions for organizing ongoing discussions within the space weather enterprise. The AIAA hosts the Atmosphere and Space Environment Technical Committee (ASETC) with its complementary Committee on Standards (CoS) that develops guidelines and standards for the user communities.

Every spring the NOAA Space Weather Prediction Center (SWPC) hosts the annual Space Weather Workshop (SWW) in Boulder Colorado. This event enables the three pillars to cross-fertilize their separate activities and has been an engine for Pasteur Quadrant programmatic and scientific/engineering application development in the space weather enterprise. Canadian, European, Russian, Japanese, Taiwanese, and South Korean space weather organizations have also participated actively in SWW. Other community forums contribute to an expansive and active space weather enterprise. These include: i) the Office of the Federal Coordinator for Meteorology (OFCM) sponsorship of the Space Weather Enterprise Forum (SWEF) held in (Summer) Washington DC to inform policy-makers of space weather; ii) the NSF-sponsored GEM, SHINE, and CEDAR (Summer) workshops which highlight new research in

space weather related discipline areas; iii) the USU-sponsored annual (Spring) Space Weather Community Operations Workshop (SpWxCOW) in Utah for space weather operational users; and iv) the NASA-sponsored (Summer) Heliophysics Summer School in Boulder to educate graduate students and professionals about the cutting-edge science related to space weather.

3.2 Commercial organizations in the space weather enterprise

3.2.1 Societal space weather needs addressed by the commercial sector

In a Decadal Survey (National Academies Press, 2012b) it was noted that, during the first decade of the 21st Century, a vibrant commercial sector has emerged that is engaged in space weather providing services and products for customers ranging from agencies and commercial aerospace to consumers. The American Commercial Space Weather Association (ACSWA), formed in 2010, is comprised of many of these companies and represents private-sector commercial interests nationally and internationally. Its formation was a milestone for maturity in commercial space weather.

The commercial sector pillar of the space weather enterprise continues to develop services and products in response to societal space weather needs. Their personnel include scientific and engineering researchers as well as users of services and products.

The activities of this commercial sector are primarily directed toward understanding, measuring, and managing the impacts of space weather upon technology. Figure 3.5 graphically shows a variety of the effects by space weather upon our technology. These include, for example: i) atmospheric drag on Low Earth Orbit (LEO) satellites caused by energy inputs into the thermosphere from solar UV, FUV, Lyman-alpha, EUV, XUV, and X-ray photons as well as by charged particle precipitation and Joule heating at high latitudes; ii) surface and internal charging from increased energetic particle fluxes, leading to effects such as discharges, single event upsets, and latch-up, on LEO to GEO satellites; iii) disrupted GPS signals caused by ionospheric scintillation leading to increased uncertainty in navigation systems such as aviations Wide Area Augmentation System (WAAS); iv) lost HF, UHF, and L-band radio communications due to ionosphere scintillation, solar flares, and geomagnetic storms; v) increased radiation to human tissue and avionics from GCRs and SEPs, especially during large solar flares, at all altitudes above 8 km (Tobiska et al., 2014); vi) increased inaccuracy in surveying and oil/gas exploration that uses the Earths main magnetic field when it is disturbed by geomagnetic

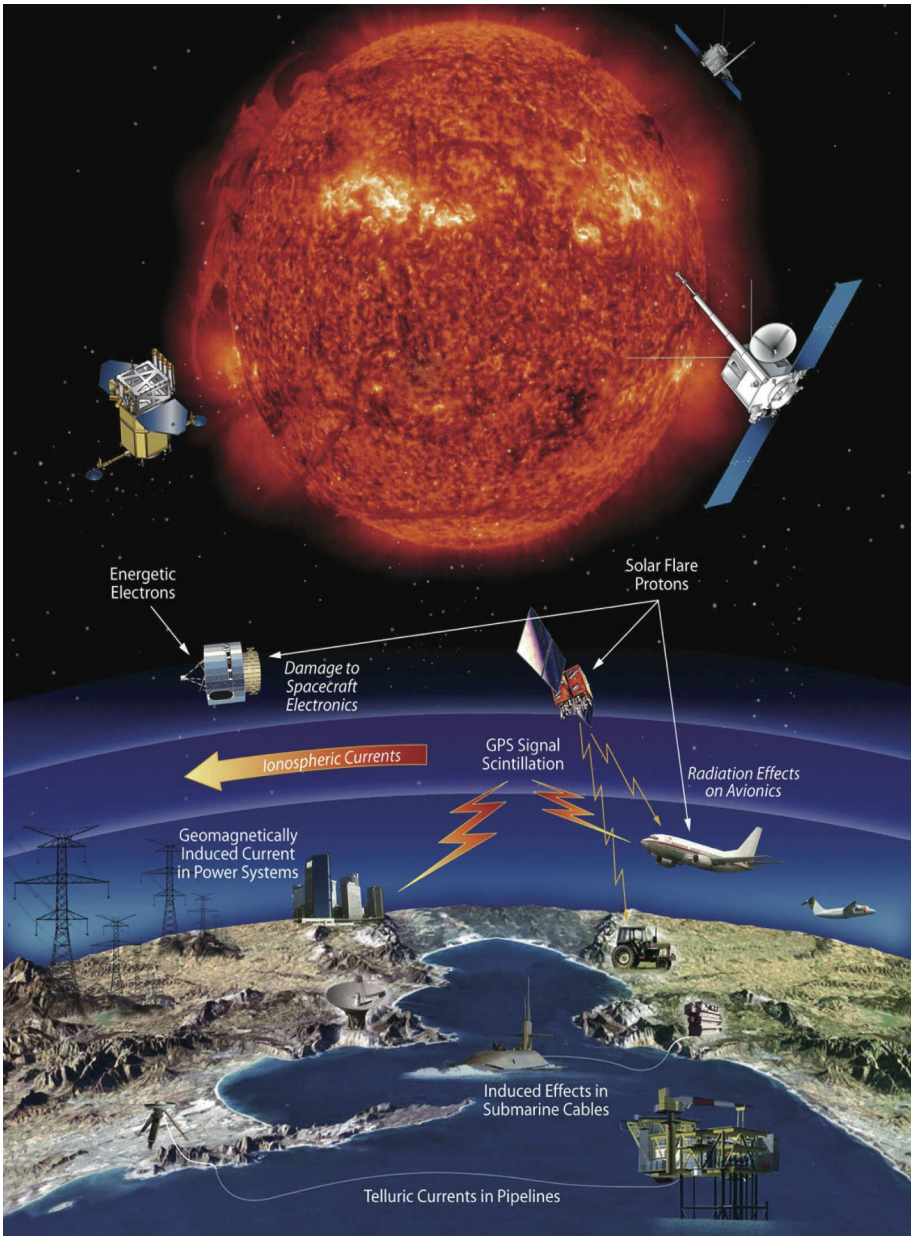

Fig. 3.5. Examples of effects of space weather on critical infrastructure (NASA, NP-2005-11-740-GSFC, NASA, Greenbelt, Md., February 2006).

storms; and vii) loss of power transmission from GIC surges in the electrical power grid and transformer shutdowns during large geomagnetic storms.

Many of these disturbances are summarized in Figures 3.6 and 3.7. Fig-

ure 3.6 outlines the NOAA SWPC customers (spacecraft, electric power, aviation, and surveying/navigation) that have impacts from space weather. Figure 3.7 shows space weather effects economic connections and interdependencies from key industrial sectors. The message from these figures is that there are a broad number of societal impacts from space weather that account for a significant part of the national Gross Domestic Product. These represent the domain of potential customers for commercial space weather services and products.

Example costs to industry from space weather events include loss of a GEO communications satellite from charging (over $500M), diversion of one commercial airline polar flight due to HF loss and radiation from solar events (over $100K/plane/diversion), power loss from transformer failure and regional electric grid outage (over $400M/unit with more than $3B from regional economic losses) (W. Murtagh, NOAA SWPC, Current Space Weather Services Infrastructure, presentation to the SWW, May 22, 2008).

A topic of particular interest has been the Geo-Magnetic Disturbance (GMD) and GIC risks to the power industry. Geomagnetically-induced currents (GICs) are damaging currents flowing through the transmission lines of the bulk power system. They are driven by electric fields that arise during large geomagnetic disturbances, which are caused by the interaction of a sharply-changing magnetic field with the underlying conductivity structure of the Earth. On average, 200 days of geomagnetic storms resulting in strong to severe conditions that could produce GICs on the surface of the Earth can be expected during a typical 11-year solar cycle (North American Energy Reliability Corporation, 2010).

One of the most impactful GIC events occurred in March 1989. This event caused wide-spread blackouts across the Canadian Hydro-Quebec power grid, resulting in the loss of electric power to more than 6 million people (Czeck, 1992; Kappenman, 2003). If a similar storm-induced blackout had occurred in the Northeastern United States, the economic impact could have exceeded $10 billion (National Research Council, 2008, 2009; Baker et al., 2009) not counting the negative impact on emergency services and the reduction in public safety associated with the loss of electric power in large cities. For more than a century, communication technologies have used long conductors and wireless methods for transmission of information. The large solar event of August 4, 1972 during the decline of Solar Cycle 20 led to a CME with a solar wind speed of approximately 2500 km s^{-1} and produced power outages in Canada and the U.S., including the disruption of a major transcontinental telecommunications cable in Illinois (Lanzerotti, 2014). On July 23, 2012, the Sun produced an event that has been described as disruptive as the 1972

Impact Area	Customer (examples)	Action (examples)	Cost (examples)
Spacecraft (Individual systems to complete spacecraft failure; communications and radiation effects)	• Lockheed Martin • Orbital • Boeing • Space Systems Loral • NASA, DoD	• Postpone launch • In orbit - Reboot systems • Turn off/safe instruments and/or spacecraft	• Loss of spacecraft ~$500M • Commercial loss exceeds $1B • Worst case storm - $100B
Electric Power (Equipment damage to electrical grid failure and blackout conditions)	• U.S. Nuclear Regulatory Commission • N. America Electric Reliability Corp. • Allegheny Power • New York Power Authority	• Adjust/reduce system load • Disconnect components • Postpone maintenance	• Estimated loss ~$400M from unexpected geomagnetic storms • $3-6B loss in GDP (blackout)
Airlines (Communications) (Loss of flight HF radio communications) (Radiation dose to crew and passengers)	• United Airlines • Lufthansa • Continental Airlines • Korean Airlines • NavCanada (Air Traffic Control)	• Divert polar flights • Change flight plans • Change altitude • Select alternate communications	• Cost ~ $100k per diverted flight • $10-50k for re-routes • Health risks
Surveying and Navigation (Use of magnetic field or GPS could be impacted)	• FAA-WAAS • Dept. of Transportation • BP Alaska and Schlumberger	• Postpone activities • Redo survey • Use backup systems	• From $50k to $1M daily for single company

Fig. 3.6. Examples of customers and impact areas for space weather data from W. Murtagh, NOAA SWPC, Current Space Weather Services Infrastructure, presentation to the SWW, May 22, 2008.

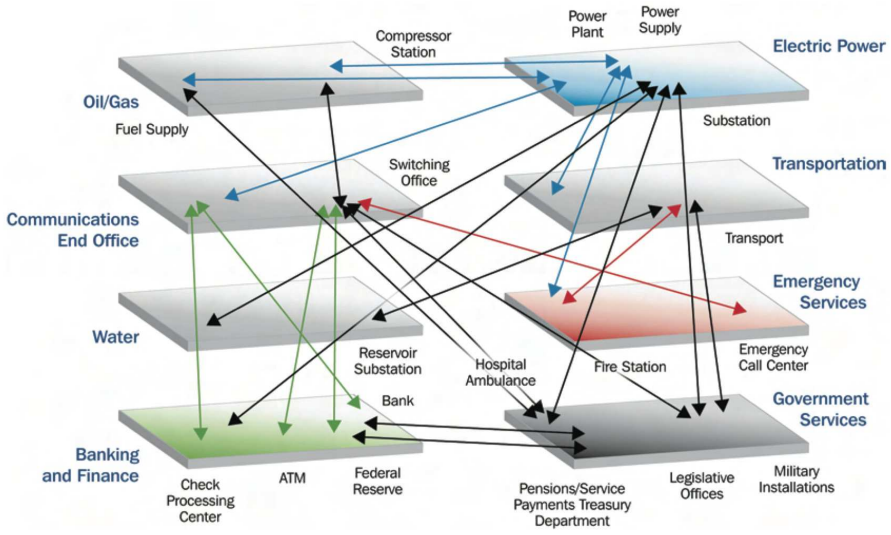

Fig. 3.7. The connections and interdependencies across the economy with their qualitative dependencies and interdependencies; courtesy of the Department of Homeland Security, National Infrastructure Protection Plan.

event and in the same league as the Carrington event of 1859. Baker et al. (2013) reported that this solar event had all of the characteristics of an extreme event that could have impacted electric power and communications systems had it occurred a week earlier. The event was not aimed at Earth but directed toward the STEREO A spacecraft 141 degrees west of the Earth-Sun

line. It is clear that space weather can significantly affect power transmission and transcontinental telecommunications technologies, especially in the period from solar cycle maximum through the decline to solar minimum.

3.2.2 Motivation for the growth of the commercial sector

It is the recognition that space weather can significantly affect technology in major industries, and that there can be economic loss from not only low-frequency, high-consequence events but also high-frequency, low-consequence events, that motivates the commercial sector to provide services and products for managing space weather risks as described below.

In the early period of the space weather industry, at the time of the NSWP Implementation Plan (2000) publication, the business model implemented by both Sterling Software (SS) (1998) and Space Environment Technologies (SET) (2000) was to sign a Cooperative Research and Development Agreement (CRADA) with NOAA SWPC as a leverage for future business. SS had a CRADA for the Magnetospheric Specification Model (MSM) and SET had one for the SOLAR2000 model. In both cases, the companies anticipated future sales of derivative products from their CRADAs to non-NOAA customers, using the CRADA as a way to leverage credibility with future customers and eliminate potential liability. This business model did not produce direct income for either company but did allow SET to develop a long-term relationship with the USAF Space Command for producing solar irradiance indices that improved thermospheric density specification and forecasting. SS abandoned its work in space weather after it was incorporated into Logicon/Northrop Grumman by 2001 while SET, starting originally as a unit within Logicon/Northrop Grumman, exited with its intellectual property to form a small company pursuing space weather business.

During most of the first decade of the 21st Century, all space weather companies used a business model of reliance on agency research and SBIR contracts to generate their primary revenue stream. Starting in mid-decade, several companies, including AER, ASTRA, EXPI, SEC, and SSI, were producing distinct products that could be sold on a per unit basis to agency and commercial customers. The SEET space environment module in AGIs Satellite Toolkit (AER), the CASES GPS unit (ASTRA), the HAF solar wind model (EXPI), the Expert System for Ionospheric Reduction – ESIR (SEC), and interferometers (SSI) were examples of such products. A partnership by SEC and SET starting in 2008 led to the first commercial, data-driven climatology ionosphere product (CAPS), which became the prototype for later GAIM derivative products of Utah State Universitys Space Weather Center. The USU SWC was unique in that Utah used federal ARRA funds to commercial-

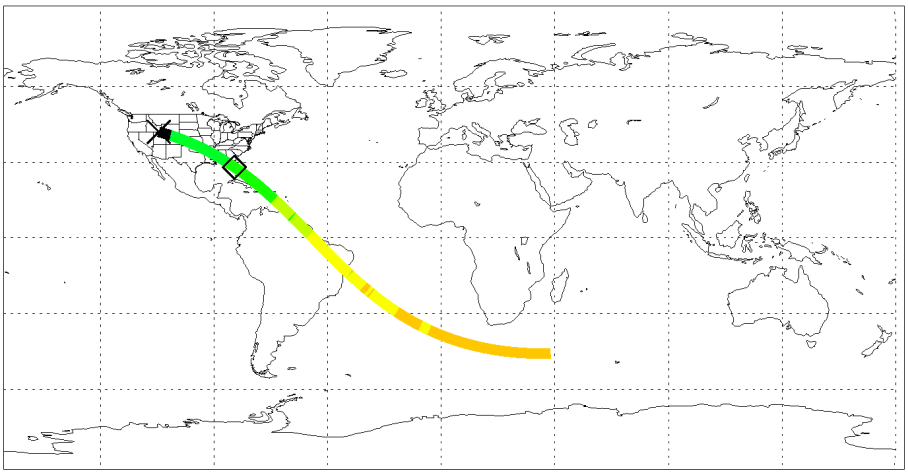

Fig. 3.8. HF signal strength for point-to-point propagation using ray-tracing through the GAIM and SECs ABBYNORMAL ionosphere. Courtesy of Q-up and Space Environment Corporation.

ize university intellectual property for the economic benefit of Utah through its USTAR program. SWC was formed in 2009 and developed GAIM derivative products of HF signal strength and GPS single frequency accuracies that are provided through its Q-upNow commercial spinoff (Figure 3.8). That partnership also produced the first smart phone app for providing real-time space weather (SpaceWx or SpaceWeather); it had a market test price of $1.99 per sale through Apple (Figure 3.4) (Tobiska et al., 2010) but was later distributed free in subsequent updates.

By the second decade of the 21st Century, the commercial space weather sector began to mature with the formation of ACSWA (2010), growing threefold to represent 18 small and medium-sized companies in 2014. ACSWA† is an association of companies that promotes space weather risk mitigation for the critical national infrastructure related to national daily life, economic strength, and national security. ACSWA, in conjunction with its member companies, helps identify important data and technology gaps that can be filled by private or government actions and develops value-added products and services for the benefit of human and property safety. By 2014, an important issue for the commercial space weather sector is the ability to sell space weather data products to the government based on private assets in space or on the

† http://www.acswa.us

ground. GeoOptics and PlanetIQ have led this work with the aim of selling ionospheric data to NOAA; SET sells its operational solar and geomagnetic indices to government and aerospace organizations.

3.2.3 Operational drivers for managing space weather risks

During the early 21st Century, the USAF has been the main engine behind the deployment of operational space weather through its procurement of space weather specification capabilities. This is because, more than any other U.S. Government agency, it has enabled the crossing of the TRL gap from 7 to 9, sometimes referred to as the valley-of-death for the lack of funding to move systems from demonstrated performance in operational environments to successfully deployed operational systems (ISO 16290). Here we make a distinction between those agencies, e.g., NASA and NSF, that have sponsored the development of scientific and engineering capabilities for space weather specification and forecasting with those that have enabled the deployment of operational systems, i.e., USAF.

Of the combination of near-Earth environments (Earth-orbiting and deep space) and technologies requiring space weather specification and forecasting for asset management, the atmospheric drag, pointing precision/attitude perturbation, end-of-lifetime, mission planning, vehicle safety/performance, radiation environment, re-entry and tracking, and telemetry and communication (command/control) issues have been important. The latter two issues (re-entry/tracking and command/control, C2) have driven the development of space situational awareness. Because tracking of space objects has been a U.S. national defense concern since October 1957 with the launch of Sputnik and because communication and navigation of space assets are key components of C2, the specification at the current epoch and the forecast for near-term out to 72-hours of the neutral atmosphere and the ionosphere have been the main focus of the USAF related to space weather in the last two decades.

Two major projects were implemented into USAF operations to address these operational space weather challenges; commercial space weather companies played key roles in developing that operational capability.

First, the HASDM project was organized in the mid-1990s as a direct result of the loss of at least 200 objects from the NORAD catalog in March 1991. That led to the goal of significantly improving LEO thermospheric density specification and forecasts to avoid a repeat of lost NORAD (now USAF Space Command) tracked objects during major space weather storms. HASDM was completed in 2002 using a dynamically calibrated atmosphere (DCA) as well as the E10.7 and ap indices; it became operational in 2004 at the Air Force Space Command (Bowman and Storz, 2003; Storz et al., 2005). Its second

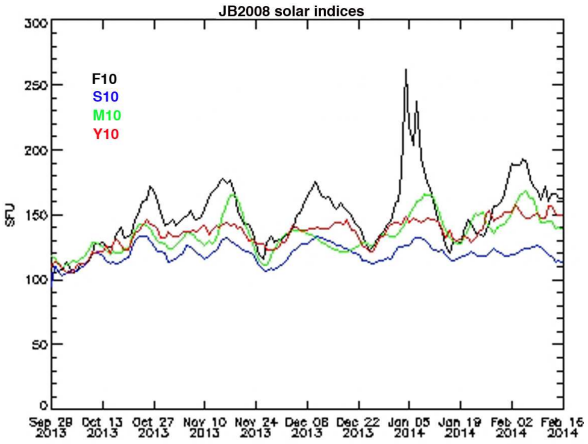

Fig. 3.9. JB2008 solar indices F10, S10, M10, and Y10 used for operations. Courtesy of Space Environment Technologies.

spiral of improvement included the development of the JB2008 model† (Bowman et al., 2008a; Tobiska et al., 2008) operationally driven by four solar indices (Figure 3.9) and two geomagnetic indices, the legacy ap and the newly incorporated Dst (Figure 3.10) (Tobiska et al., 2013); all have operational versions that were developed by SET and the real-time Dst is available on the web‡. HASDM with this upgrade became operational in 2013 at the AF Space Command. The JB2008 thermospheric density model became the most significant improvement in accurate LEO density specification since the 1960s Jacchia models and is now part of the ISO 14222 (ISO 14222, 2013) International Standard and the 2014 COSPAR International Reference Atmosphere (CIRA§).

Second, the Global Assimilation of Ionospheric Measurements (GAIM) project was organized in the late-1990s as a direct result of the need for an improved ionosphere. Physics-based data assimilation models of the ionosphere were developed at Utah State University and University of Southern California/Jet Propulsion Laboratory as part of a DoD Multidisciplinary University Research Initiative (MURI) program. The USU effort was called the Global Assimilation of Ionospheric Measurements (GAIM) Gauss-Markov Kalman Filter (GMKF) model (Schunk et al., 2004, 2005; Figure 3.11) and was selected for operational implementation at the USAF Weather Agency (AFWA), becoming operational there in 2006. It uses the Ionosphere Forecast Model (IFM) from SEC for the physics-based model of the ionosphere and it assimilates 10,000 global mea-

† http://sol.spacenvironment.net/~JB2008/
‡ http://sol.spacenvironment.net/~sam_ops/
§ http://spaceweather.usu.edu/htm/cira

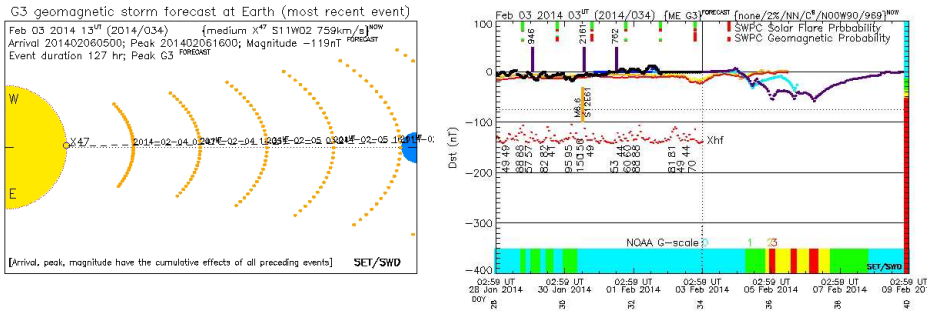

Fig. 3.10. (a) The left panel shows a CME from the Anemomilos Dst prediction by SET. (b) The right panel shows the operational Dst with both ENLIL/Rice (stream A, gold) and Anemomilos (stream B, purple and aqua) used in the operational JB2008 thermospheric density model. Sources: (a) and (b) courtesy of Space Environment Technologies.

surements every 15 minutes to correct the physics ionosphere with the GPS TEC data. GAIM-GM is described as part of the updated ISO 16457 (2014) international standard for the ionosphere. In 2014, the GAIM Full Physics (FP) model was delivered for operations to AFWA by the USU/SEC GAIM team and now represents the gold standard for ionosphere specification and forecasting. While the DoD operational version runs at AFWA, the commercial version runs at the USU Space Weather Center and serves data to the Q-upNow commercial services company for accurate real-time and forecast HF signal strengths between any global points.

While these example systems have been deployed operationally, there is still a need for substantial improvement in both current epoch specification and forecasting. Particularly important areas of improvement for Dst predictions from CMEs include the need to characterize Bz and velocity along the transit from Sun to Earth as well as improved coupling of the solar ejected plasma with the magnetosphere. The communities continue to develop the metrics of current state-of-art operational systems.

3.2.4 Managing risks to operational space weather systems

The overarching architecture for managing risk in operational systems is that from the NIPP (National Infrastructure Protection Plan†). The NIPP defines risk as a function of threat identification, vulnerability (probability or likelihood), and consequence (impact). The approach to managing space weather risks includes five elements (National Academies Press, 2008):

† http://www.dhs.gov/national-infrastructure-protection-plan

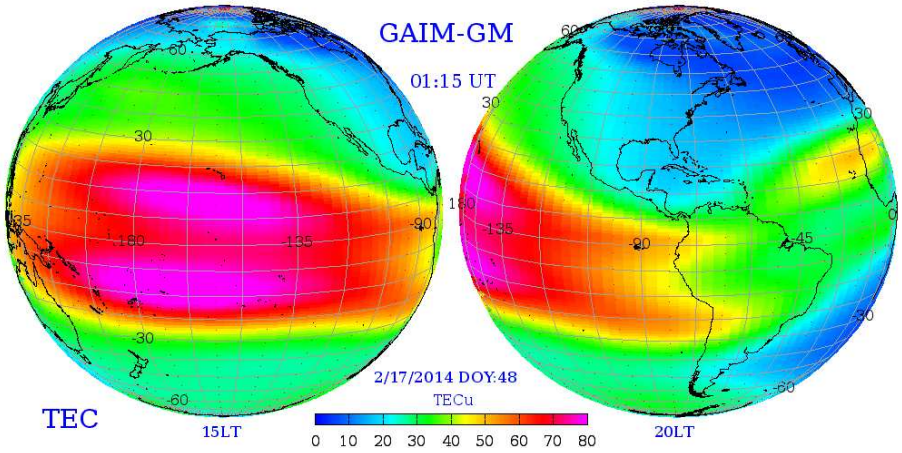

Fig. 3.11. The GAIM-GM model running in commercial operations at the USU SWC. Courtesy of Utah State University Space Weather Center.

- Detection: identify potential threats and validate and/or communicate the information, as appropriate;
- Defense: protect assets by preventing or delaying the threat or reducing its effect on an asset, system, or network;
- Mitigation: lessen the potential impacts of a threat by introducing system redundancy and resiliency, reducing asset dependency, or isolating downstream assets;
- Response: enable rapid reaction and emergency response to threat incidents, such as conducting exercises and having adequate crisis response plans, training, and equipment; and
- Recovery: allow businesses and government organizations to resume operations quickly and efficiently, such as by using comprehensive mission and business continuity plans that have been developed through prior planning.

Using this approach, a first example of a risk management applied to space weather operational systems is the SET Corporate Mission Assurance Standard (MAS) Risk Management Process Plan† (see the Standards Link: Space Weather Operational Standards). The document is derived from the AIAA S-102 Mission Assurance Standard that also has its heritage in MIL-STD-882C. This Corporate Standard defines an approach for implementing a Risk Management Process, describing the roles and responsibilities of the Project Manager (PM), project personnel, major subcontractors, and the customer. Each identified risk is documented, assessed, tracked, and updated in a project Risk Database that complies with the risk metrics defined in this Standard.

† http://www.spacewx.com/

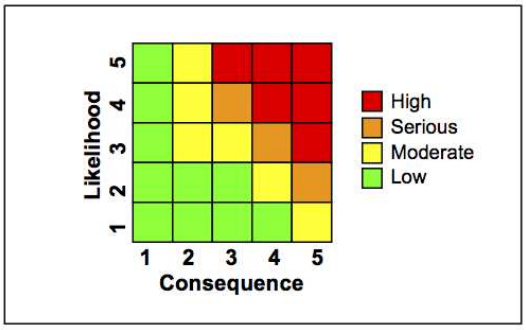

Fig. 3.12. Matrix where risk is determined by multiplying probability impact (MAS). Source: Space Environment Technologies Corporate Mission Assurance Standard (MAS) Risk Management Process Plan.

All five elements of the approach described in the NIPP are covered in the SET MAS document and the operational space weather community uses it as a foundation. Using the type of matrix in Figure 3.12 for risk management, the space weather operational community is able to assess a risk level for a given threat and develop a system plan for managing it. Important concepts in risk management for this process include:

- *Risk identification* is the identification of uncertainty for successfully completing a task.
- *Risk probability* is the likelihood of occurrence of a risk; values are: 1 = improbable, 2 = remote, 3 = occasional, 4 = probable, 5 = frequent).
- *Risk impact* is an events consequences if it occurs (values are: 1 = inconvenience, 2 = minor impairment, 3 = major impairment, 4 = severe impairment, 5 = failure to perform). By multiplying probability (likelihood or vulnerability) impact (consequence) it is possible to obtain a value in the range of 1-25 (Figure 3.12).
- *Risk level* is the overall evaluation of a risk from the risk matrix. This risk matrix provides an assessment for four risk levels: low = negligible impact on success (green); moderate = marginal impact on success (yellow); serious = critical impact on success (orange); and high = catastrophic impact on success (red). High-risk items (unacceptable technical, schedule, or cost risk) are risk management drivers and require detailed management tasks. Serious-risk items (adverse effect on interfaces of designated system) are risk management drivers and require detailed management tasks. Moderate-risk items (minor impairment of margin, design life, or secondary missions) require preliminary assessments and documentation. Low-risk items (inconveniences or inefficiencies in systems) require documentation and tracking.

- *Risk mitigation* is the path for reducing risk; it is usually important to add explanations of the rationale for assessment of the probability and management of a risk. This includes the sources of risk, such as immature technology, new processes, new designs, high levels of design complexity, tight tolerance requirements, new operational requirements or customer needs, new mission assurance requirements (safety, reliability, maintainability, dependability, availability, or quality assurance), changing requirements, engineering change orders, cost and schedule estimating assumptions, resource availability (people, materials, facilities, tools), under-qualified personnel (design, engineering, production), and limited mission assurance capability.
- *Risk metrics* are evaluative methods by which one can determine if a risk has been reduced or not.

A new tool for managing risks in the distributed network of service providers is being developed. Quality, consistent, and validated operational products between operational space weather services are needed so companies and organizations have begun to develop common best practices. This activity has been led by the SpWxCOW workshops.

3.3 Emergent companies in commercial space weather

3.3.1 Lower-tier companies as the innovators

The term tier is used to describe the relationship of a commercial sector company to the defense technology industrial base, as described by the U.S. Congress Office of Technology Assessment. Here we use the term for categorizing companies that provide an operational space weather capability to the DoD, NASA, NOAA, or FAA. The first (or top) tier companies are the large primes that assemble, integrate, and often operate the national space weather capacity. Mid-tier companies usually provide components directly to the top tier group, while lower-tier companies provide components and services to other lower-tier, mid-tier, or top-tier companies. For our purposes, we note that lower-tier companies are often small businesses in the space weather commercial sector. Many of them are found in ACSWA as of 2014 and they play the role as innovators of new products and services in the national space weather enterprise commercial sector (Lanzerotti, 2012). Examples of these innovators include:

- Space Environment Corporation providing IFM to USU which, in turn, incorporated IFM into GAIM-GM for use by AFWA as integrated by the top-tier Northrop Grumman prime contractor for the SWAFS project;
- Space Environment Technologies providing JB2008 solar and geomagnetic

indices for use by Space Command as integrated by the top-tier Lockheed Martin prime contractor for the ISC2 project; and
- Atmospheric and Environmental Research (acting as a lower-tier here) providing the SEET (Space Environment and Effects Tool) module to Analytic Graphics, Inc. for the Satellite Toolkit which is integrated into mission design and planning by mid- and top-tier companies.

3.3.2 Mid-tier companies as the expanders

Mid-tier companies are often those that play the role as expanders of implemented solutions in the national space weather enterprise commercial sector. Examples of those mid-tier expanders include:

- Analytic Graphics, Inc. providing the Satellite Toolkit which is integrated into mission design and planning by mid- and top-tier companies as well as government agencies; and
- Atmospheric and Environmental Research (acting as a mid-tier here) providing algorithm implementation of the GOES-R space weather sensors to top-tier Harris Corporation, which is the integrator of the GOES-R satellite system for NOAA.

3.3.3 Top-tier companies as the integrators

Top-tier companies are often those that play the role as integrators of multi-component systems in the national space weather enterprise commercial sector. Examples of those top-tier expanders include:

- Northrop Grumman providing integration services for the AFWA SWAFS project;
- Lockheed Martin providing integration services for the Space Command ISC2 project; and
- Harris Corporation providing integration services for the NOAA GOES-R satellites.

3.4 Standards solidify the space weather enterprise foundation

3.4.1 International standards

Progress is occurring toward the development of operational space weather prediction and monitoring systems. However, a situation will soon be reached in the next few years where specification and prediction will become ubiquitous and where coordinated management of the space environment becomes a necessity. Coordination will continue to develop within the context of new air

and space traffic management systems, which will manage continued government launches, commercial space tourism, and the growing satellite debris environment. Agencies such as the U.S. Department of Defense (DOD), NASA, NOAA, and the U.S Federal Aviation Administration (FAA) provide programmatic directions, but international organizations such as the Inter-Agency Space Debris Coordination Committee (IADC), the International Standards Organization (ISO), the World Meteorological Organization (WMO), and the International Civil Aviation Organization (ICAO) also lend their guidelines and standards expertise. The risk of not using foundational guidelines and standards to integrate operational monitoring and prediction of space weather within larger technical systems will lead to added costs, damage of assets, and lost opportunities to use space for improving human conditions on 21st-century Earth (Tobiska, 2008).

Nations and regional organizations outside the United States are developing their own systems that utilize space weather operations. For example, the European effort is growing substantially†. With growing international activity, international standards for the space environment are required and are vital for successful space weather management. Such standards serve as a reference framework, or a common technological language, between suppliers and their customers, which facilitates trade and the transfer of technology.

As described by Tobiska (2008) compliance with an international standard means compliance with a set of requirements that facilitates the exchange of data or products among diverse communities. The work of preparing international standards is normally carried out through ISO‡ technical committees and their working groups that are convened under the direction of member bodies. The main task of technical committees is the preparation of draft international standards. In the course of developing a standard, there may not be consensus to proceed to publication. Alternative documentation routes exist for providing technically accepted guidelines that are not international standards but that are useful for user communities. These types of documents include technical specifications (TS) or technical reports (TR), both of which require a consensus vote by member countries even though they are used as best practices rather than standards.

ISO Technical Committee 20 (TC20) organizes all standardization issues related to aircraft and space vehicles. There are six active subcommittees (SC) in TC20. Two subcommittees work with space issues and are considered sectoral committees. They have large areas of responsibility distributed among several working groups (WGs). Of the two space subcommittees, Space Data and Information Transfer Systems (SC13) and Space Systems and Operations

† http://www.spaceweather.eu/
‡ http://www.iso.org/iso/home.htm

(SC14), the latter organizes the standardization of the space environment (natural and artificial) under its Working Group 4 (WG4).

Since 1993 ISO TC20/SC14 WG4† has been active in developing consensus on international space environment standards. Thirteen space environment International Standards, Technical Specifications, and Technical Reports have now been published, including:

a) IS 15390:2004 Galactic cosmic ray model;
b) IS 21348:2007 Process for determining solar irradiances;
c) IS 22009:2009 Model of the Earth's magnetospheric magnetic field;
d) IS 15856:2010 Simulation guidelines for radiation exposure of non-metallic materials;
e) TR 11225:2011 Guide to reference and standard atmosphere models;
f) IS 16698:2012 Methods for estimation of future geomagnetic activity;
g) TS 12208:2013 Observed proton fluences over long duration at GEO and guideline for selection of confidence level in statistical model of solar proton fluences;
h) IS 14200:2013 Guide to process-based implementation of meteoroid and debris environmental models (orbital altitudes below GEO+2000 km);
i) IS 14222:2013 Earth upper atmosphere;
j) IS 10788:2014 Lunar simulants;
k) IS 16695:2014 Geomagnetic reference models;
l) IS 16457:2014 The Earths ionosphere model: international reference ionosphere (IRI) model and extensions to the plasmasphere; and
m) TR 18147:2014 The method of the solar energetic protons fluences and peak fluxes determination.

There are four standards in development during 2014 including (document titles are italicized): CD 17761 *Model of high-energy radiation at low altitudes (300-600 km)*; CD 16709 *Realtime solar activity and space environment information for spacecraft operation*; CD 17851 *Space environment simulation at material tests. General principles and criteria*; and CD 17520 *Cosmic ray and solar energetic particle penetration inside the magnetosphere: Method of effective vertical cut-off determination*. In addition, WG4 is drafting documents related to the following areas: *Procedure for obtaining worst case and confidence level of fluence using the quasi-dynamic model of the Earths radiation belts*, *Spacecraft charging potential estimation in the worst case environments*, Spacecraft Charging Standard-Earth orbit, Nanomaterials in space, A process based standard for the solar energetic proton environment, satellite drag,

† http://www.iso.org/iso/home.htm

radiation belts, atomic oxygen, solar wind, solar cell degradation due to energetic particles, Lunar radiation environment, Mars radiation environment, electrostatics and lunar dust, worst case solar events, protection of materials from MMOD impact, solar wind data in the OMNI database, space weather information for use in space systems operations, a guide to Ionosphere and Plasmasphere Reference Models, and a guide to Solar Reference Spectra and Irradiance Models.

Existing and future standards enable safety, efficiency, and commercialization of space activity within the context of managing the adverse effects of space weather. The international space physics community has actively participated in discussions to develop these standards and has provided concept reviews through the Committee on Space Research (COSPAR) scientific congress session C0.1 starting in 2002.

3.4.2 National standards

American, Russian, European, Japanese, and Chinese national standards bodies are among those countries that have been very active in developing space environment standards. In the U.S., the American National Standards Institute (ANSI) facilitates voluntary consensus standards as well as actively audits and accredits U.S. organizations that create standards. The American Institute of Aeronautics and Astronautics (AIAA) is an ANSI-accredited standards-making organization in the U.S. that is actively developing guidelines and standards related to the space environment. Seven AIAA space environment guidelines and standards being developed through the Atmospheric and Space Environments Technical Committee (ASETC) Committee on Standards (CoS) include:

a) G-083-1999 Guide to Modeling Earths Trapped Radiation;
b) SP-078-2007 Space and Planetary Environments;
c) G-003C-2010 Guide to Reference and Standard Atmosphere Models;
d) S-115-2013 Low Earth Orbit Spacecraft Charging Design Standard Requirement and Associated Handbook; and
e) G-034A-2014 Guide to Reference and Standard Ionosphere Models.

In addition, the AIAA ASETC CoS is developing projects during 2014 in the following areas: *Guide to Spacecraft Charging and Mitigation Methods of Spacecraft Charging, Guide to Solar Irradiance Models, and Guide to Atmospheric Turbulence Models for Aeronautical and Aerospace Application.*

3.4.3 Corporate standards

As referenced above, the SpWxCOW workshops have begun the effort to develop best practices, guidelines, and standards for commercial space weather operations. A key heritage document used by this community is the AIAA S-102 *Mission Assurance Standard*; it was derived from MIL-STD-882C. The Space Environment Technologies Infrastructure and Standards Division (ISD) used these documents to develop its *Corporate Mission Assurance Standard (MAS) Risk Management Process Plan*† (Standards Link: Space Weather Operational Standards). This Corporate Standard is a living document and is the first to define an approach for implementing a risk management process for commercial space weather operations.

3.5 Challenges for the space weather enterprise

3.5.1 Present-day challenges

As identified above, key industrial sectors all feel impacts from space weather to their technologies. However, it is still the case in the second decade of the 21st Century that some of these sectors do not consider space weather risks in their risk management plans. For those that have identified their risks from space weather, it represents a first step in a successful, broad, two decades-long customer education campaign by the space weather community.

At the beginning of the 21st Century the primary challenges were to understand the physics of the space weather phenomena, to identify the risks from space weather, and how to build applications for managing that risk. With the success of the National Space Weather Program (National Academies Press, 2012b) and the emergence of the commercial sector ACSWA organization, these original challenges have seen progress toward resolution while new challenges have begun to evolve.

3.5.2 Near-term challenges

During the second and third decades of this century, challenges for the space weather enterprise start with the element of institutional provincialism. The not-invented-here syndrome stems from both a legacy of competition for limited funding, which will persist for the foreseeable future, and a legitimate desire in each organization to maximize its own benefit for developing the capacity of the space weather domain. This syndrome occurs across all elements of the space weather enterprise including agencies, academia, and industry.

† http://www.spacewx.com/

Examples of enterprise collaborations do occur, for example with the hosting of models or the CME Scorecard comparisons by the NASA Community Coordinated Modeling Center (CCMC) and their respect for the intellectual property of the code developers. Separately, the commercial sector both competes and collaborates on proposals that are linked to improving the space weather enterprise.

However, major challenges still loom in the form of natural hazard and disaster recovery, for example, which can be worsened by untimely and severe space weather. Outside of space weather impacts, the U.S. sustains $50B in destroyed property annually while globally (2010) there were $124B property losses with 297,000 lives lost and 217 million people affected. We now know that hazards to our technology and our society clearly exist from space weather for communication outages and navigation position uncertainties; we saw this during the Gulf Coast Hurricane Katrina recovery from August 29 into early September 2005. If unmanaged, space weather hazards create additional stress during emergencies, compounding disasters. How to integrate this risk management into our technology infrastructure is a challenge we still face. In an era of climate change we may see an increased coupling of global natural disasters with severe space weather.

There have been numerous forums, including the Decadal Survey (National Academies Press, 2012b), that address the strengthening of the U.S. space weather enterprise. We know that government policies, funding, and requirements can degrade or strengthen global competitiveness of the U.S. space enterprise and its ability to sustain the nation's security. When a go-it-alone approach occurs, it tends to degrade security and is usually a by-product of persistent funding limitations; it can restrict our ability to compete globally. On the other hand, security improvement can occur with: i) data and model innovation; ii) using all assets of the national space weather enterprise, e.g., operational, research, and commercial satellites; iii) government purchases of commercial data and services that spur rapid advances and competitive innovation; and iv) long-term funding of the academic research base.

3.5.3 Societal impact challenges

We face major societal challenges in this century, particularly from shortages of energy and fresh water. Solving those issues will be fundamental to ensuring the progress and security of our global society. A real challenge for the space weather enterprise is to make itself relevant to solving these fundamental challenges facing humanity this century. Historians some 300 years into the future will judge our efforts based on how successful we made the relevance of space weather to solving fundamental social problems. Making space-related

assets useful for improving life on Earth, and understanding how to manage risks from space weather to those technology assets, is the start for making our enterprise relevant to society. Commercial space weather organizations are at the forefront for innovation, expansion, and integration of solutions as our enterprise responds to societal needs of managing the risks from space weather.

4

The impact of space weather on the electric power grid

David Boteler

4.1 Introduction

Severe space weather storms have been the cause of power system problems for over seventy years. The first reported impact is from the magnetic storm that occurred in March 1940 which caused power swings and transformers to be tripped out on power utilities in the northern eastern US and Canada (Davidson, 1940). Increased awareness of geomagnetic effects on power systems was stimulated by the work of Albertson and co-workers (Slothower and Albertson, 1967; Albertson et al, 1973, 1974; Albertson and Thorson, 1974). Subsequent studies examined the effect of geomagnetically induced currents (GIC) on transformers (Bolduc and Aubin, 1978) and on system operation (Albertson et al., 1981). In Europe, Lehtinen and Pirjola (1985) developed a method for modelling GIC that was applied to the power system in Finland (Pirjola and Viljanen, 1989).

The extent to which space weather can affect power grids was illustrated by the great magnetic storm that occurred on 13 March 1989 (Allen et al., 1989). This caused a 9h blackout of the 21,000 MW Hydro-Qu/'ebec, electric power system (Blais and Metsa, 1993; Bolduc, 2002). Many other power utilities in North America and Europe experienced problems ranging from minor voltage fluctuations to tripping out of lines and capacitors and transformer overheating (Gattens, 1989; Cucchi and Ponder, 1991). This event prompted a surge of work on GIC effects and their economic impact (Barnes and Van Dyke, 1990; Elovaara et al., 1992; Viljanen and Pirjola, 1994; Boteler, 1994). Reviews of geomagnetic effects on power systems are provided by, e.g., Boteler et al. (1998), Molinski (2002), and Kappenman (1996, 2001).

Later space weather storms caused further problems including a blackout in

Malmö in southern Sweden during the Halloween storm of 2003 (Pulkinnen et al., 2005). Transformer overheating seen in South Africa was also attributed to geomagnetically induced currents (Gaunt and Coetzee, 2007). Studies in many parts of the world (Trichtchenko et al., 2007; Trivedi et al., 2007; Liu et al., 2009; Wik et al., 2009; Watari et al., 2009; Marshall et al., 2012, 2013; Torta et al., 2012) including problems in New Zealand in 2006 (Beland and Small, 2004) showed the GIC that could occur in power grids at any latitude. Also events such as the August 2003 blackout in northeastern USA and Canada, while not due to space weather, showed the cascading effects of power system problems and the economic impact of a power outage (Kappenman, 2003a).

Although major space weather effects on power systems are infrequent, modern societies' dependence on electricity means that any power interruption will have widespread impact (Baker et al., 2008). There is also concern that damage to a significant number of transformers during a space weather storm could take many years to replace and restore the integrity of the power system (Kappenman, 2010). Thus there has been renewed effort to understand the space weather impact on power systems and to examine the feasibility of various mitigation strategies (GMDTF, 2012). This chapter provides a description of what happens during a space weather storm to cause power system problems. An examination is then made of the key parameters influencing each stage of the process. Finally it is shown how these factors combine to determine the risk of problems to power systems and influence the forecasting of space weather for the power industry.

4.2 Cause of power system problems

The different stages of how space weather storms affect power systems are shown in Figure 4.1. Magnetic field variations produced during space weather storms induce electric fields in the Earth and in long conductors, such as power lines, at the Earth's surface. These electric fields drive electric currents along the power transmission lines and through power transformers to ground. These geomagnetically induced currents (GIC) shift the operating point of the transformers causing half-cycle saturation resulting in transformer heating, generation of harmonics and increased reactive power consumption (all discussed in this chapter). These respectively can lead to transformer overheating, to misoperation of protective relays, and to system stability problems.

To understand why some space weather storms cause more problems than others or why some power systems are more affected than others it is necessary to examine the response functions at each stage of the process and determine how that influences the total response. Obviously the magnitude of the initial disturbance is important, but the frequency content of the magnetic distur-

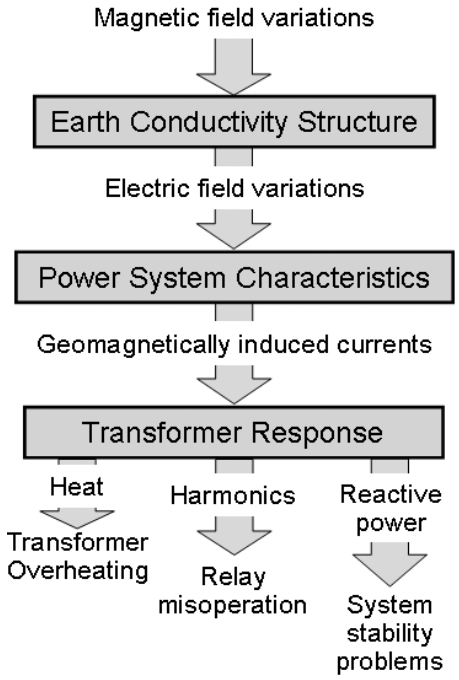

Fig. 4.1. Overview of space weather impacts on power systems

bance is also significant. It will also be shown that the frequency response of the Earth is important and a frequency domain approach is useful for analyzing how the responses of the component parts of the process combine to determine the final outcome.

4.3 Magnetic disturbances

This section presents the characteristics of geomagnetic disturbances that are significant for assessing the risk to power systems. The physics of the processes leading to the various types of geomagnetic field variations have been well covered elsewhere including the Heliophysics series (see, e.g., Vol. I, Ch. 10 and Vol. II, Ch. 10). Any magnetic field variation will lead to the occurrence of GIC in power systems; the important question is whether these variations will cause GIC that are large enough to impact power system operation.

4.3.1 Magnetic storm (main phase)

The temporal variation of a magnetic storm is shown in Figure 4.2. The Storm Sudden Commencement (SSC) at the start of the storm will be examined in

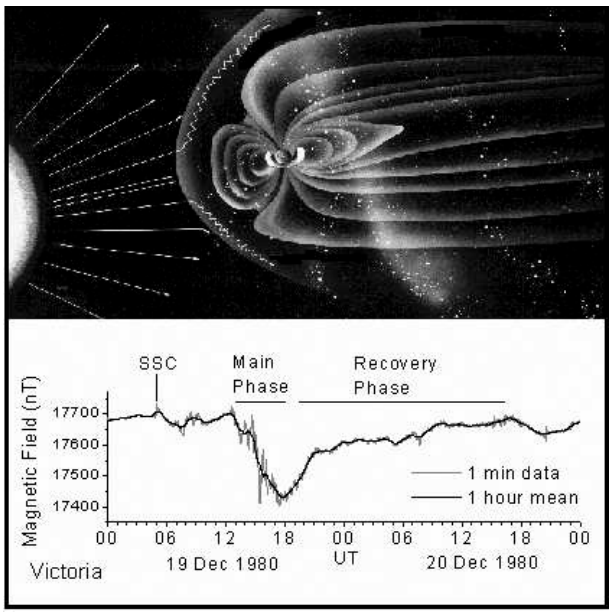

Fig. 4.2. Phases of a magnetic storm

section 4.3.4. Here, we focus on the later stages of the storm. These are characterized by the main phase where there is an increasing depression of the magnetic field strength for 6 h to 12 h followed by a recovery phase lasting a day or two. The storm main phase is seen worldwide, although more clearly at low and mid latitudes away from substorm activity in the auroral zone.

The main phase depression is generally attributed to the magnetic field produced by a ring current in the outer radiation belt (Tsurutani, 2001). A measure of the globally-symmetric part of the main phase disturbance is obtained from four low-latitude magnetic observatories whose records are combined to form the Dst ("disturbance storm time") index. A magnetic storm is defined as a storm with a maximum excursion giving a Dst exceeding -50 nT and a major magnetic storm is classed as one with Dst exceeding -100 nT. Significant storms can have even larger Dst excursions: for example the March $13-14$, 1989 magnetic storm had a Dst of -574 nT. The Carrington storm of September 1859 is estimated to have had a Dst of -1600 nT (Tsurutani, 2001).

4.3.2 Magnetic substorms

Magnetic substorms consist of shorter period bays in the magnetic field recordings lasting 15 minutes to a few hours (Figure 4.3). The substorms are pro-

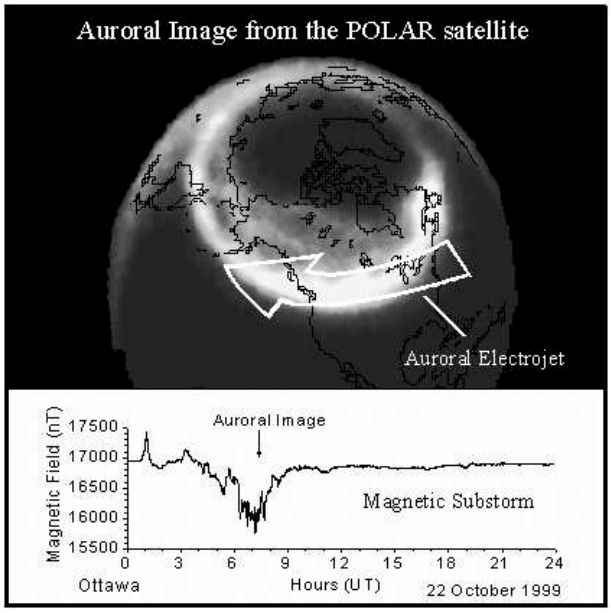

Fig. 4.3. Example of a magnetic substorm

duced by currents in the auroral ionosphere at a height of about 100 km and with intensities of approximately 10^6 Amperes. Analysis of current systems in the auroral zone often distinguishes between convection electrojets: eastward in the evening sector and westward in the morning sector and the "substorm" electrojet in the midnight sector. Earlier authors claimed that the convection electrojets only produced slowly varying disturbances that were not a problem for power systems and that only substorm electrojets varied fast enough to cause problems; however some power system problems can be attributed to rapid variations of the convection electrojets (Boteler, 2001).

Auroral electrojets are typically located at approximately 65° magnetic latitude. However, during large magnetic storms the electrojets move to lower latitudes where they can represent more of a threat to mid-latitude power grids. The complete substorm current system also involves field-aligned currents and these contribute a significant part of the magnetic disturbance seen at mid latitudes (Turnbull et al, 2009). Viljanen et al. (1999) have also examined how the detailed characteristics of the ionospheric currents influence the GIC produced in a power grid.

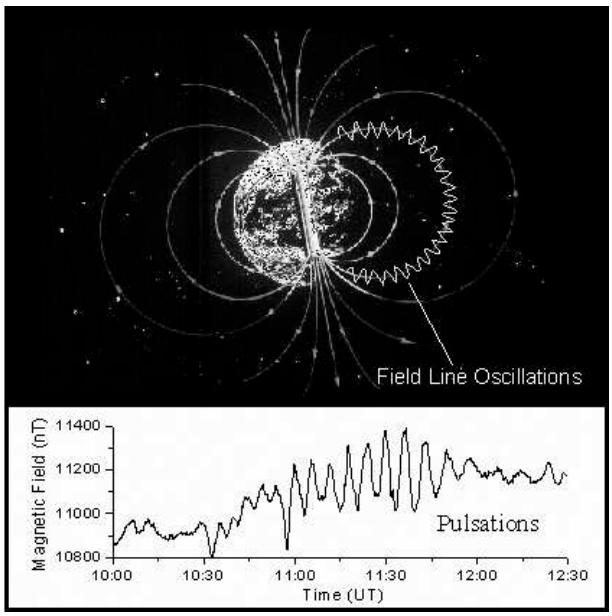

Fig. 4.4. Schematic picture of field line oscillations in the Earth's magnetic field that are the most common cause of magnetic pulsations on the ground.

4.3.3 Magnetic pulsations

Magnetic pulsations, also referred to as ultra low frequency (ULF) waves are oscillations in the frequency band from 1 mHz to 1 Hz (periods 1000 s to 1 s). These are classified as pulsation continuous (Pc) or pulsation irregular (Pi), with each class subdivided into particular frequency bands. Magnetic pulsations exist in the magnetosphere and have a wide variety of causes including Kelvin-Helmholtz instabilities on the magnetopause and field-line resonance (FLR) (McPherron, 2005). FLR, illustrated in Figure 4.4, is the most common cause of magnetic pulsations observed on the ground. MHD waves incident on the ionosphere drive electric currents that produce the electromagnetic wave seen on the ground as magnetic pulsations. Of particular interest for power systems are the Ps6 pulsations associated with substorms (Connors et al., 2003). These arise from modulation of the auroral electrojet by particle precipitation changing the ionospheric conductivity (McPherron, 2005).

4.3.4 Storm sudden commencement (SSC)

The storm sudden commencement and sudden impulse are a short-lived (few minutes) pulse in the magnetic field caused by the impact of an interplanetary shock on the magnetosphere: the two names referring to whether the

magnetic pulse is followed by a magnetic storm main phase or not. The interplanetary shock causes compression of the magnetosphere and enhancement of the magnetopause currents. These produce a magnetic signature with similar amplitude across all latitudes, suggesting that SSC could be a risk to power systems at low and mid latitudes (Kappenman, 2003b). In the August 1972 space weather storm, power system and phone system problems coincided with a shock arrival that caused compression of the magnetopause inside geostationary orbit (Anderson et al., 1974). This initially suggested that magnetopause currents were responsible. However, subsequent analysis showed that the magnetic disturbance observed on the ground was too localized to be caused by currents on the magnetopause and was instead consistent with currents at the height of the ionosphere (Boteler and Jansen van Beek, 1999).

Further linkages between GIC and the characteristics of particular space weather storms are contained in Lam et al. (2000), Boteler (2001), Kappenman (2005) and Trichtchenko et al. (2007).

4.4 Electromagnetic induction in the Earth

To understand the GIC that will be produced by the various types of magnetic field variations described above it is necessary to determine the electric fields produced by these variations. The primary sources of the magnetic field variations are electric currents in the ionosphere and magnetosphere, but the magnetic field variations also induce currents in the Earth and these currents themselves create magnetic fields that contribute to the total magnetic field observed at the Earth's surface. The induced currents in the Earth act to cancel the inducing magnetic field producing a fall-off of the magnetic field variation with increasing depth. This fall-off is characterized by the "skin depth" which, for a uniform conductivity σ is given by

$$\delta = \sqrt{\frac{2}{\omega \mu \sigma}} \tag{4.1}$$

where ω is the angular frequency and μ is the magnetic permeability. Equation (4.1) shows that lower frequencies and lower conductivities will result in larger skin depth values. For the frequencies of concern for GIC (0.0001 Hz to 1 Hz) the skin depths range from kms to hundreds of kms (Figure 4.5) and the Earth conductivities down to these depths affect the electric fields produced at the Earth's surface.

At the surface of the Earth there are considerable differences in the conductivities of different regions. Igneous rocks, such as the Canadian Shield, at the core of continental blocks have low conductivities while sedimentary rocks have a higher conductivity. Deeper in the Earth the crust has a generally low

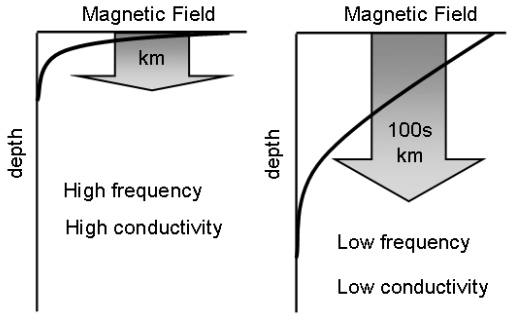

Fig. 4.5. Penetration of magnetic fields into the Earth

conductivity, while below that in the mantle the increasing pressure and temperature lead to higher conductivities (Lanzerotti and Gregori, 1986). How the conductivity values for each of these layers influence the electric fields at the Earth's surface and the influence of surface lateral conductivity changes are considered in the next two sections. The electric fields produced in any particular situation are also influenced by the spatial scales of the magnetic disturbance, but to more clearly demonstrate the Earth conductivity influence the following calculations assume a spatially uniform source field, sometimes referred to as the "plane wave" approximation.

4.4.1 Effect of conductivity variation with depth

The surface impedance relating the electric field and magnetic field at the Earth's surface can be calculated for a 1-D Earth conductivity model by using the recursive relation (Weaver, 1994; Trichtchenko and Boteler, 2002)

$$Z_n = i\omega\mu_0 \left(\frac{1 - r_n e^{-2k_n \ell_n}}{k_n (1 + r_n e^{-2k_n \ell_n})} \right) \tag{4.2}$$

where μ_0 is the permeability of free space, ℓ_n and $k_n = \sqrt{i\omega\mu_0\sigma}$ and r_n are the thickness, propagation constant, and reflection coefficient of layer n, respectively, with

$$r_n = \frac{1 - k_n \frac{Z_{n+1}}{i\omega\mu_0}}{1 + k_n \frac{Z_{n+1}}{i\omega\mu_0}}. \tag{4.3}$$

For the bottom half-space layer N, $r_N = 0$ (no reflections) and

$$Z_N = \frac{i\omega\mu_0}{k_N}. \tag{4.4}$$

Layered earth models have been produced for a number of regions (Ferguson

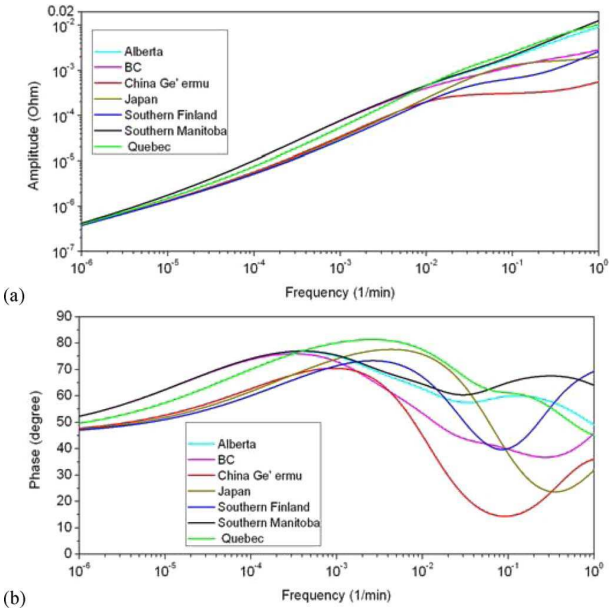

Fig. 4.6. Surface impedance as a function of frequency for the seven representative earth conductivity models: (top) amplitude, (bottom) phase (from Zheng et al., 2013).

and Odwar, 1997; Adam et al., 2012). The effect of different Earth models and how they would affect GIC in a power system has been examined by Zheng et al. (2013). Figure 4.6 shows the surface impedances they calculated for a range of Earth models. The general trend is for the surface impedance E/H to increase with increasing frequency and decreasing conductivity. The Earth model for southern Manitoba featuring a high resistivity crust produced the highest transfer function values while the model for China with a low resistivity crust produced the lowest transfer function values. For the event considered by Zheng et al. (2013) these surface impedance differences give electric field amplitudes that are 4-10 times higher with the resistive Earth model compared to the low resistivity structure.

4.4.2 Effect of lateral variations in conductivity

The Earth conductivity varies both vertically, as considered above, and horizontally. Adjacent regions with different conductivities will have different electric fields. In addition, at the boundary between the two regions there will be localized enhancements of the electric field on the resistive side of the boundary. A good explanation of the physics is provided by Price (1973) who points out that small amounts of charge at the boundary produces the larger electric fields on the higher resistivity side of the boundary needed to give

current continuity across the boundary. This effect can occur at the boundary between geological regions with different conductivities (McKay and Whaler, 2006; Fernberg et al., 2007), but is most noticeable at the coast because of the conductivity contrast between the land and sea.

The coast effect on the electric fields can be calculated for simple, idealized situations using analytical formulas developed by Gilbert (2005) and Pirjola (2013). However, for more realistic situations it is necessary to use 2-D or 3-D modelling techniques such as the finite difference method (Brewitt-Taylor and Weaver, 1976) or finite element method (Wannamaker et al., 1987). To illustrate the coast effect we consider the model shown in Figure 4.7. Calculations made using the finite element method of Wannamaker et al. (1987) for a magnetic field variation parallel to the coast of 1000 nT and period of 300 s are shown in Figure 4.8. These show the increase in the electric field perpendicular to the coast. The right-hand axis shows the electric field values normalized by dividing by the electric field value on the land side away from the effect of the coast. This shows that the electric field is increased by a factor of 7.3 at the coast compared to its inland value. The electric field enhancement falls-off with distance from the coast and, in this example, reduces to within 5% of the inland value at a distance of 73 km from the coast. Other model calculations show that the relative size of the coastal enhancement and its extent inland both get larger as the frequency decreases. These characteristics all influence the electric fields that drive GIC in power systems.

4.5 GIC flow in power systems

The flow of geomagnetically induced currents (GIC) depends on the paths through the power network. High voltage power transmission networks use 3-phase alternating current (AC) where the transformer windings for the 3 phases are often connected together at a neutral point as shown in Figure 4.9. In normal operation the AC currents in the 3 phases have the same amplitude but are 120° out of phase and sum to zero at the neutral point. However, during fault conditions there may be a significant unbalance current or lightning strikes can produce large currents in the lines and transformers; a safe discharge path for these currents is provided by connecting the transformer neutral points to ground. These neutral-ground connections allow the geomagnetically induced currents to flow through the transformer windings to ground.

Power transmission networks use multiple voltages: the highest voltages (e.g., 345 kV, 500 kV, 735 kV) are used for long distance power transmission; medium voltages (e.g., 135 kV, 220 kV) are used for shorter distance power transmission; and lower voltages (e.g., 10 kV, 15 kV) are used for local power

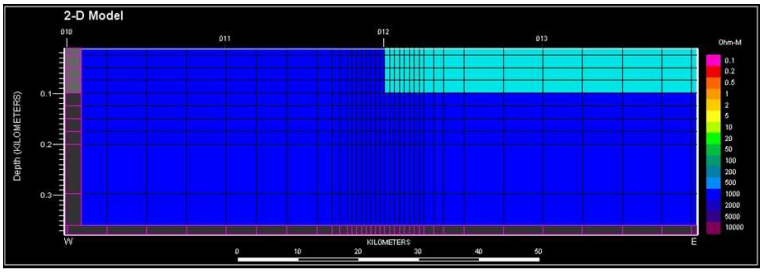

Fig. 4.7. Finite-element 2-D conductivity model of a coast for an Earth conductivity of 1000 ohm-m (dark blue) and with a sea layer 100 m deep (light green). The associated model electric field for specific values of B_x and the frequency of the field perturbation is shown in Fig. 4.8.

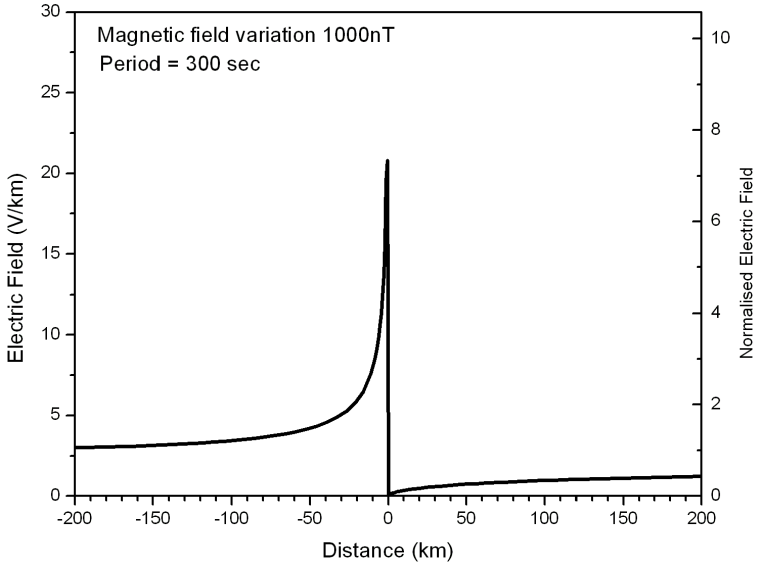

Fig. 4.8. Model electric field, E_y (mV/km) across a coast for $B_x = 1000\,\mathrm{nT}$, for model properties as shown in Fig. 4.7: seawater depth = 100 m, frequency = 0.0032 Hz. The left-hand axis shows actual electric field values; the right-hand axis shows electric field normalized by dividing by E field value at surface of land away from the effect of the coast.

distribution. The lower voltages are normally connected by delta windings that are ungrounded so are unaffected by GIC. For the medium and high voltages the higher voltage transmission lines are comprised of multiple conductors to minimise losses and reduce corona effects. This means that higher voltage lines have lower resistances so experience higher levels of GIC (Kappenman, 2004).

The GIC flow in a network can be calculated using a model of the network comprising the resistances of the transmission lines, transformer windings and

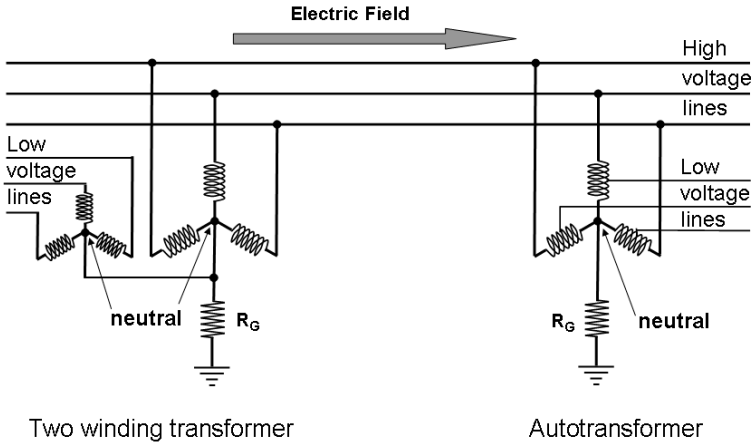

Fig. 4.9. Three-phase transmission lines and substations with a two winding transformer and an autotransformer (a transformer with a single coil in which one winding acts both as primary and as secondary winding).

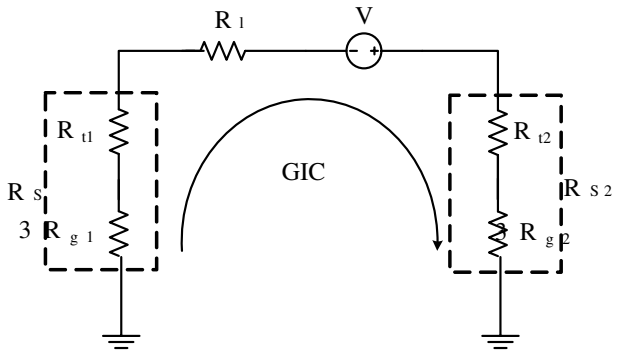

Fig. 4.10. GIC in a single phase circuit (from Zheng et al., 2013).

ground connections with the induced electric fields. All three phases experience the same GIC so it is sufficient to model a single phase network. This is comprised of the single phase resistances except for the substation grounding resistance. The GIC from all three phases share the path through the substation grounding resistance so produce three times the voltage drop of that produced by the current from one phase. To account for this in a single phase network model a value of three times the substation grounding resistance is used. The relative influence of the different resistances can be examined by considering a simple network as shown in Figure 4.10.

The driving force for GIC is the induced electric field in the transmission lines (Boteler and Pirjola, 1998). This is represented in the model by a voltage

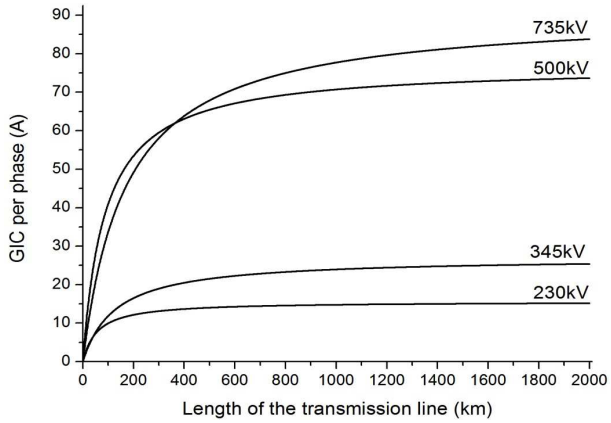

Fig. 4.11. GIC dependence on line length (from Zheng et al., 2013).

source equal to the integral of the electric field along the length of the transmission line. For a uniform electric field and a straight transmission line this reduces to the electric field component in the direction of the transmission line E_ℓ multiplied by the line length, ℓ, i.e. $V = E_\ell \cdot \ell$. $R_\ell = r \cdot \ell$ is the DC resistance of the transmission line with resistance r per unit length; R_t is the resistance of the transformers, R_g is the substation grounding resistance, so the resistance of each substation as a whole for a single phase model is $R_s = R_t + 3R_g$. The GIC driven by this voltage is simply given by Ohm's law, i.e., by dividing the induced voltage by the resistance of the circuit:

$$GIC = \frac{V}{R_\ell + (R_{S1} + R_{S2})} = \frac{E_\ell \cdot \ell}{r \cdot \ell + (R_{S1} + R_{S2})}. \tag{4.5}$$

This shows that the induced voltage is dependent on line length so longer lines experience a larger induced voltage. The resistance of the circuit is the resistance of the line plus the resistance of the substations at each end of the line. The substation transformer and grounding resistances are fixed but the line resistance is dependent on the length of the line. Figure 4.11 shows the GIC calculated for different lengths of line for different voltage levels. As well as showing the larger GIC in higher voltage systems, this shows that the GIC is larger in longer lines, because of the increased induced voltage mentioned above. However, at very long line lengths the line resistance becomes the dominant resistance in the circuit and then the induced voltage and the resistance increase at the same rate so the GIC approaches a limiting value. This represents the largest value of GIC that a particular electric field can produce in a transmission line.

The concern about GIC is not the flow in the transmission lines but where

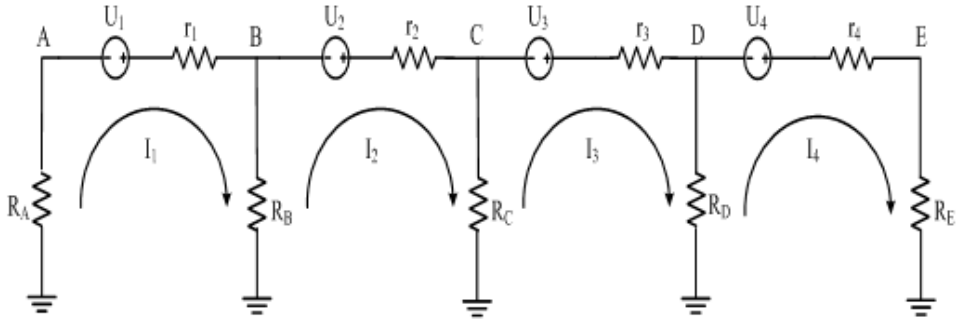

Fig. 4.12. GIC in adjacent loops cancel at the middle substations and largest GIC occurs at substations at the edge of the network.

they flow through transformers to ground. Not every substation will be affected by GIC. Consider the simple network shown in Figure 4.12. At the middle substations there are similar GIC flow in the transmission lines going into and out of the substation so little GIC flows to ground at these substations. Most of the GIC flow in and out of the network occurs at the edges of the network. Examination by Zheng et al. (2014) of factors influencing the GIC values at the end substations in a network shows that it is not the individual line length that is important but the length across the system. Exact values of GIC in real networks can be calculated using network modelling techniques (Boteler, 2014) or the Lehtinen-Pirjola (1985) method.

4.6 GIC effects on transformers

The concerns about GIC in a power system all arise from the effect of GIC on transformers (Whalling and Khan, 1991; Dong et al., 2001; Price, 2002; Girgis and Vedante, 2013). GIC flowing through the transformer windings create an extra magnetic field inside the core of the transformer. GIC frequencies are low compared to the 50 Hz or 60 Hz AC frequency so produce a varying DC offset to the transformer operation as shown in Figure 4.13. Using the magnetising curve for the transformer it is possible to determine the current waveform under DC offset conditions. This shows that during each part of the AC waveform when the combined DC and AC magnetic field take the transformer into the saturation region of the magnetising curve there is a spike in the current waveform. Spectral analysis of the distorted current waveform shows that the distorted waveform has a high harmonic content with both even and odd harmonics. Also, the transformer is operating less efficiently

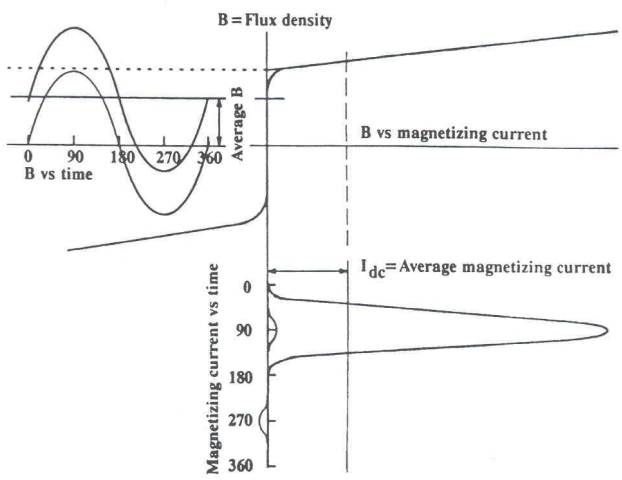

Fig. 4.13. Hysteresis curve for a single phase power transformer showing the spikey current waveform produced when the flux offset takes the transformer into saturation (from Bolduc and Aubin, 1978).

and draws more magnetising current, representing increased consumption of reactive power.

During saturation the magnetic field spills out of the transformer core and into the surrounding air and support structures for the transformer. Depending on the transformer construction, there can be flux concentrations that cause hot spots that can damage the transformer windings. Figure 4.14 shows recordings of transformer temperatures during a GIC event and shows the hot spot temperature following the GIC variation while the bulk transformer temperature, given by the oil temperature, does not change.

4.7 System impacts

4.7.1 Protective relays

To protect the power system during hazardous conditions many different relays are used to detect a variety of conditions and switch out threatened equipment. Some relays are designed to sense conditions that would normally be indicative of a fault on the system, but also occur at times such as system energization. To distinguish between these conditions other signals (e.g., harmonics) are used to restrain the relay operation during the "safe" occurrences. There are thus three classes of response by relays to GIC: i) to correctly operate when GIC has created unsafe conditions that the relay is designed to detect, ii)

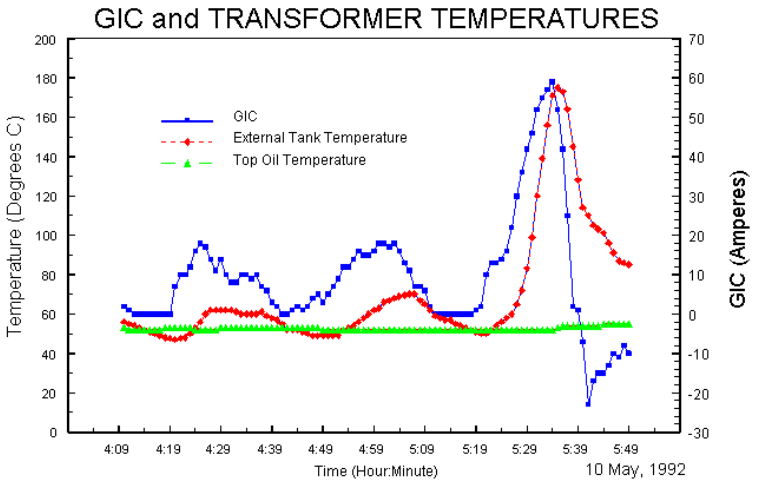

Fig. 4.14. Geomagnetically induced current (GIC), tank temperature, and oil temperature measured on a transformer on the Allegheny Power system (redrawn from results from P. Gattens reported by Kappenman, 2010). GIC do not affect the overall transformer temperature (shown by the oil temperature) but can produce hot spots on the external tank wall.

to operate when GIC create a false signature of a fault, and iii) to restrain operation of a relay when fault conditions do exist.

Bozoki et al. (1996) reviewed the effect of GIC on protective relays. They consider different relays used to protect capacitor banks, transformers, and generators. Buchholz relays detect gassing from transformer oil caused by overheating. Many relays are designed to detect excess currents in various parts of the power system. The settings for these relays are usually based on levels of the fundamental AC but many studies have found that they also inadvertently respond to increased harmonics.

The harmonics produced by GIC can interfere with operation of transformer differential relays. Differential relays are designed to detect a departure from the normal ratio of input and output currents which is usually indicative of a fault in the transformer. However different currents also occur during transformer energization and relay operation is not wanted at this time. To distinguish between these two conditions the presence of harmonics during energization is used to restrain the operation of the relay in this case. With respect to GIC, the concern is that the harmonics generated by GIC cause either the differential relay to operate inappropriately under normal load or inhibit proper operation during transformer internal faults.

The susceptibility of relays to harmonics varies with manufacturer and type

so it is very difficult to generalise about which relays will mis-operate. Tests are needed for the relays used on a specific system. The move towards digital filters is changing the GIC sensitivity, though it is uncertain whether relays are becoming more or less sensitive to GIC effects. A key characteristic of digital filters is that they allow greater flexibility of settings which perhaps could be used to optimise their performance during GIC events.

4.7.2 Reactive power

The power delivered to customers usually has the AC current in phase with the AC voltage and is termed real power. In contrast the AC magnetising current drawn by the transformers is out of phase with the AC voltage and this combination is termed reactive power (also referred to as "VAR" standing for volts times amps reactive). Reactive power has to be supplied to the system in order for the transformers to operate correctly. This can be done either by dedicated generators or by static VAR compensators (SVC) that convert real power to reactive power. When there is insufficient reactive power to maintain voltage stability, voltage collapse may occur causing system outages and interruption of service to customers (Maquire and Woodford, 1990).

When GIC cause transformer saturation there is an increase in magnetising current and, by association, an increase in the reactive power demand (see Figure 4.15). Because of the widespread nature of GIC many transformers on a power system can be going into saturation simultaneously, creating a significant increase in the total reactive power demand on the system. During the March 1989 magnetic storm GIC in the Hydro-Québec system caused transformer saturation and increased reactive power demand. At the same time harmonics caused SVC relays to trip removing a source of reactive power, leading to voltage collapse and the system wide blackout.

Management of reactive power is becoming more of a concern as the operation of the transmission network and the operation of power generation are split into separate companies and purchases of power have to be negotiated ahead of time. Erinmez et al. (2002) estimated that in England and Wales a geomagnetic storm could increase the system reactive power demand by several thousand MVARs requiring deployment of tens of reactive power resources.

The impact of a widespread power blackout on a modern power system can be examined by considering the August 2003 blackout of the Northeast USA and Canada. This blackout was not produced by a magnetic storm but there are many similarities with the way the system failures spread, especially the role of reactive power, and the August 2003 storm provides a well documented example of the costs of a power blackout (Kappenman, 2003a). The August

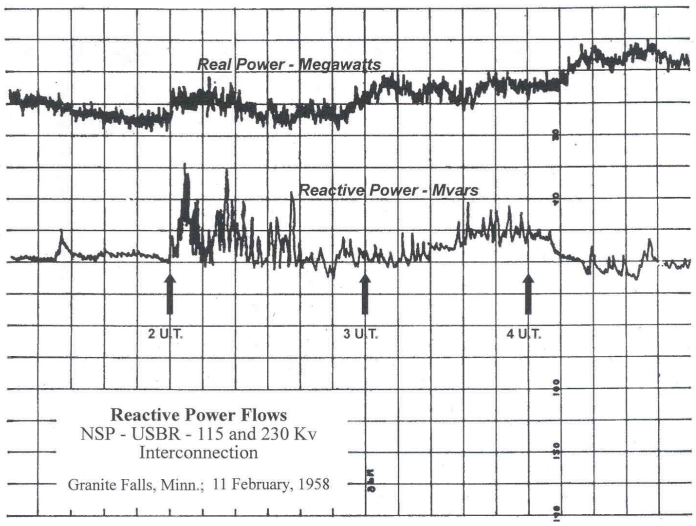

Fig. 4.15. Increased reactive power flows during the February 1958 magnetic storm (from Slothower and Albertson, 1967).

2003 blackout started when a tree fell on a power line in Ohio. Tripping out of this line caused a redistribution of power flows to other lines which then became overloaded and tripped out of service themselves. Investigations of the event document a whole series of lines becoming overloaded, tripping out, and pushing the power flow problems to an even wider area, resulting eventually in blackouts in Ontario, Ohio, Michigan and New York state (Task Force, 2004).

The US-Canada Power System Outage Task Force identified insufficient reactive power as a significant factor in allowing the blackouts to spread. These problems occurred because there was not enough reactive power for normal system operation and single contingencies. Thus it is easy to imagine the effects a geomagnetic storm, that creates an abnormal demand for reactive power, would have on the power system.

4.8 Hazard assessment

The above sections show how geomagnetic disturbances create electric fields that drive GIC in power systems causing transformer saturation leading to increased harmonic levels and reactive power consumption that can cause problems with power system operation. During any geomagnetic disturbance there will be some GIC flowing in a power system causing low levels of harmonics that are not troublesome for system operation. The key question is what types

and levels of geomagnetic activity and what Earth and system conditions combine to give GIC that can cause problems to power system operation.

To start we consider the main phase of a magnetic storm. Although the Dst index is often used as an indicator of large disturbances, it is strictly only a measure of the main phase itself which, in most circumstances, varies too slowly to produce large enough electric fields to cause significant GIC. However, many associated variations (substorms and pulsations) may cause large GIC. Generally the Dst value is not a good proxy for the magnitude of these other magnetic field variations and it is better to use indices that more directly measure these phenomena when evaluating GIC risk.

Magnetic substorms produce large and rapid changes in the magnetic field that produce significant spikes in the electric field. The Hydro-Québec power system blackout in 1989 coincided with a substorm onset. Other power system problems during March 13 and 14, 1989 also occurred during substorms. Not all of this activity was associated with the westward substorm electrojet in the midnight sector. Problems in the evening sector on March 13 coincided with the occurrence of a strong eastward electrojet that extended down over the US. The transformer failures at the Salem generating station on the east coast of the US have also been attributed to this part of the event. Power system problems during other space weather storms are also associated with rapid variations of the convection electrojets (Boteler, 2001).

Storm sudden commencements produce the most rapid magnetic field variations, but their amplitude is usually not sufficient to cause problems. However, ground system effects in US in August 1972 (Anderson et al., 1974) and in New Zealand in November 2001 (Beland and Small, 2004) coincided with SSC. This would be a significant risk factor for lower latitude systems if the magnetopause currents were the cause. However, close inspection of these events showed the causes were surges in the convection electrojets associated with the compression of the magnetosphere and increased magnetopause currents, rather than the magnetopause currents themselves. A recent study has found that some SSC signatures show a high latitude enhancement that cannot be explained by the magnetopause currents and is consistent with a simultaneous surge of the convection electrojets in the auroral ionosphere and contributes to the risks for power grids at high latitudes (Fiori et al., 2014).

Magnetic pulsations are another type of magnetic field variations that are varying rapidly enough to produce large electric fields. However, the variations do not seem to be large enough to produce the catastrophic effects such as seen in the March 1989 storm. Close inspection of the magnetic field variations around the time of the Hydro-Québec blackout shows that the magnetic substorm was accompanied by large pulsations that persisted for over an

hour. While the rapid onset of the magnetic substorm caused the system collapse for Hydro-Québec there is now concern that long-lasting pulsations as seen after the substorm onset may, because of their persistence, contribute to transformer heating.

A number of studies have examined the overall risk of extreme geomagnetic activity for power grids (Viljanen 1997; Boteler, 2001; Pirjola et al., 2005; Marshall et al., 2011; Thomson et al., 2011). These have determined the occurrence statistics of particular geomagnetic indices or data that could then be used to estimate the levels of GIC in a power grid. Thomson et al. (2011) illustrated how extreme value statistics could be applied to estimate the occurrence of the infrequent most severe space weather storms that are a problem for power grid operation. Now, these techniques are being used to assess the GIC levels expected once in 100 years that can be used as design criteria for power grids (Pulkkinen et al., 2012; Ngwira et al., 2013).

4.9 Space weather forecasting for power grids

When the hazard assessment has identified that a power grid is at risk from space weather storms then plans have to be made to mitigate the effects. One option is technological changes to the power grid, such as installing blocking devices (Kappenman et al., 1991) or use of particular transformer designs (Girgis and Vedante, 2013). However, apparently simple measures can have adverse consequences: for example, tests of blocking capacitors in the power grid in England showed that this changed the GIC flow across the network such that the reactive power demand actually increased (Erinmez et al., 2002). Thus, although various technological solutions are being investigated their costs or practicality have, so far, limited their application. Instead, power grid operators are looking for space weather forecasts to provide them with sufficient warning to implement operating strategies to safeguard the power grid.

The space weather forecast requirements for the power industry have been considered in a number of papers (e.g., Thomson, 2000; Kappenman, 2001, Pirjola et al., 2005). Thomson (2000) points out that the forecasts of geophysical parameters commonly produced need to be translated into parameters that are relevant to the users. He shows how decision theory can be used to evaluate forecasts of conditions above an "action theshold" at which a power grid would invoke particular operating procedures. Determining these threshold levels is where the hazard assessment work described in the previous section is relevant. Providing forecasts of specific GIC levels for a power grid can be split into three parts: (1) forecasting the occurrence and propagation of solar eruptions, (2) forecasting the magnetic disturbances produced when these

eruptions reach the Earth, and (3) forecasting the GIC produced by these disturbances.

The general occurrence of solar phenomena such as coronal mass ejections and high speed solar-wind streams follows the solar cycle, but the most severe storms that represent a threat to power grids can be characterized as "rogue" events that can occur with any level of solar activity. A good example of this is the July 2012 CME that occurred during a weak solar cycle. This CME missed the Earth but simulations based on in-situ measurements made by the STEREO-A spacecraft that was in the path of the CME indicate that if it had been Earth-directed it may have had a serious impact on power grids (Baker et al., 2013). The problem with this or any prediction of CMEs is knowing if they will be "geo-effective". This involves two key properties: the speed of the CME and the orientation of the associated interplanetary magnetic field (IMF). Faster CMEs would generally be considered more likely to cause problems and the short transit time between the 1859 Carrington solar flare and the following geomagnetic disturbance would support this. However, the August 1972 event featured an even shorter transit time and although the initial shock caused problems there was no major magnetic storm. In contrast, the March 1989 event did not involve a fast CME speed, yet produced widespread and significant effects on power systems. The problem with prediction is knowing the IMF orientation associated with the CMEs. Tsurutani (2001) examines answers to common questions and misconceptions about using information about CMEs to predict magnetic storms.

Information about solar wind speed and IMF are available from the ACE satellite at the L1 point upstream of the Earth and have been used in many models to try and predict geomagnetic activity (e.g., Wintoft, 2005; Pulkkinen et al. 2010). The question is what is the appropriate geomagnetic activity to forecast. Often the focus is on forecasting the magnetic storm main phase as measured by the Dst index. The main phase variations are too slow to cause significant GIC themselves; however the Dst value may be useful as guide to the expansion of the auroral zone that is a risk factor for GIC in many power systems. Pulkkinen et al. (2011), comparing different forecast models with observations, found that the performance of the models depended on the metric used and also varied with different events. The difference in performance for different events suggests that forecast models to use could be chosen based on the event. If users could identify the characteristics of a disturbance that are important for them, then the appropriate metric can be chosen for evaluating which are the best forecast models to use.

Forecasts of magnetic field variations can be used with an Earth model to calculate electric fields which are then used as input to a power system

model to calculate GIC. This relies on forecasts of the actual magnetic field variations in order to calculate the electric fields. An alternative approach is to determine empirical relations between the magnetic activity and resulting GIC. This can be done with data or with indices. Trichtchenko and Boteler (2004) obtained better correlations using hourly or 3-hourly indices than the correlation obtained with 1-min data. This shows that it is more practical to forecast the envelope of the GIC rather than the GIC variations themselves.

Power grid response to a forecast space storm will inevitably involve some costs so power utilities may be reluctant to take such action unless the forecast is reliable (Pirjola et al., 2005). Forecast accuracy is inversely related to the lead time. Thus the solar observations are best used to provide a general advance warning of potentially hazardous space weather while more specific alerts are produced from models driven by solar wind data from an upstream monitor (Cargill, 2001). Even these forecasts may not be reliable enough for power system operators to take action and some power grids are using GIC measurements and real-time simulations to monitor the condition of the power grid (Marti et al., 2013, 2014). As the action taken in response to a forecast of activity may involve ongoing costs such as using less cost-effective generation (eg oil-fired instead of hydro) or restricting exports of power, it is also important to provide forecast or notification of the end of a space weather disturbance. Provision of such space weather services would make a significant contribution to help deal with space weather effects on power grids.

5

Radio waves for communication and ionospheric probing

Norbert Jakowski

5.1 Introduction

Radio waves play a significant role in our modern society in telecommunication, navigation and remote sensing. At present days we cannot imagine a world without using radio waves. It is surprisingly that the fundamental theory of electromagnetic waves was founded not earlier than about 150 years ago. The British physicist James Clark Maxwell summarized the existing knowledge on electricity and magnetism at that time in his famous theory of electromagnetism. The four Maxwells equations describe the fundamental relationship and interaction between electromagnetic fields, electric charges and currents. It took further 20 years until the German physicist Heinrich Rudolf Hertz could experimentally verify Maxwells theory by demonstrating that electricity can be transmitted via electromagnetic waves travelling at speed of light. He also brought evidence that light is a form of electromagnetic radiation. In honor to Heinrich Hertz the unit of radio and electrical frequencies is expressed in Hertz (Hz) in the international metric system since 1933. The unit 1 Hz means that there is one oscillation per second (1Hz = 1/s). Maxwells theory and its experimental verification by Hertz led finally to the development of wireless telegraph and the radio.

About 10 years later many engineers and scientists started the racing to improve transmitters and detectors to bridge increasing distances. Among these wireless communication pioneers were the Serbo-American engineer Nicola Tesla, the Russian physicist Alexander Popov and the Italian engineer Guglielmo Marconi. Concerning the matter of this paper there was a remarkable experiment conducted by Marconi in December 1901. Marconi claimed that he has successfully transmitted a signal from Poldhu, Cornwall, England to Signal

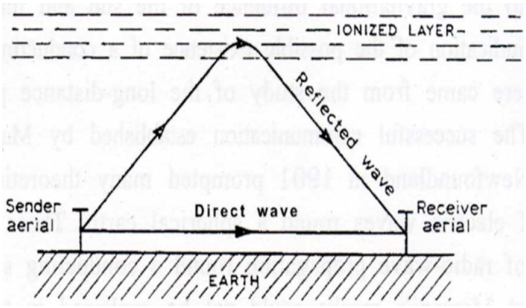

Fig. 5.1. Illustration of the propagation of radio waves in the presence of the ionosphere (E.V. Appleton Nobel lecture, 1947).

Hill in St John's, Newfoundland over a distance of about 3500 km. Further improvement and installation of more effective transmitter and receiving stations made it possible to send a message from US president Theodore Roosevelt to the King of the United Kingdom via Marconis Glace Bay station in Nova Scotia, Canada, across the Atlantic on 18 January 1903.

To explain the long distance transmission of radio waves, the American electrical engineer Arthur Edwin Kennelly and the British physicist Oliver Heaviside assumed an upper conducting layer from 80 km altitude upward already in 1902. In honor of these two men the upper conducting layer was named Kennelly-Heaviside layer over many years. In 1926 the British scientist Watson-Watt used the term Ionosphere at the first time for describing the ionized layer in the upper atmosphere. In the subsequent years the term Ionosphere came into use widely and is now well accepted. Edward Appleton and Miles Aylmer Fulton Barnett in 1925 reported direct evidence for the existence of the conducting and therefore reflecting layer by using medium frequency (MF) radio waves. In the same year the American physicists Gregory Breit and Merle Antony Tuve came to the same result by detecting reflected pulses of High Frequency (HF) radio waves. These experiments led to the development of RADAR technique in subsequent years.

In his Nobel Lecture on December 12, 1947, Sir Edward Appleton described the matter as follows: Now the most striking feature of the atmospheric air at high levels is that it is ionized, and for that reason the spherical shell surrounding the earth at the levels with which we are concerned is called the ionosphere (cf. Fig. 5.1).

Generally speaking, the practical use of electromagnetic radio waves for long-distance communication led to the development of radio and electronic technologies including the need of more detailed knowledge of the propagation environment.

The historical review shows clearly that the detection and exploration of the ionosphere is closely related to radio waves and their interaction with the charged particles in the ionosphere. On the other hand, also the wireless communication technique and related applications have developed in close relationship to the knowledge about the propagation medium ionosphere. Radio wave propagation via the ionosphere was of great practical importance during the first half of the 20th Century. Below frequencies of 30 MHz the ionosphere is an essential part of the terrestrial radio wave propagation. At higher frequencies the ionosphere is a source of system perturbation or even disruptions in Earth - space communications such as navigation systems. On the other hand, the availability of radio signals permanently transmitted by a fleet of satellites belonging to Global Navigation Satellite Systems (GNSS) such as the Global Positioning System (GPS) has opened a new dimension for ionosphere sounding. Therefore, this chapter is focusing on GNSS signal propagation and related capabilities for probing the ionosphere.

5.2 Propagation medium ionosphere

To better understand the radio wave propagation in the ionosphere we will briefly consider composition, vertical structure and dynamics of the ionosphere (for further reading see also Fuller-Rowell and Schrijver, 2009 and Solomon, 2010).

The ionosphere is the ionized part of the Earth atmosphere, ranging from about 60 km up to about 1000 km. The upper part of the ionized and co-rotating atmosphere is usually called the plasmasphere or protonosphere reaching up to the plasmapause height which describes the boundary to the outer magnetosphere. The ionospheric plasma is mainly formed by the solar radiation in the Extreme UltraViolet (EUV) range at wavelengths below 130 nm. The electron production is a direct consequence of the interaction of the solar radiation with atoms and molecules in the Earth's upper atmosphere. The atoms and molecules of the main constituents (i.e., O, O_2, N, N_2, NO) of the upper atmosphere are mainly ionized by the solar radiation in the far and extreme ultraviolet regions as well as by solar X-rays. In addition to this photoionization also cosmic rays and energetic particles originating from the solar wind contribute to the ionization but to a less extent.

The plasma is composed by a variety of different atomic and molecular ions interacting in a complex way by photochemical reactions. Basic processes can be described by the continuity equations, energy equations and equations of motion for the individual charged particles taking into account that the total number of ions is equal the number of electrons in the ionospheric plasma (Davies, 1990).

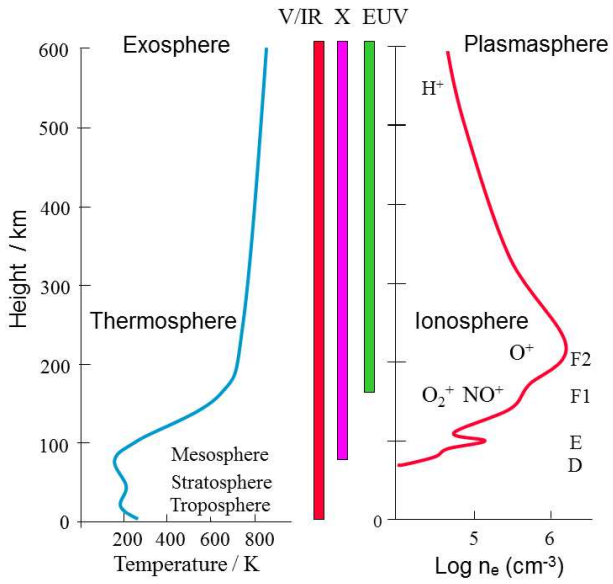

Fig. 5.2. Vertical structure of the electron density of the ionosphere including symbols of main contributing ions (right) in comparison with the neutral atmosphere temperature (left) and solar radiation penetration depths (middle).

The fundamental continuity equation for the electrons is written by:

$$\frac{\partial n_e}{\partial t} = Q - L - \nabla(n_e \cdot v), \tag{5.1}$$

where n_e is the electron density, t is the time, Q is the rate of electron production, L is the rate of electron loss, and v is the mean velocity of the electrons. The divergence term represents the net loss/gain due to transport. It is evident that composition and density of the neutral gas have a severe impact on the production and loss term in the continuity equation, whereas forces such as thermospheric winds and electric fields penetrating from the magnetosphere essentially determine the transport term.

The complex dynamics of production, loss and motion of the ionospheric plasma, including strong coupling in particular with the thermosphere and magnetosphere, leads to a typical vertical structure of the ionospheric electron density as shown in Fig. 5.2. The different layers (D, E, F1, F2 named in order of increasing heights) characterize regions where specific processes dominate such as the E layer named by Appleton as that region where electric currents maximize. As it will be demonstrated in subsequent sections, the ionization at altitudes around 100 km is strongly impacted by high energetic particles and

radiation such as X-rays accompanying solar flare eruptions. The additional ionization significantly impacts the radio wave propagation.

The vertical electron density distribution can effectively be described by Chapmans theory (Chapman, 1931). Considering a horizontally stratified layer of an one-component isothermal gas which is ionized by a monochromatic beam of solar radiation at an incidence angle χ and assuming equilibrium conditions, the height dependence of the electron density is then given by the Chapman layer function:

$$n_e = N_0 \exp\left(\frac{1}{2}\left[1 - z - \sec(\chi)\exp(-z)\right]\right), \tag{5.2}$$

with

$$z = \frac{h - h_0}{H} \tag{5.3}$$

and n_e is the electron density, N_0 the peak density, h_0 the peak height and H the pressure scale height of the neutral gas.

Although the assumptions are rather specific, this Chapman layer formula describes the general features of the vertical structure of the ionospheric electron density very well. Thus, the total vertical electron density structure as shown in Fig. 5.2 can be described by different Chapman layer functions representing different layers.

5.3 Radio wave propagation and ionosphere

When traveling through the ionospheric plasma, it is evident that electromagnetic waves characterized by oscillating electric and magnetic fields interact with the charged particles. The degree of interaction is described by the refractive index n which has been derived in the late 1920s and early 1930s by Appleton, Lassen and Hartree (for further reading see Budden, 1985 and Rawer, 1993 and references therein).

Starting with Maxwells equations it can be shown (e.g. Davies, 1990) that the refractive index n for a cold, homogenous and collisionless plasma is given by the equation

$$n^2 = 1 - \frac{f_p^2}{f^2}, \tag{5.4}$$

where the plasma frequency f_p is given by

$$f_p^2 = \frac{n_e e^2}{4\pi^2 m_e \epsilon_0}, \tag{5.5}$$

and n is the index of refraction for a wave of frequency f; e is the electron charge; m_e is the electron mass; and ϵ_0 is the dielectric constant of vacuum.

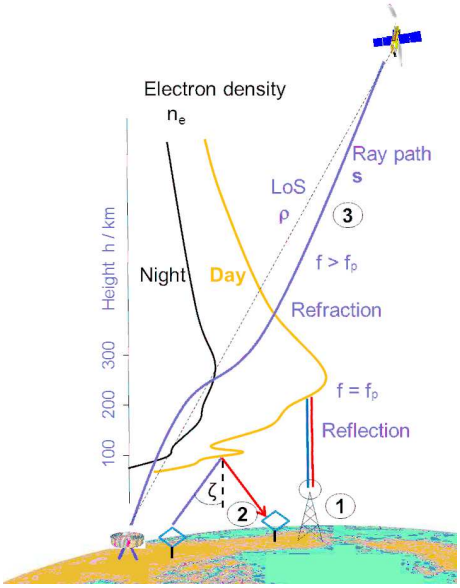

Fig. 5.3. Illustration of radio wave propagation effects in the ionosphere (1) Vertical sounding, (2) HF propagation, (3) Transionospheric propagation, LoS: Line of sight

When taking into account the real ionosphere, i.e., considering the fact that due to the presence of the geomagnetic field the ionosphere is anisotropic and collisions between neutrals and charged particles (ions and electrons) are allowed, the refractive index n is given by the Appleton-Lassen formula which is not considered here in detail (for details see Budden, 1985, or Rawer, 1993).

Although simplified, Eqs. (5.4) and (5.5) provide already some basic information for discussing propagation effects at high frequencies.

Considering Eq. (5.5) the vertical electron density profile illustrated in Fig. 5.2 can directly be converted into a vertical profile of plasma frequency. If the frequency of a propagating radio wave becomes equal to the plasma frequency, the refractive index in Eq. (5.4) becomes zero, meaning that the wave is reflected. This fact is systematically used by the vertical sounding technique practically established by Breit and Tuves first experiment (see (1) in Fig. 5.3) If the frequency of a vertically directed radio wave is increased step by step, the reflection takes place at growing heights where the wave frequency reaches the plasma frequency f_p.

While measuring the propagation time, the reflection height for the transmitted frequency can be determined. Thus, the electron density profile of the bottomside ionosphere can be determined step by step until the critical frequency fc is reached. The critical frequency corresponds with the peak electron

density NmF2 at the peak height hmF2 via Eq. (5.5). The measurement devices are usually called ionosondes which have been systematically used since the mid-1920s and have provided the basic knowledge about the ionosphere. The ionosonde record is called ionogram which traces the reflected echoes as a function of frequency (electron density) and time (height). Because there are usually several propagation modes such as multiple reflections between the ionosphere and ground or sporadic E-layer reflections and absorption phenomena, the reconstruction of the bottomside electron density profile up to hmF2 height is a challenging task in particular under conditions of a perturbed ionosphere. Nevertheless, the relatively low cost of ionosondes has allowed them to be installed worldwide forming a global network of more than hundred permanent stations. Modern ionosondes such as the digisonde are able to operate automatically in near real time to monitor key parameters such as the peak electron density and height (Reinisch et al., 2005). So, operational services such as DIAS (Belehaki et al., 2006) can provide regional and global maps of the peak electron density NmF2.

It is interesting to note that the same vertical sounding technique can be applied from above for transmitting signals from satellite orbits down to Earth and recording the echoes. This topside sounding technique was successfully used at a number of satellites such as Alouette 1 and 2, Explorer 20, Isis 1 and 2 and Cosmos resulting in a huge data basis. Before transionospheric measurements became available to a greater extent, bottomside and topside sounder data were extensively used to develop global ionospheric models such as the International Reference Ionosphere (IRI) (e.g. Bilitza et al. 1993, Bilitza, 2001).

If the frequency of the vertically transmitted radio wave exceeds the plasma frequency ($f > f_p$), the radio wave can travel through the ionosphere, i.e., in case of bottomside sounding the wave leaves the Earth, in case of topside sounding the wave reaches the Earth surface.

Radio waves used for telecommunication (see (2) in Fig. 5.3) or oblique sounding have incidence angles which are not equal zero. In this case the maximum usable frequency (MUF) to get a reflection becomes greater than the plasma frequency according to refraction rules. The MUF can be estimated as $MUF \approx f_p/\cos(\zeta)$.

To better discuss different types of radio waves covering a very broad spectrum in relation to their different behavior and associated application potential it is convenient to separate the spectrum into frequency bands which are listed up in Table 5.1.

Whereas for terrestrial communication all frequency bands can be used, transionospheric radio wave propagation starts commonly at the VHF range.

Table 5.1. *Frequency bands of radio waves*

Symbol of freq. band	Frequency range	Wavelength range	Freq. band (ITU-R) symb.
ELF Extr. Low Freq.	<300 Hz	>1000 km	
ULF Ultra Low Freq.	300 Hz - 3 kHz	1000 - 100 km	
VLF Very Low Freq.	3 kHz - 30 kHz	100 - 10 km	
LF Low Freq.	30 kHz - 300 kHz	10 - 1 km	
MF Medium Freq.	300 kHz - 3 MHz	1000 - 100 m	
HF High Freq.	3 MHz - 30 MHz	100 - 10 m	
VHF Very High Freq.	30 MHz - 300 MHz	10 - 1 m	
UHF Ultra High Freq.	300 MHz - 3 GHz	1000 - 100 mm	1-2 GHz - L
SHF Super High Freq.	3 GHz - 30 GHz	100 - 10 mm	2-4 GHz - S
			4-8 GHz - C
			8-12 GHz - X
EHF Extr. High Freq.	30 GHz - 300 GHz	10 - 1 mm	12-18 GHz - Ku
			18-27 GHz - K

Terrestrial propagation up to the HF band is usually strongly impacted by the ionosphere, e.g. due to the interference of the direct ground wave with the so called sky wave reflected at the ionosphere as already shown in Fig. 5.1. Besides vertical sounding described above, several other radio techniques which we cannot discuss here are utilized to probe the different layers of the ionosphere from ground (e.g. Hunsucker, 1991).

Because we focus in this chapter on transionospheric radio wave propagation, we consider here only propagation measurements in the VLF band which can provide some valuable information on solar flares. As Table 5.1 indicates, the wavelengths of VLF radio waves ranging from 10 km to 100 km are in the same order as the distance between the bottomside ionosphere and the ground. In this case the space between the bottomside ionosphere and the Earth surface forms a so-called waveguide in which the radio wave can travel over large distances around the Earth. Any modification of the lower and upper boundary conditions of this waveguide will lead to a change in the received signal. Hence, X-rays accompanying a solar flare will change amplitude and phase of VLF waves rapidly according to the intensity or class of the solar flare (cf. Fig. 5.4).

Because VLF signals are closely correlated with solar flare eruptions and in addition simple signal strength measurements of signals from numerous transmitters are easy to handle, the Solar Center at the Stanford University has initiated an international students project on occasion of the International Heliophysical Year (IHY) in 2007. The Center developed an inexpensive Space Weather Monitor capable to measure Sudden Ionospheric Disturbances (SID)

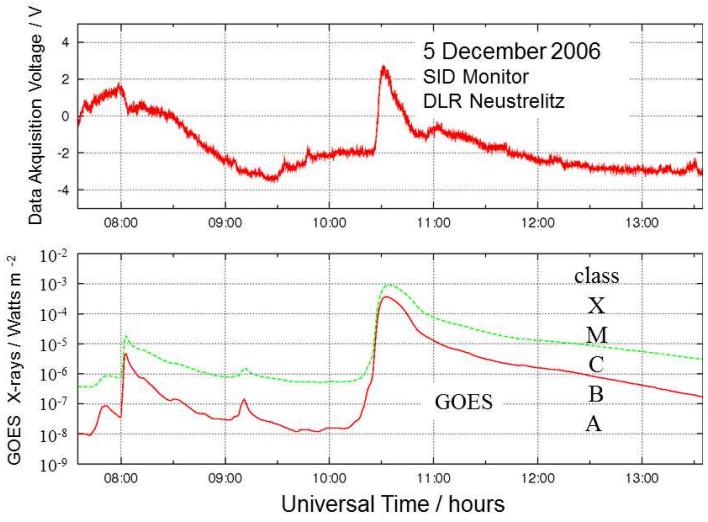

Fig. 5.4. SID (Sudden Ionospheric Disturbance) Monitor output in comparison with GOES X-ray measurements from 2006/12/05.

for installation at high schools and universities around the globe†. During the IHY an international network of SID Monitors has been successfully set up and data have been collected at Stanford University from all over the world. To simplify the data collection, a VLF receiver has been developed within the project SOFIE (SOlar Flares detected by Ionospheric Effects) at the German Aerospace Center (DLR) site Neustrelitz. The new receiver is able to transfer data directly to a server without the help of a PC‡. Due to their relative stable propagation over long distances and their skin depth of several kilometers, VLF waves are commonly used for worldwide telegraphy to ships, submarines and for subterranean communication, e.g. in mines.

5.4 Transionospheric radio wave propagation

Transionospheric radio wave propagation became important after the first artificial satellite, Sputnik I which has been launched in October 1957, has transmitted radio waves to the Earth for communication. The Sputnik I Majak beacon transmitter allowed first transionospheric radio sounding of the ionosphere. In subsequent decades up to now radio beacons onboard Low Earth Orbiting (LEO) satellites such as NNSS, Cosmos, CHAMP and For-

† http://solar-center.stanford.edu/SID/sidmonitor/
‡ http://swaciwebdevelop.dlr.de/ueber-sofie/

mosat/COSMIC have provided a lot of information on the structure and the behavior of the ionosphere under regular and perturbed conditions. Since the mid of 1990s a growing number of signals of Global Navigation Satellite Systems (GNSS) such as GPS, GLONASS and Galileo are available for precise and reliable positioning and navigation but also for ionospheric sounding.

5.4.1 Fundamentals

5.4.1.1 Refraction

Principally, when utilizing radio techniques to probe the ionosphere, typical radio wave parameters such as amplitude, phase and polarization are measured. Thus, amplitude measurements tell us something about changes at the bottomside ionosphere during solar flares (Fig. 5.4), phase or travel time measurements provide direct information on the density and distribution of plasma along the ray path. So linearly polarized VHF signals transmitted by geostationary satellites such as ATS 6, SMS, GOES in the 1970s and 1980s allowed measuring the Faraday effect to derive the Total Electron Content (TEC) of the ionosphere for ionospheric studies (e.g. Davies 1990, Jakowski et al. 1983, 1990, 1991). Here it becomes already evident that the simplified formulation of the refractive index as given in Eqs. (5.4) and (5.5) is not sufficient because the Faraday effect is a result of the anisotropy of the ionospheric plasma caused by the geomagnetic field.

Principally, there are some propagation effects which cannot be ignored when considering the strong requirements of precise and Safety of Life (SoL) applications utilizing space based techniques such as Global Navigation Satellite Systems (GNSS). So we have to consider in particular ray path bending, higher order terms in the refractive index and signal distortions due to diffraction and scattering. The refractive index n given by the Appleton-Lassen formula (e.g. Rawer, 1993) can be approximated for frequencies $f \gg f_p$ by:

$$n = 1 - \underbrace{\frac{f_p^2}{2f^2}}_{\text{1st order}} \pm \underbrace{\frac{f_p^2 f_f}{2f^3}\cos(\theta)}_{\text{2nd order}} - \underbrace{\frac{f_p^4}{8f^4}}_{\text{3rd order}} \quad . \tag{5.6}$$

Here f_g is the gyro frequency of the electron ($f_g \leq 1.4\,\text{MHz}$) defined by:

$$f_g = \frac{eB}{2\pi m_e}, \tag{5.7}$$

where the parameter B is the geomagnetic induction or flux density and θ is the angle between the ray path and the geomagnetic field.

Assuming that the wavelength $\lambda = c/f$ of a radio wave traveling through

the ionosphere is much smaller than characteristic spatial scales of the ionosphere S_I ($\lambda \ll S_I$), principles of geometrical optics can be applied. Thus the propagation follows Fermats law of fastest arrival given by the phase integral or Eikonal

$$L = \int n \mathrm{d}s. \tag{5.8}$$

becomes a minimum (Budden, 1985). In terms of carrier phase ϕ of a radio wave the Eikonal is given by

$$\phi = \frac{2\pi f}{c} \int n \mathrm{d}s. \tag{5.9}$$

The Eikonal can be rewritten in terms of ray path s according to:

$$s = \int \mathrm{d}s_0 + \int (n-1)\mathrm{d}s + \left(\int \mathrm{d}s - \int \mathrm{d}s_0 \right). \tag{5.10}$$

$$s \equiv \rho + \Delta s_\phi + \Delta s_B \tag{5.11}$$

Here ρ is the true range between the transmitting satellite and the ground receiver along the vacuum or line of sight ray path (cf. Fig. 5.3), Δs_ϕ represents the range error terms measured by phase changes and Δs_B is the optical ray path excess due to bending. Ray path bending effects on positioning and their estimations are described by Hoque and Jakowski (2006 and 2008).

Whereas the true range shall be determined in positioning, ionosphere probing techniques analyze in particular the residual terms of phase measurements in s as defined in Eqs. (5.10) and (5.11). The two signs in Eq. (5.6) indicate double refraction for radio waves travelling through the non-isotropic plasma of the ionosphere. The anisotropy is due to the presence of the geomagnetic field causing a gyration of charged particles around the magnetic field lines. Thus, electrons oscillate clockwise around field lines in field direction. The upper (+) sign in Eq. (5.6) represents the ordinary wave (left-hand side circularly polarized) whereas the negative sign refers to the extraordinary wave (right-hand side circularly polarized).

Because a linearly polarized wave can be considered as the superposition of right hand side and left hand side circularly polarized waves, their difference in phase speed leads to a rotation of the polarization plane. The effect is named after Michael Faraday who described at first time the change of the polarization plane of light in the presence of a magnetic field.

Taking into account Eqs. (5.6) and (5.7) the Faraday rotation angle ϕ_{FR} is determined by the phase difference of both waves (represented by n_+ and n_-) according to:

$$\phi_{FR} = \phi_+ - \phi_- = \frac{2\pi f}{c} \int (n_+ - n_-)\mathrm{d}s. \tag{5.12}$$

This can be rewritten in the form

$$\phi_{FR} = \frac{K_F}{f^2} \int n_e B \cos(\theta) \mathrm{d}s, \tag{5.13}$$

with $K_F = 4.73\,10^4\,\mathrm{m^2 s^{-2}}$ in SI units.

Because the geomagnetic field and the angle between the ray path and the geomagnetic field vary only slightly along the ray path, their weighting in Eq. (5.13) can be averaged and the Faraday rotation angle can be approximated by the expression:

$$\phi_{FR} = \frac{K_F}{f^2} \langle B\ \cos(\theta) \rangle \int n_e \mathrm{d}s. \tag{5.14}$$

Here we see that Faraday rotation measurements allow estimating the Total Electron Content,

$$TEC_S \equiv \int n_e \mathrm{d}s, \tag{5.15}$$

of the ionosphere along the ray path s. Because the magnetic field B decreases with the radial distance r according to $1/r^3$, the geomagnetic field weighting pronounces the contribution of the electron density distribution to the integral from the bottomside up to about 2000 km height which is called in the beacon literature "Ionospheric TEC". This fact has been extensively used for sounding the ionosphere in former years by measuring the Faraday effect on linearly polarized signals, e.g. transmitted from geostationary satellites in the VHF range (e.g. Davies, 1980, Jakowski et al., 1991)

Because the GPS signals are transmitted in right-hand circular polarization, the described anisotropy leads to an asymmetry of ionospheric range errors at a selected GPS receiver site in particular in North -South direction (Kedar et al., 2003, Hoque and Jakowski, 2006, 2008). Due to its systematic character, the effect is meaningful in precise geodetic measurements and satellite orbit determination where millimeter accuracy is required (Hernandez-Pajares et al., 2007).

In GNSS applications the first order phase error (cf. Eq. 5.6) is the most significant ionospheric range error reaching even more than 100 m during severe space weather events. Modeling and measurement of this range error is a challenging task in a variety of GNSS applications.

5.4.1.2 Diffraction and scattering effects

If characteristic scale of ionospheric electron density variations is comparable with the radio wavelength, principles of geometric optics are no longer valid. The propagation of radio waves must be described by diffraction and scattering theories (Hunsucker, 1991, Barclay, 2003) which cannot be considered

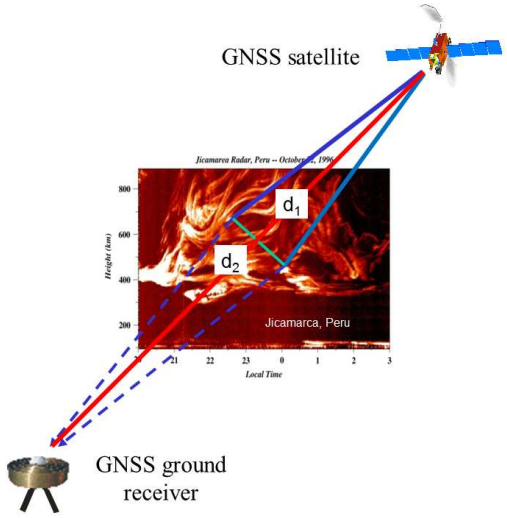

Fig. 5.5. Schematic of radio wave propagation through a turbulent plasma characterized by spatial electron density irregularities illustrated by Incoherent Scatter measurements at Jicamarca/Peru

here due to their complexity. So we confine our attention to describe the phenomenological impact on radio signals.

Small scale irregularities in the ionosphere cause rapid changes in the amplitude and/or phase of radio signals commonly called as radio scintillations. Such scintillations reduce the accuracy and reliability of radio systems and may even result in a complete loss of lock of the signal. Transionospheric scintillation effects cover a broad frequency range from 30 MHz up to 10 GHz.

To estimate the spatial size of ionospheric irregularities which should have a significant impact on a radio wave of wavelength λ the first Fresnel zone can be considered whose radius F_1 is defined by

$$F_1 = \sqrt{\frac{\lambda d_1 d_2}{d_1 + d_2}}. \tag{5.16}$$

Here d1 and d2 mean the distance from the transmitter and from the receiver, respectively. In case of GNSS applications ($\lambda \approx 20\,\mathrm{cm}$, scintillation volume in the ionospheric F layer at around 250-400 km height) the first Fresnel radius is of the order of 300 m. Irregularities of this size or smaller are most effective in producing diffracted or scattered radio waves which interfere at receiver antenna.

A typical radio wave propagation scenario through small scale plasma turbulences is sketched in Fig. 5.5. Small scale electron density irregularities (illustrated here by an Incoherent Scatter based reconstruction of local elec-

tron densities over Jicamarca/Peru) split the primary ray into many different rays due to diffraction and forward scattering. At GNSS receiver level these different rays interfere and cause strong and rapid signal fluctuations. If the fading depth is strong enough, the receiver loses signal tracking, reducing the availability of signals for positioning and navigation.

Ionospheric irregularities may be caused by different processes related to plasma instabilities. One of them is the Rayleigh Taylor Instability (RTI) causing also Equatorial Spread F (ESF) at ground based ionosonde measurements (Kelly, 1989). The RTI describes the behavior of two fluids or plasmas moving in opposite directions. This may happen in the low latitude ionosphere in particular during the sunset hours when plasma diffusion is directed downward due to plasma cooling. On the other hand it is typically for the low latitude evening ionosphere that an eastward directed field is generated which forces the ionospheric plasma to lift up. Although the actual geophysical conditions modify the establishment of the RTI, the occurrence of ESF and related enhanced scintillation activity between sunset and midnight is a well-known phenomenon as will be seen later in section 5.6. Furthermore, enhanced scintillation activity can be observed along strong ionization gradients probably initiated by the gradient drift instability (e.g. Alfonsi, 2006). At high latitudes irregular precipitation of energetic particles from the solar wind may also cause chaotic plasma structures resulting in radio scintillations (Smith et al., 2008, Fuller-Rowell and Solomon, 2010).

Specific phenomena observable at low latitudes are so-called equatorial plasma bubbles (EPBs) which are formed by nonlinear plasma processes probably closely related to the RTI. Inside a plasma bubble the electron density is extremely low (less than 10% of the outside value). Hence, there is a sharp gradient of electron density when crossing the surface of an EPB. This can nicely be seen in TEC data by a rapid fall of TEC values when the ray path enters the EPB and recovers when the ray path leaves the EPB. Due to acting electromagnetic forces in the presence of the geomagnetic field EPBs are shaped along magnetic field lines up to more than 1000 km. Perpendicular to field lines EPBs are rather thin (up to about 100 km) meaning that several bubbles may coexist in a certain region. As RTI is establishing near sunset, EPBs occur and drift eastward at a velocity of about 100-200 m/s (Fukao et al., 2006). The occurrence probability of EPBs depends on solar activity and on season with highest values around equinoxes over Africa and around solstices at the American sector (Nishioka et al., 2008).

Geomagnetic activity affects the generation of EPBs in different ways: increasing magnetic activity at low level is anti-correlated with the generation of EPBs, whereas severe magnetic storms may cause enhanced generation of

EPBs. To characterize the scintillation strength of the received signal, commonly the scintillation index S_4 is used. Other parameters useful for measuring scintillations are the phase standard deviation σ_ϕ , the probability and duration of fades and their depth in the signal strength.

The scintillations level is frequency dependent. As a first approximation it increases with the inverse of the frequency in the range $1.7 < f < 4GHz$. The S_4 index is commonly defined via the signal intensity SI by

$$S_4 = \left(\frac{\langle SI^2 \rangle - \langle SI \rangle^2}{\langle SI \rangle^2} \right)^{1/2}, \tag{5.17}$$

where $\langle \ldots \rangle$ means the average value. S_4 index values are usually between 0 and 1. Values lower than 0.2 represent low, values around 0.5 medium and values greater than 0.7 severe scintillation activity. The phase scintillation index widely used is defined by

$$\sigma_\phi = \sqrt{\frac{1}{N-1} \Sigma_{i=1}^{N} (\phi_i - \langle \phi \rangle)^2}, \tag{5.18}$$

where ϕ means the signal carrier phase and N the number of observations. Both parameters S_4 and σ_ϕ are commonly defined over a period of 1 min.

To learn more about scintillations in the L-Band range, high rate GNSS measurements are well suited to monitor them systematically as reported in section 5.6.

5.4.2 Telecommunication

As pointed out in the introduction, ionospheric impact on radio wave propagation guided wireless communication from the earliest days. On the one hand ionosphere enables transmission over large distances, on the other hand ionosphere acts as a disturber in a broad frequency range up to the SHF band (cf. Table 5.1), i.e., including both terrestrial as well as space based communication. Communication technologies have developed enormously since Marconis experiment and became very robust.

As seen in Eq. (5.4) the refractivity index becomes nearly 1 at very high frequency bands primarily utilized in space based telecommunication. Furthermore, the phase delay is not as crucial for communication as for navigation. Nevertheless, there remains some ionospheric impact on a number of services using frequency bands ranging from VLF to UHF in particular during severe space weather events. The signals of geostationary communication satellites may be impacted even in present days by ionospheric irregularities and plasma bubbles. Thus, ionospheric scintillations on the 4 GHz signal from Intelsat (701) have been observed at low latitudes in the South Pacific region

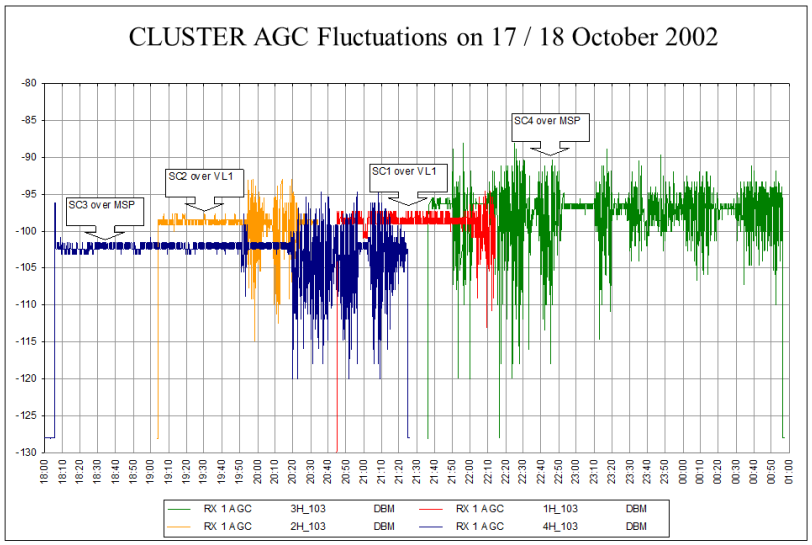

Fig. 5.6. Fluctuations of the Automatic Gain Control (AGC) voltage of CLUSTER spacecraft receivers at different ground stations (marked by different colors) in Spain (Source: ESA Report CL-COM-RP-1001-TOS by Billig et al., 2003)

by Kumar et al., 2007. In particular, if transmitted radio power is low, signals are vulnerable against radio scintillations due to ionospheric irregularities as described in the previous section.

To give an example, corrupted signals have been reported by the European Space Agency (ESA) concerning the reception of Cluster satellites in Spain as shown in Fig. 5.6 (Billig et al. 2003).

Scintillation effects as observed on GNSS signals in the L-band (cf. section 5.6.6) demonstrate the overall vulnerability of L-band satellite communications in particular during severe space weather effects. To better understand the impact and to develop mitigation techniques, more research is needed.

5.4.3 Satellite navigation

Critical infrastructure and economy of our modern society are increasingly dependent on services provided by global navigation satellite systems. Accuracy and reliability of positioning, navigation and timing (PNT) services depend on the ability to determine the travel time of the coded radio signal (modulation phase) with high precision. Although sophisticated atomic clocks onboard GNSS satellites are already precise at picosecond level, there is a slow drift of the clock oscillator which needs to be corrected in the measurements.

So, in addition to measurements for the three space coordinates, a fourth measurement for time correction is required for positioning.

When measuring the travel time of the code or modulation phase of the radio signals, we have to take into account the group refractive index n_{gr}. Using the group refractive index (e.g. Budden, 1985, Davies, 1990) defined by

$$n_{gr} = n + f\left(\frac{\mathrm{d}n}{\mathrm{d}f}\right), \tag{5.19}$$

we get for the first order effect

$$n_{gr} = 1 + \frac{f_p^2}{2f^2}. \tag{5.20}$$

Please note that the absolute value of the ionospheric phase delay is the same as for the carrier phase as seen in Eq. (5.6) but always positive leading to $n_{gr} > 1$. Hence, the travel speed $v_{gr} = c/n_{gr}$ is less than the velocity of light in vacuum whereas the phase velocity $v = c/n$ is higher than the velocity of light in vacuum leading to a phase advance.

The ionospheric code phase delay t_{Dgr} is then given by

$$t_{Dgr} = \frac{1}{c}\frac{K}{f^2}\int n_e ds = \frac{1}{c}\frac{K}{f^2} TEC_S, \tag{5.21}$$

with $k = 40.3\,\mathrm{m^3 s^{-2}}$. TEC_s defines the slant Total Electron Content, which is the number of electrons per square meter along the ray path s. TEC is commonly expressed in TEC units [1 TECU=10^{16} electrons per square meter]. GPS satellites transmit radio waves at frequencies of L1=1575.42 MHz and L2=1227.60 MHz justifying the first order approach in the refractive index (Eqs. 5.6 and 5.20) for most of applications. The observation equation of the GNSS code phase Φ and carrier phase ϕ can be written as:

$$\Phi = \rho + c(dt - dT) + d_I + d_T + d_M + b_C + \epsilon_C, \tag{5.22}$$

$$\phi = \rho + c(dt - dT) - d_I + d_T + d_M + b_L + N\frac{c}{f} + \epsilon_L, \tag{5.23}$$

where Φ is the code phase, ρ is the geometrical distance to be determined, dt and dT are the receiver and transmitter clock offsets, d_I is the ionospheric range error, d_T is the tropospheric range error, d_M is the error due to multipath, $b_{C,L}$ are the instrumentation offset of code/carrier phase measurements, $\epsilon_{C,L}$ is the phase noise of code/carrier phase measurements and N is the phase ambiguity integer of carrier phase measurements. Because carrier phase measurements are much less noisier than code measurements they are used in precise positioning in addition to code measurements. Various techniques have been developed to determine the unknown phase ambiguity N.

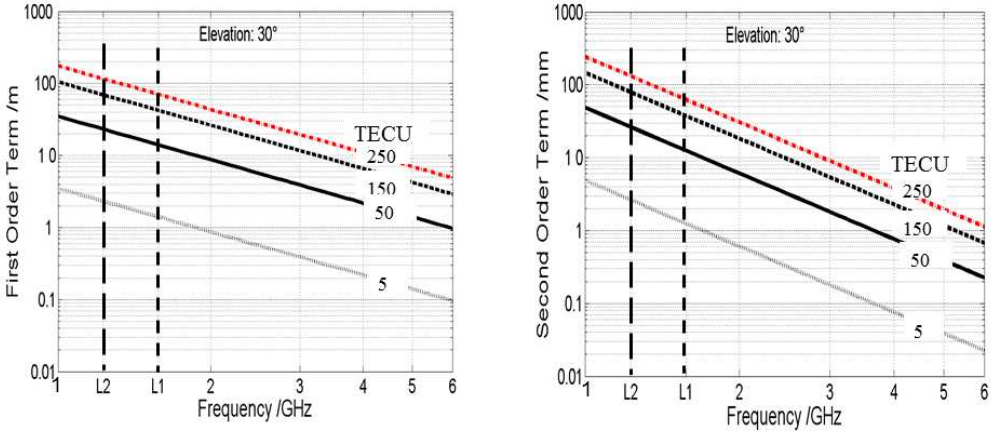

Fig. 5.7. Frequency dependence of first and second order (longitudinal propagation) ionospheric errors in radio systems at different levels of vertical TEC for 30° elevation angle of the radio link. GPS frequencies L1 and L2 are marked by dashed lines.

According to Eq. (5.21) the first-order ionospheric range error d_I is given by

$$d_I = \frac{k}{f^2 TEC_s}. \tag{5.24}$$

Because the total electron content is usually measured along slant ray paths, we define for further use in this paper TECs as slant TEC whereas the vertical TEC along a vertical ray path is simply called TEC. The geometry free vertical total electron content TEC is an ionospheric key parameter comparable with the air pressure in the atmosphere (mass, or the number of atoms and molecules per square meter).

As indicated in Eq. (5.24), the first-order range error in GNSS (99.9% of the total ionospheric error) is proportional to TECs. This means that ionospheric monitoring of TEC can essentially help to correct GNSS based positioning and navigation. Typical ionospheric range errors of first and second order effects are shown as a function of the frequency for different TEC levels in Fig. 5.7. On the other hand, due to the frequency dependence of the refractive index (dispersion) there is a unique opportunity to derive TECs or the ionospheric range error by combining signals at two different frequencies. Knowing TECs, the first order ionospheric error can easily be removed. This is the reason why GNSS satellites transmit signals at least at two frequencies.

Neglecting the frequency independent terms and assuming that the ray paths are the same at both frequencies, the differential phase $\Delta\Phi$ of coherent

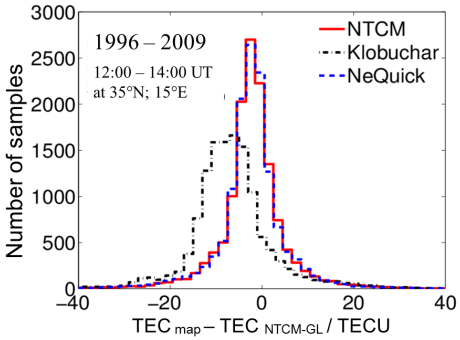

Fig. 5.8. Comparison of the performance of 3 ionospheric models for estimating vertical TEC at 50°N;15°E at 12:00-14:00 UT over more than one solar cycle from 1996 to 2009.

signals at frequencies f_1 and f_2 can be expressed by

$$\Delta\Phi = \Phi_2 - \Phi_1 = K\frac{f_1^2 - f_2^2}{f_1^2 f_2^2} TEC_s + b_{\Delta C} + \epsilon_{\Delta C}, \tag{5.25}$$

where $b_{\Delta c}$ refers to a constant or very slowly varying bias value and $\epsilon_{\Delta C}$ is the residual code phase noise. Here we see as mentioned above that the ray path related TECs can easily be deduced from differential GNSS phases. Thus, on the one hand the 1st order ionospheric range error can directly be corrected in a dual frequency GNSS, on the other hand, Eq. (5.25) can effectively be used to derive TEC from dual frequency GNSS measurements for ionospheric monitoring. As we will see later in section 5.6, such monitoring results can be provided to single frequency GNSS users for ionospheric corrections.

To enable single frequency GPS users a quick estimation of the ionospheric range error, GPS permanently broadcasts a set of 8 coefficients for running a simple GPS correction model. These coefficients are adjusted by the GPS master control station for the best fit to current ionospheric conditions and are broadcasted to users finally every day. This model, well-known also as the Klobuchar model, is able to correct about 60% of the ionospheric error in average (Klobuchar, 1987). The European countries are establishing an autonomous GNSS called Galileo that will use the three-dimensional NeQuick model (Nava et al., 2007) for estimating the ionospheric propagation error. Whereas the numerous model coefficients of NeQuick are fixed, the model is adapted to the actual ionization level provided by Galileo via an effective solar index parameter A_z.

Recently, another simple TEC model running with only 12 coefficients (the Klobuchar model needs 8 coefficients, NeQuick several thousands) has been

published which achieves the performance of the NeQuick model (Jakowski et al., 2011a). Solar activity dependence is introduced to the model via the solar F10.7 cm radio flux. The performance of this model is compared with the Klobuchar and the NeQuick model in Fig. 5.8 for more than one solar cycle at a mid-European site.

Besides modeling of ionospheric propagation errors utilizing empirical or physics based models, the ionospheric state can also directly be monitored by using GNSS data as mentioned before. As we will discuss later in section 5.6 in more detail, Wide Area Augmentation Systems (WAAS) in US and the European Geostationary Navigation Overlay Service (EGNOS) in Europe operate a number of so-called monitor stations (e.g. for EGNOS these are about 30 Ranging and Integrity Monitoring Station RIMS) to monitor the service area and to derive TEC as the key parameter for estimating ionospheric range errors for users. In a similar way TEC data provided by the SWACI service of DLR† were used in a single-frequency Precise Point Positioning (PPP) experiment (Le et al., 2008). For the vertical as well as for the horizontal positioning accuracy of 2-3 decimeter was achieved (95% level).

5.4.4 Remote sensing

Similar as for GNSS positioning the operation of space-based, transionospheric VHF and UHF radars requires knowledge of ionospheric impact on signals. The ionospheric impact is more serious for remote sensing radars such as the Synthetic Aperture Radar (SAR) because the signals cross the altitude range of peak electron density, the F2 layer, usually twice. In addition to transionospheric propagation effects the transmitted signal can be backscattered by small scale ionospheric irregularities which interfere with the received radar signal on board the radar satellite. Furthermore, the two-way radio wave propagation causes a doubling of the phase variance. Both effects degrade the performance of the radar system (e.g. Xu et al., 2008).

Most prominent ionospheric effects on radar signals are range error or group delay, distortions of the shape of radar pulses due to dispersion, rotation of the polarization plane due to the Faraday effect (cf. section 5.4.1.1) and distortion of phase coherence across synthesized aperture and over pulse integration period.

Radar signal degradation problems arise when the level of ionospheric ionization (TEC) and/or temporal and spatial variations of ionospheric electron density structure are high, commonly observed in years of enhanced solar activity and/or during severe space weather events. Assuming vertical TEC

† http://swaciweb.dlr.de

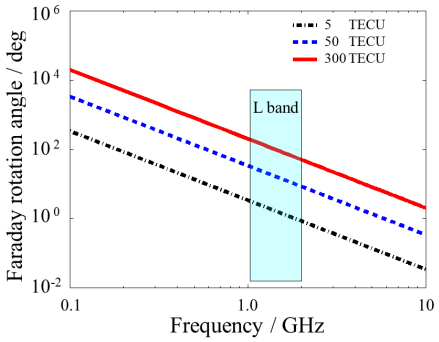

Fig. 5.9. Frequency dependence of Faraday rotation angle (longitudinal propagation) at different ionization levels characterized by the vertical TEC.

values of more than 200 TECU the related vertical range error is around 30 meters in the L-band. These high values are crucial because the accuracy requirements are challenging. For example, SAR Interferometry (InSAR) for tectonic deformation measurements require accuracy of the order of millimeters over hundreds of kilometers. Because the ionospheric delay is proportional to TEC as seen in Eq. (5.21), a strong horizontal gradient structure of TEC causes different phase shifts at pixels across the image. Thus, large- to medium scale structures over the target area result in geometrical distortions of the SAR image. It is evident that a high TEC level usually observed at day time in particular at low latitudes enhances the broadening of radar pulses due to the dispersive nature of the refractive index as discussed in section 5.4.1.1, which also affects the image resolution.

Furthermore, since the anisotropic ionosphere causes a double refraction of radio waves, polarimetric measurements will suffer from the Faraday effect described by Eq. (5.13). When a linearly polarized wave travels through the ionospheric plasma which is embedded in the geomagnetic field, the radio wave splits into two oppositely rotating circularly polarized waves traveling along slightly different ray paths with different phase velocities. Thus, when considering the superposition of both waves at the receiving antenna, the polarization angle has been changed as a function of the electron density and the geomagnetic field along the ray path according to Eq. (5.13). Considering the $1/f^2$ frequency dependence, the Faraday effect is much more significant at UHF than at SHF frequency band (cf. Fig. 5.9). This fact has to be taken into account when using the lower frequency band. Microwave remote sensing using low-frequency SAR technique can provide a lot of information on forest characteristics such as spatial coverage, density, height of trees and species.

Monitoring of vegetation and biomass is an important issue in the context of environmental monitoring program of countries. Thus, in May 2013, the biomass mission concept of ESA was selected to become the next in a series of satellites exploring the Earth system. The polarimetric radar shall operate at 435 MHz at a 6 MHz bandwidth. To derive realistic biomass information, the contribution of the ionospheric Faraday rotation of up to one cycle at this wavelength must be estimated and corrected in a proper way.

Because TEC is the main contributor, attempts have successfully been made to estimate the 2nd order range error which is equivalent to the Faraday rotation angle over the image area from TEC maps (Hoque and Jakowski, 2006, 2008).

It is worth notice that vice versa SAR measurements can also be used to get TEC information about the ionosphere (e.g. Meyer et al., 2006; Jehle et al., 2010). Whereas the absolute TEC accuracy doesnt reach GNSS based estimations (see sections 5.5 and 5.6) the relative TEC has the advantage that measurements can be made with a resolution of 1 kilometer. This capability could be used to study the structure of ionospheric irregularities in upcoming years. Besides the range and dispersion effects due to high ionization level measurable by TEC, small scale ionospheric irregularities are a significant threat of SAR performance. As discussed in the previous section, the irregularities may cause severe amplitude scintillations. SAR applications may additionally suffer from angular scintillations and interference with backscattered waves causing defocussing. In addition, a highly structured electron density distribution causes severe fluctuations of the refractive index along the ray path leading to enhanced phase noise which also degrades the performance of SAR.

In order to mitigate ionospheric impact on radar systems such as SAR, external information provided by GNSS measurements using global geodetic networks is beneficial. How such information can be generated is considered in the subsequent section.

5.5 GNSS probing of the ionosphere

Due to the strong dependence of GNSS phase measurements on the ionospheric key parameter TEC, ground and space based dual-frequency measurements are very effective in probing the ionosphere.

Nowadays exist numerous national and international GNSS networks with high station density at distances of about 50 km. High quality open data sources are provided by the geodetic community such as the International GNSS Service (IGS) (Dow et al. 2009) or EUREF (Bruyninx et al., 2011). In particular IGS provides near real time data in 1 s streaming mode via

the Real Time Pilot Project (RTPP†). To measure ionospheric scintillations, higher sampling rates than 1Hz are required. Taking into account the need of more systematic observations, high rate measurement networks using sampling rates of 20 100 Hz are established worldwide on national level e.g. as the Scintillation Network Decision Aid (SCINDA) in US (Carrano and Groves, 2006) or via international organizations like ESA (MONITOR project, Prieto-Cerdera and Beniguel, 2011).

5.5.1 Ground-based techniques

To derive the total electron content (TEC) of the ionosphere from dual frequency ground based GNSS measurements the differential code phase defined in Eq. (5.25) is used. To mitigate strong multipath of code measurements, differential carrier phases are combined with the absolute code measurements (e.g. Jakowski, 1996). Unfortunately the higher precise differential phase delays yield only a relative measure of TEC due to the unknown number N of phase lengths contributing to the absolute phase. In analogy to Eq. (5.25) the differential carrier phase $\Delta\phi$ can be expressed by

$$\Delta\phi = \phi_1 - \phi_2 = K\frac{f_1^2 - f_2^2}{f_1^2 f_2^2} TEC_s + b_{\Delta L} + \epsilon_{\Delta L}, \tag{5.26}$$

where $b_{\Delta L}$ refers to the remaining constant or very slowly varying delays including the difference of ambiguities N, and $\epsilon_{\Delta L}$ is the residual phase noise which is much smaller than the noise of doce phase $\epsilon_{\Delta C}$ For saving the high accuracy of the differential phases, it is a common practice to level them into the code phases by least squares techniques. Naturally, the chosen approaches to calibrate the absolute code phase measurement by determining the instrumental delays $b_{\Delta C}$, are different by different research groups (e.g. Wilson and Mannucci, 1993, Sardón et al., 1994, Ciraolo et al., 1994, Jakowski, 1996).

To derive vertical TEC values serving as a geometry free reference, the slant measurements must be converted to the vertical by a so-called mapping function as illustrated in Fig. 5.10.

For doing this, the altitude dependent electron density distribution is compressed to a thin spherical layer commonly fixed at a height of $h_I \approx 350$ to 450 km. This simple assumption provides the possibility to locate the measurement at the Ionospheric Piercing Point (IPP) of the radio link with the ionospheric layer.

Applying simple geometric relationships, the mapping function $M(\epsilon)$ for converting a measured slant TEC_s to the vertical TEC at the piercing point

† http://www.rtigs.net/pilot/index.php

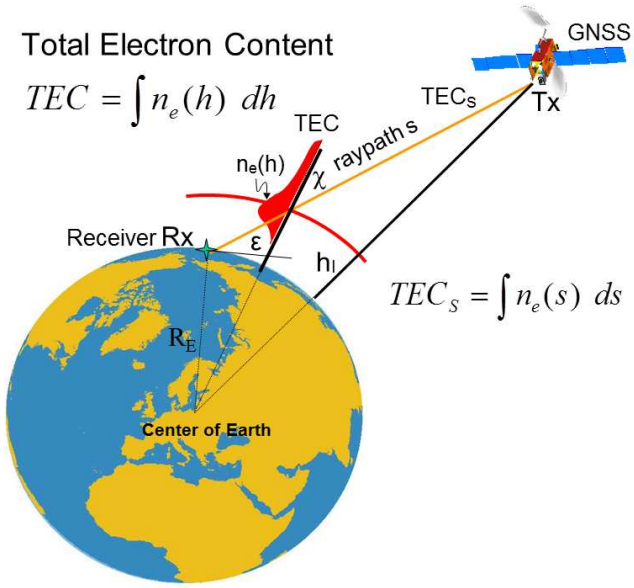

Fig. 5.10. Illustration of TEC measurements along slanted ray paths providing TECs and their transformation to the vertical TEC via a thin layer mapping function.

of the ray path with the ionospheric shell at h_I is given by:

$$M(\epsilon) = \frac{TEC_s}{TEC} = \left(1 - \left[\frac{R_E \cos(\epsilon)}{R_E + h_I}\right]^2\right)^{-1/2}, \tag{5.27}$$

where R_E is the Earth radius, h_I is the height of thin ionosphere shell and ϵ is the elevation angle.

After fixing TEC at several IPPs it is quite useful for applications to construct a vertical TEC map from the actual data. From such a reference TEC map all corrections along any slant ray paths can be made utilizing the mapping function $M(\epsilon)$) for the back transformation from vertical to slant TEC.

It is evident that the accuracy and spatial resolution of generated TEC maps depend on the availability of GNSS measurements. Again, as noticed earlier in conjunction with the bias estimation, different approaches are applied by different research groups (e.g. Wilson and Mannucci, 1993, Jakowski, 1996, Hernández-Pajares et al., 1999). As reported by Jakowski et al. (2011b) in DLR a model assisted technique is successfully used for calibrating and mapping the measured TEC over Europe since 1995 and globally since 2010. The inter frequency bias b_C can be split into a satellite bias and a receiver bias for each ray path. They are obtained by least squares fit to the NTCM model developed in DLR (Jakowski et al., 2011a). Furthermore, the model is

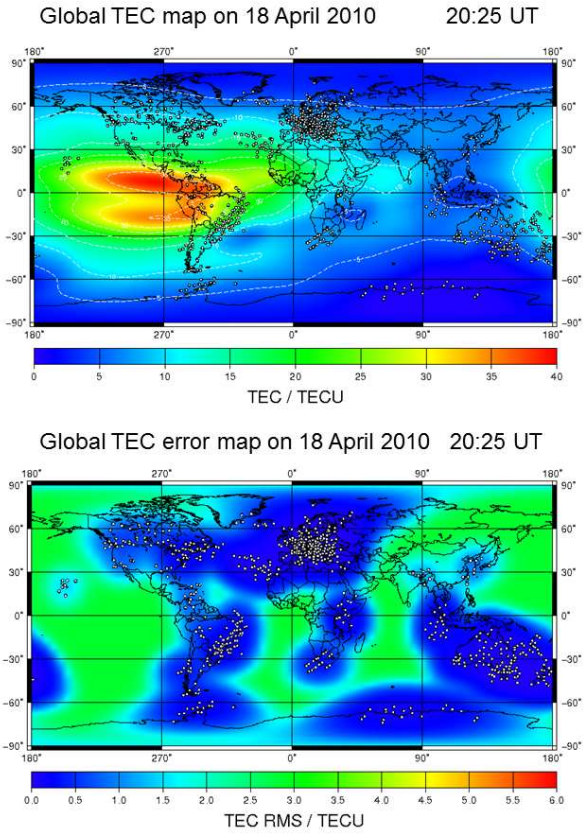

Fig. 5.11. Sample TEC map (upper panel) and corresponding TEC error map (Lower panel) generated for 18 April 2010 at 20:25 UT in the Space Weather Application CenterIonosphere of DLR (SWACI, http://swaciweb.dlr.de). Piercing points of radio links are indicated as white dots. At areas without data an average RMS error of 3.5 TECU (≈ 55 cm range error at L1) is assumed.

used as a background model to assist the mapping procedure. This procedure has the advantage that even in case of a low density GNNS network, e.g. over the oceans, sufficiently accurate TEC maps for range error corrections can be obtained (cf. upper panel of Fig. 5.11). For generating global TEC maps (grid values spaced by 2.5 degrees in latitude and 5 degrees in longitude) permanent operating GPS ground stations of the IGS network are used in DLR†. Because a user is principally interested to know the accuracy and resolution of the utilized TEC maps, it is quite useful, to create not only TEC maps but also related error maps as shown in the lower panel of Fig. 5.11. Once TEC maps

† http://swaciweb.dlr.de

have been generated, a number of secondary information can be derived such as gradient maps, or Rate of TEC (RoT) maps. Taking into account also the high temporal resolution of 1s, perturbation processes can be monitored in detail as considered in section 5.6.

For Space Based Augmentation Systems (SBAS) systems like WAAS and EGNOS a regional ionospheric correction model is defined by a grid of correction values (Grid Ionospheric Vertical Error - GIVE) at regular spacings in latitude and longitude of 5 degrees. These grid values are transmitted to single-frequency users via geostationary satellite downlink. SBAS receivers must be capable receiving the correction (TEC) map from which the individual user can derive specific link related correction information using a mapping function as defined in Eq. (5.27). SBAS systems like WAAS and EGNOS achieve an accuracy of about 1-3 m. Integrity checks made within the SBAS system provide user warnings on malfunctions within an alert time interval of 6 seconds and decide whether GIVE values can be trusted or not. Grid values are set as not monitored if the accuracy requirements cannot be guaranteed by the system in cases when the error exceeds a certain protection level. This is crucial for safety-critical aviation applications. For instance, any solution of internal system computations that exceeds a Vertical Protection Level (VPL) of 20 meters is considered as not monitored in WAAS. Thus, during ionospheric storms the number of such data gaps may increase considerably, making the SBAS service unavailable (see section 5.6).

5.5.2 Space based techniques

Dual frequency GNSS measurements can use the same observation equations Eqs. (5.24) and (5.25) for deriving ionospheric information as used in ground based techniques.

Space based GNSS measurements on board Low Earth Orbiting (LEO) satellites may essentially contribute to monitor the Geo-plasma. Thus, on the one hand GNSS radio occultation measurements are capable of monitoring the vertical ionization of the ionosphere on global scale (e.g. Hajj and Romans, 1998, Jakowski et al., 2005). On the other hand, regular navigation data used for satellite positioning can effectively be utilized to monitor the threedimensional electron density distribution of the topside ionosphere/plasmasphere near the orbit plane (Heise et al., 2002). The effectiveness of radio occultation measurements has been demonstrated by several satellite missions such as Microlab-1 with the GPS/MET experiment (Hajj and Romans, 1998), CHAMP (Jakowski et al., 2005) and in particular by the Formosat /COSMIC mission in recent years (Rocken et al., 2000).

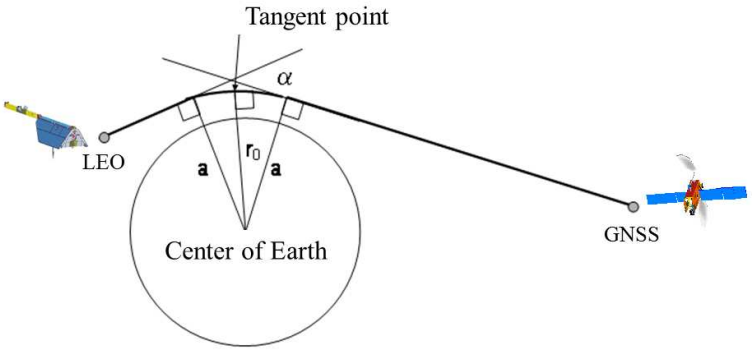

Fig. 5.12. Illustration of GNSS radio occultation geometry for retrieving the vertical electron density profile of the ionosphere.

5.5.2.1 Radio occultation technique

The radio occultation technique enables the retrieval of the vertical refractivity profile of a planetary atmosphere. Measured is the change of ray path bending, phase or signal strength of the radio wave while approaching the planetary surface in the limb sounding geometry until it is completely occulted by the planet. Thus, planetary atmospheres from Mars and Venus were explored by radio communication link occultations of spacecrafts such as Mariner IV (Kliore et al., 1967) and Venera 4, respectively. In the late 1980s, when the occultation science possibilities of GPS were recognized, it was proposed to apply the radio occultation technique also to the Earths atmosphere sounding using the L-band signals of the global positioning system GPS that was just established (Yunck et al., 1988). To prove this concept, the GPS/MET experiment onboard the Microlab 1 satellite mission, was launched in April 1994. The results of the GPS/MET experiment have demonstrated that the GPS radio occultation technique is a powerful tool for remote sensing of the Earth's neutral atmosphere and ionosphere (e.g. Hajj and Romans, 1998). More recently, a full constellation of 6 LEO satellites (COSMIC/FORMOSAT-3 mission) was deployed bringing on board radio-occultation GPS receivers among other equipment (Rocken et al. 2000). The multi-satellite COSMIC/FORMOSAT-3 mission can provide up to ≈2500 daily occultations whereas a single satellite mission like Microlab 1 or CHAMP can provide about 200-400 measurements. Indeed, FORMOSAT-3/COSMIC constellation provides a rather dense global coverage of radio occultations.

The well-known scheme of radio occultation is shown in Fig. 5.12. The refraction angle α, between the ray path asymptotes can be derived from the GNSS carrier phase measurements on board the LEO satellite with high

accuracy. Because the bending angle is principally less than one degree, the orbit data must be measured with high precision (centimeter range) and clock drifts have precisely to be removed. Introducing the impact or approaching parameter $a = \mathbf{n} \cdot \mathbf{r}$ that describes the refractive distance of the asymptotic ray path from the center of the Earth, the refraction angle α can be expressed by the refraction index n via the integral equation

$$\alpha(a) = -2a \int_{r_0}^{\infty} \frac{1}{\sqrt{r^2 n^2 - a^2}} \frac{\mathrm{d}\ln(n)}{\mathrm{d}r} \mathrm{d}r. \tag{5.28}$$

This integral equation can then be inverted by the Abel integral transform providing the vertical profile of the refractive index in terms of α and a (cf. Fjeldbo et al, 1971).

Thus, measuring the bending angle α at the refractive distance a from the satellite orbit height down to the bottom of the ionosphere, one can retrieve the vertical refractivity profile.

Taking into account Eqs. (5.4) and (5.5), it becomes clear that the Abel inversion described in Eq. (5.28) provides the vertical electron density profile from the bottom ionosphere up to the satellite orbit height. In the lower atmosphere the vertical refractive index profile reveals the neutral gas temperature in conjunction with the water vapor profile.

Instead of measuring the small refractive angle, Ionospheric Radio Occultation (IRO) measurements can take advantage of the dispersive nature of the ionosphere. Thus, differential GNSS carrier phases simply derived from dual frequency GNSS measurements on board the LEO satellite (Eq. 5.26) can effectively be used to retrieve the vertical electron density profile (e.g. Jakowski et al. 2002). When using a sampling rate of 1 Hz as in case of CHAMP and other satellites, the height resolution is a few kilometers and can be improved by taking into account ray path bending (Hoque and Jakowski, 2010, 2011a) So the IRO measurements allow collecting enormous data sets for ionospheric studies (Jakowski, 2005) and for developing and/or improving models of ionospheric key parameters such as the peak density NmF2 (e.g. Hoque and Jakowski, 2011 b) or the peak height of the F2 layer hmF2 (e.g. Hoque and Jakowski (2012).

Typical electron density profiles obtained from the CHAMP IRO data base are shown in Fig. 5.13 for years of high and low solar activity in 2002 (left panel) and 2006 (right panel).

5.5.2.2 Topside measurements

Whereas the IRO retrieval technique can utilize non-calibrated differential carrier phase measurements (Jakowski et al. 2002), the topside reconstruction technique requires calibrated TEC data measured along the numerous radio

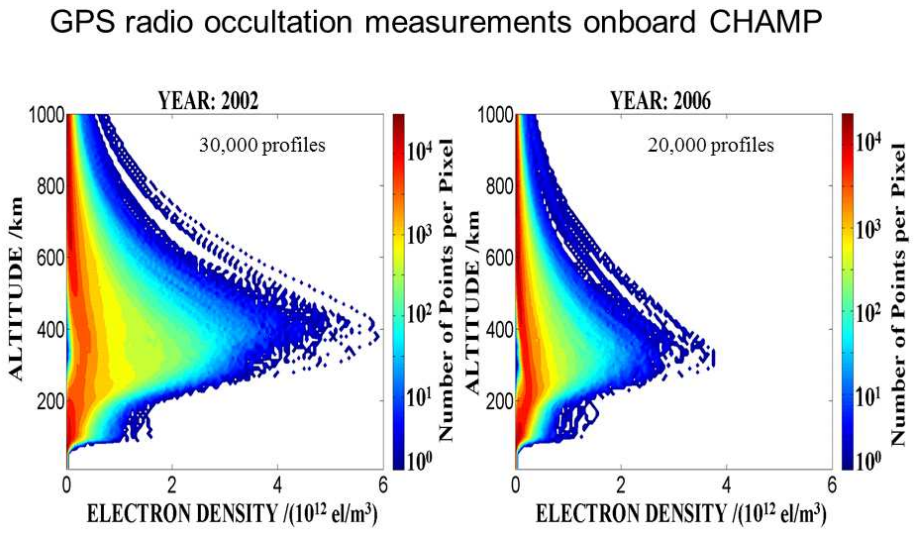

Fig. 5.13. Superposed plots of vertical electron density profiles profiles retrieved from GPS radio occultation measurements performed onboard CHAMP in2002 (left) and 2006 (right).

links between the GPS satellites and the navigation antenna onboard the LEO satellite. As a data sample from GPS measurements onboard CHAMP shows, the CHAMP-GPS satellite constellation, i.e. the data coverage changes permanently. Usually the data are not homogeneously distributed as demonstrated in Fig. 5.14. To overcome this problem, the reconstruction can be made via data assimilation into a reliable background electron density model.

Depending on the data quality up to 4000 GPS radio links are available for one revolution period. To simplify the reconstruction it is assumed that the ionosphere doesnt significantly change during one revolution (93 minutes). This is justified in most cases for large scale processes but not for medium and small scale processes.

To assimilate the link related TEC data into an ionosphere/plasmasphere model, a global three-dimensional voxel structure has been constructed by Heise et al. (2002). The voxel structure has been initialized by the Parameterized Ionospheric Model (Daniell et al., 1995). In the following an iterative process is carried out that modifies the electron density inside the voxels crossed by the CHAMP - GPS radio links to meet the link related TEC measurements. This procedure resembles the well-known Multiplicative Algebraic Reconstruction Technique (MART).

Although the reconstruction will not be an absolute correct reproduction of the real state of the topside ionosphere and plasmasphere, the result is an

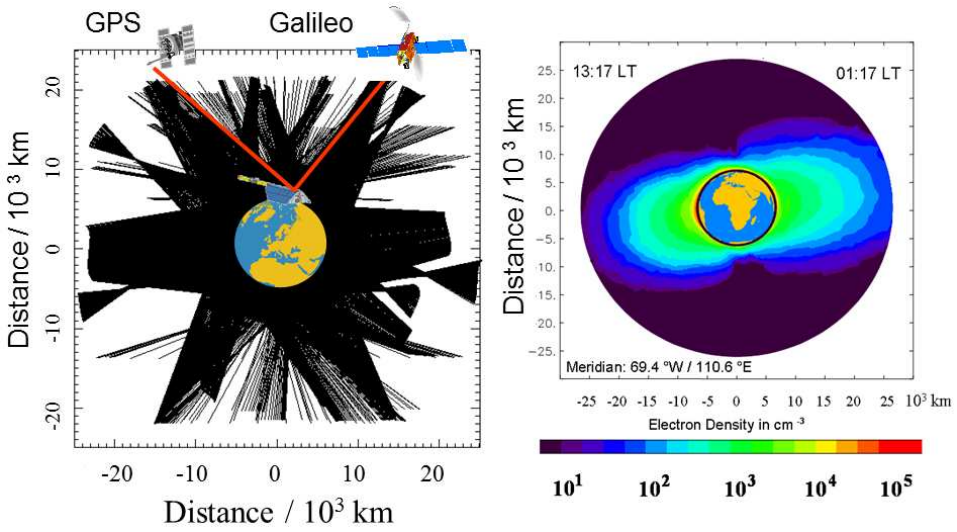

Fig. 5.14. Illustration of the topside radio link distribution in the CHAMP orbit plane to the visible GPS satellites during one satellite revolution (left panel). Reconstruction of the electron density distribution of the topside ionosphere based on GPS data received onboard CHAMP (right panel). The reconstruction is based on medians obtained for 21:00 UT over 10 consecutive days in August 2005. Thus, the right side shows the ionosphere/plasmasphere shortly after midnight whereas the left side images the plasma environment shortly after noon.

improved model output. Independent on data coverage the result is always stable and physically reasonable. The assimilation process results in a three-dimensional electron density distribution near the CHAMP orbit plane as it is seen in Fig. 5.14 (right panel). It becomes evident that the global view on the Earths plasma environment enables studying magnetospheric-ionospheric coupling processes. Here, the compression of the plasmasphere at the day-side and the enlarged extension of the plasmasphere at the night-side are clearly visible. Thus, it becomes evident that this type of space based GPS measurements can provide essential contributions to a space weather monitoring of the ionosphere and coupling processes with the Earths magnetosphere (see Vasyliunas, 2009). General speaking, the three-dimensional reconstruction of the electron density distribution of the full global ionosphere/plasmasphere systems is a challenging task in upcoming years. The reconstruction will take great benefit from ground and space based measurements considered in previous sections.

5.6 Space weather monitoring of impacts on radio systems

Whereas the principles of different radio sounding techniques have been considered in previous sections, in this section we will demonstrate the use of GNSS signals for permanent ionospheric sounding which is an integral part of space weather monitoring (for further reading see also articles in Heliophysics books by Fuller Rowell and Schrijver, 2009, Vasyliunas, 2009, Bastian, 2010, Fuller-Rowell and Solomon, 2010, Solomon, 2010, Lean and Woods, 2010). The utilization of ground and space based GNSS signals is attractive because of the rapidly growing number of ground and space based radio links, the robustness of measurements and their high accuracy. To illustrate the broad spectrum of scientific studies based on GNSS measurements typical observations for quite different studies have been selected in the following sections.

5.6.1 Direct solar radiation impact

Solar radiation bursts known as solar flares usually transmit electromagnetic waves at a broad frequency spectrum from Gamma via X-rays down to radio waves. Sudden Increase of TEC (SITEC) is a typical space weather effect in the ionosphere caused by enhanced photoionization due to solar radiation bursts at wavelengths below 130 nm were observed since many years.

Principally there is a close correlation between TEC and the solar radiation. Whereas photoionization acts immediately, the total ionization follows the solar cycle and solar irradiation changes (see Lean and Woods 2010) with a delay of 1-2 days (Jakowski et al., 1991).

During a SITEC event TEC may rapidly change up to 20 TECU or even more. The strong impact could nicely be seen during the SITEC caused by the solar flare on 28 October 2003 (Garca-Rigo et al., 2007). As Fig. 5.15 (bottom panel) shows, TEC jumps by several TECU within a few minutes and therefore may seriously limit the accuracy and reliability of GNSS applications. During this event the number of usable GPS measurements dropped down from 30 to 7 in the SWACI system. As shown by Afraimovich et al. (2002), the response of the ionosphere to faint and bright solar flares can be deduced from global GPS network data. Global GNSS networks can be used to detect in particular flares characterized by a strong EUV increase (e.g. Garcia-Rigo et al., 2007).

During solar flares besides energetic ionizing radiation also radio waves covering a broad spectrum are emitted called radio bursts (Bastian, 2010). On December 6, 2006 the radio burst intensity at GPS frequencies at L1=1575.42 MHz and L2=1227.60 MHz was extremely high so that GPS measurements at the sunlit side of the Earth were disturbed (Cerruti et al., 2006).

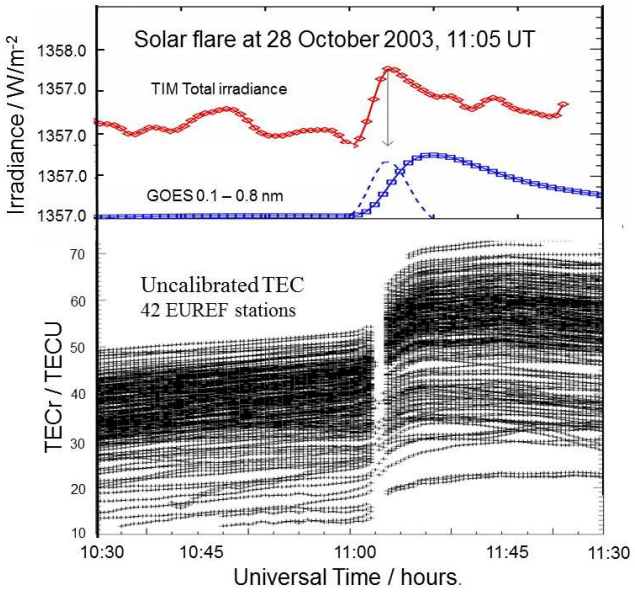

Fig. 5.15. The strong solar flare on 28 October 2003 at 11:05 UT caused an enhancement of the total solar irradiance by 267 ppm and a strong increase of TEC at all GPS measurements over Europe (range error up to about 3.5 m).

5.6.2 Solar eclipse

A solar eclipse can be considered as an active large scale plasma experiment in the ionosphere (e.g. Baron and Hunsuker, 1973; Jakowski et al., 1983; Cohen, 1984). The photoionization is switched off and switched on according to a well-defined obscuration function.

The obscuration function of the solar radiation during a solar eclipse is very helpful for studying the interaction of spatial and temporal ionosphere/thermosphere processes. The simultaneous attenuation of the solar EUV irradiation and the thermosphere heating initiates a number of closely related phenomena in the ionosphere. It has been found that the plasma redistribution during eclipses may essentially change not only the ionization level but also the electron density profile shape. Principally, it is expected that the relative depletion of ionization is more significant in the bottom-side ionosphere, at around 200 km altitude, where the photoionization is strongest, and the recombination is still significant. Observations made during the annular solar eclipse on 3rd October 2005 (Jakowski et al., 2008) indicated a change of the profile shape in the equivalent slab thickness τ derived from vertical sounding and TEC measurements according to $\tau = TEC/NmF2$. The computations revealed an increase of the equivalent slab thickness of about 30-40 km around the maxi-

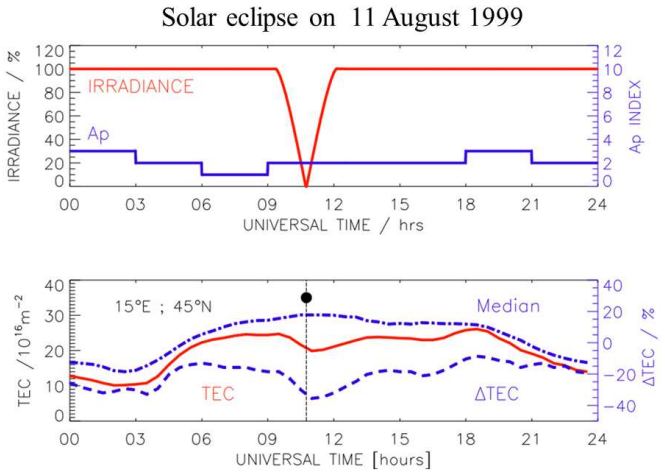

Fig. 5.16. Ionospheric depletion of the total ionization of the ionosphere (TEC) in the zone of totality at 15°E; 45°N during the solar eclipses on 11 August 1999 in comparison with the corresponding monthly median TEC.

mum eclipse phase. Whereas the total plasma depletion during the eclipse on 11 August 1999 (Fig. 5.16) reached 40% (25 − 30 TECU), the depletion was about 30% on 3rd October 2005 (15 − 20 TECU). This is in agreement with TEC observations reported earlier (Tsai and Liu, 1999; Rashid et al., 2006). The supersonic motion of the Moons cool shadow through the atmosphere can generate atmospheric gravity waves that propagate upward and are detectable as traveling ionospheric disturbances at ionospheric heights. The generation of such waves on 3rd October 2005 was indicated by ionosonde data but could not be confirmed by TEC data (Jakowski et al. 2008).

5.6.3 Particle precipitation

Instead of electromagnetic radiation also particle radiation of solar origin may increase the ionospheric ionization level (see Fuller-Rowell and Solomon, 2010). This effect is measurable by ground and space based dual frequency GNSS measurements. In this section only space based IRO retrievals from CHAMP and Formosat-3/COSMIC satellites are considered to identify particle precipitation events. Because particle precipitation of magnetospheric origin usually causes additional ionization in the auroral zone at E-layer heights, numerous IRO data sets of CHAMP and Formosat-3/COSMIC data sets have been screened to select those profiles which indicate higher ionization at E-layer heights than at F2 layer heights (Mayer and Jakowski, 2009). The E-layer

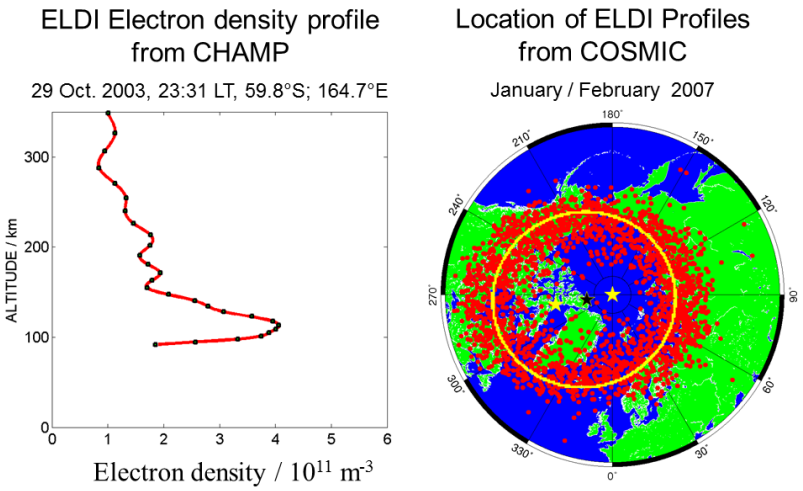

Fig. 5.17. Electron density profile retrieved from CHAMP IRO measurements on 29 October 2003 at high latitudes illustrating the E-layer dominated ionosphere (ELDI) (left panel) established during the Halloween storm. Ellipse fit to the distribution of Formosat-3/COSMIC profiles of Jan/Feb 2007 satisfying the ELDI condition (right panel). The yellow stars mark the focal points of the ellipse, the black star marks the center point of the circle fit.

dominated ionosphere (ELDI) is a clear indication of particle precipitation during space weather events. Thus, data from CHAMP collected since 2002 and from Formosat-3/COSMIC collected since 2006 were used to study the local-time and the solar cycle dependence of the observed E-layer enhancements. As shown in Fig. 5.17, selected ELDI profiles (left panel) are well distributed around the auroral zone (right panel) which has been described by an ellipse formula (Mayer and Jakowski, 2009).

During ionospheric storms the particle precipitation is essentially enhanced, often associated with fascinating polar lights. The enhanced irregular electron density distribution in the aurora zone may directly cause disruptions of GNSS measurements and services like EGNOS at high latitudes (e.g. Jakowski et al., 2012). Thus, for instance, the performance of the Norwegian geodetic network degraded due to distortions of numerous ground stations even during the moderate storm on 10/11 March 2011.

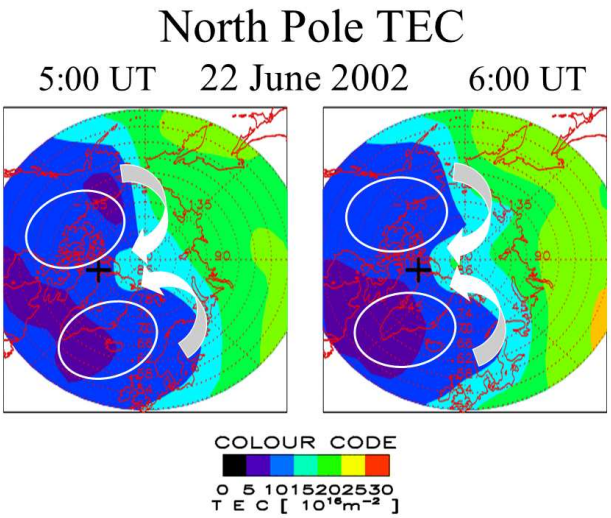

Fig. 5.18. Formation of the tongue of ionization in TEC on 22 June 2002 moving the plasma across the North Pole. Measurements have been derived from ground based GPS measurements of the IGS station network in DLR (Jakowski et al., 2011b).

5.6.4 Large scale effects - ionospheric storms

During severe space weather events enhanced solar wind energy couples into the ionosphere thus generating large perturbations in the high-latitude ionosphere and thermosphere. These perturbations are characterized by significant plasma density, composition and temperature variations as well as transport processes directed primarily towards lower latitudes (e.g. Prölss, 1995, Fuller-Rowell and Solomon, 2010).

Ground and space based GNSS measurements are well suited to monitor these perturbations (e.g. Foerster and Jakowski, 2000) as will be shown in this section. Thus the storm driven convection electric field from magnetosphere (see Vasyliunas, 2009) may move the ionospheric plasma across the pole via $E \times B$ drift from the dayside to the night side thus forming a tongue of ionization in TEC as illustrated in Fig. 5.18 for the moderate storm on 22 June 2002. A severe ionospheric storm was globally observed end of October 2003, called Halloween storm. The storm was initiated by a huge solar flare of class X17 on 28 October followed by two severe coronal mass ejections (CMEs) on subsequent days. Whereas there was an immediate TEC response on the flare (cf. Fig. 5.15) by more than 10 TECU, persistent large scale perturbations were observed later when the CMEs reached the Earth on 29 and 30 October 2003. This storm has demonstrated the reality of ionospheric threats when WAAS over the US failed for several hours (Komjathy et al., 2004). Over the

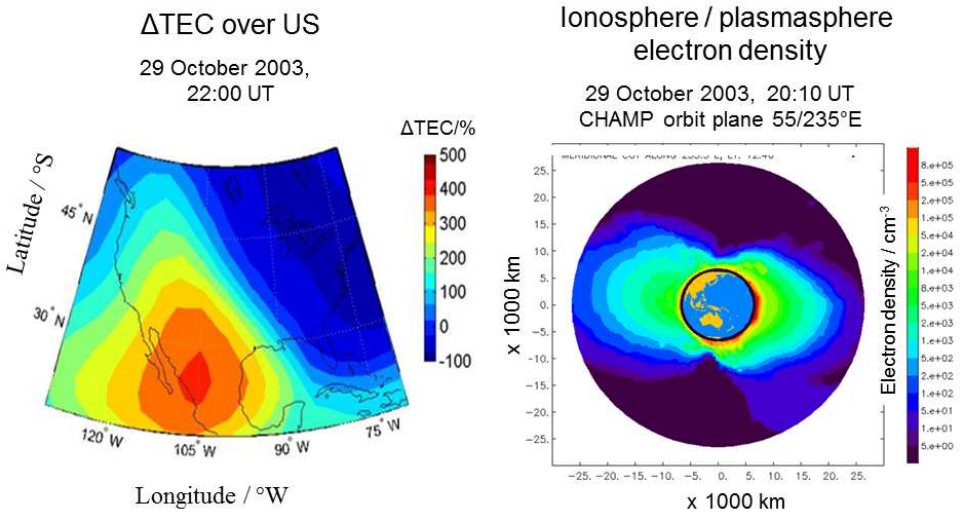

Fig. 5.19. Percentage deviations of TEC over US from corresponding monthly medians on 29 October 2003 at 22:00UT (left panel). Topside reconstruction of the electron density distribution in the CHAMP orbit plane for 29 October 2003 around 20:10 UT (right panel).

US absolute TEC values of the order of 250 TECU and deviations from the monthly mean of about 500% were observed (cf. Fig. 5.19). Severe ionization fronts as seen here are often generated in the course of space weather initiated ionospheric storms (Ho et al., 1996, Jakowski et al., 1999). A moving ionization front may cause hazardous misleading information (HMI) in a ground based augmentation system at an airport (Luo et al, 2003, Mayer et al. 2009). Consequently, the high safety standards in aviation require the development of ionospheric threat models which are specific for Europe or North America.

Anomalies have been detected at this storm also in space based GNSS measurements as Fig.5.20 shows. The strong plasma enhancement observed over US is also indicated in the plasmasphere in particular at the southern hemisphere around 125°W a little bit outside the center as shown in Fig. 5.19.

Corresponding electron density profiles derived from CHAMP IRO are summarized over October 29, 2003 in latitudinal zones along 15°E meridian and compared with corresponding average values as shown in Fig. 5.20. At the European sector we notice a strong enhancement of the electron density from about 30 up to 70°N latitude whereas the crest region around 20°N indicates a reduced electron density. It seems that a storm-driven strong $E \times B$ drift caused a severe plasma transport perpendicular to the magnetic field lines, moving northward and upward.

It is worth noting that ground and space based GNSS measurements pro-

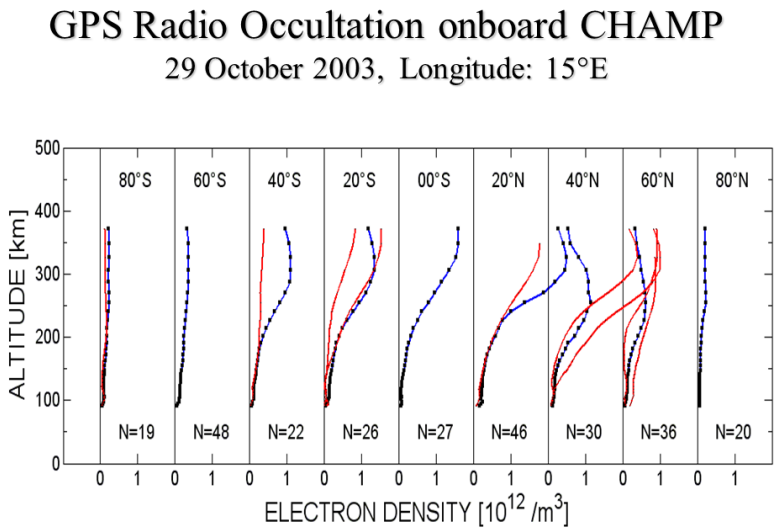

Fig. 5.20. IRO retrieved electron density profiles retrieved for 15°E longitude and different latitude zones on October 29, 2003 (red line). Comparison is made with corresponding median profiles, number N of profiles used for calculation is given.

vide valuable insight into ionospheric processes from a different point of view and therefore the observation results complete each other to get a better understanding of ionospheric processes.

Improving our understanding of ionospheric perturbations in their complexity may help developing proper mitigation techniques and forecast tools for practical applications such as satellite navigation.

Ionospheric storms degrade GNSS systems in different ways. Large and localized deviations of TEC from average behavior as mentioned above cause problems in SBAS such as WAAS and EGNOS due to mismodeling, e.g. underestimating the GIVE and related gradients in these networks as reported by Skone and Coster (2008) after analyzing storms in October and November 2003. During the Halloween storms on 29 and 30 October 2003 WAAS was unreliable during a 15-hours and 11-hours period, respectively.

EGNOS, which entered into operation for Safety of Life in March 2011, was impacted even by the moderate storm on 24/25 October 2011 (Jacobsen and Schaefer, 2012). The Norwegian real-time kinematic (RTK) network CPOS became unavailable at certain regions up to more than 90% during this storm. According to the NOAA space weather scales this was a moderate G3 storm.

Because about 200 storms of this strength can be expected during one solar cycle, network operators and users should be prepared for such events.

Differential GNSS techniques (DGNSS/RTK) rely on at least one reference station at well-known location. Ranging errors including clock, orbit and propagation errors can be estimated by comparing the computed and the known location. The residuals are broadcasted to the mobile user assuming that the same correction is required there. This assumption is justified if the user is located close to the reference receiver site. However, at some distance from the reference site the user measures errors which depend on the spatial gradient of the ionospheric delay (TEC) and the distance from the reference site. Under solar storm condition on 20 November 2003, horizontal gradients of TEC of up to 300 ppm (mm/km) were observed at mid-latitudes which would result in a zenith ionospheric error of 6 m at 20 km distance from the reference site (Powell and Walter, 2010).

5.6.5 Medium scale effects - Travelling Ionospheric Disturbances

As known from GPS studies, precise and Safety of Life applications of GNSS are not only sensitive to ionospheric gradients but also to wavelike phenomena well-known as Traveling Ionospheric Disturbances (TIDs). Medium scale TIDs (MSTIDs) are ionospheric signatures of atmospheric waves, with amplitudes of a few TECU at solar cycle maximum conditions. Their propagation velocity ranges from about 50 to 300 m/s (e.g. Hernandez-Pajares et al., 2006).Typical periods range from several minutes to about one hour.

The physical origin of MSTIDs is not well known yet. There are several options how the neutral atmosphere could generate MSTIDs, e.g. due to the perturbed atmosphere during storms, atmospheric turbulences or perturbations initiated by the solar terminator.

It is worth notice that the performance of geodetic techniques such as precise GNSS navigation and VLBI can degrade in the presence of MSTIDs in particular in winter when the occurrence probability is high. On the other hand, GNSS technique allows studying and modeling main features of MSTIDs (e.g. Hernndez-Pajares et al., 2012). Fig. 5.21 shows an example of TIDs associated with a moderate storm on 24 August 2005 (Borries et al., 2009, Saito et al. 1998). To characterize the propagation of such wave events, the TID amplitude may be traced in a Time-Latitude-Plot. So the southward propagation of the TIDs is immediately visible.

Because RTK systems primarily use carrier phase measurements for positioning, their errors are typically at the cm level providing that the correct integer number N of carrier phases in the observation equation (cf. Eq. 5.23) has been determined. The process to find the correct integer numbers N is

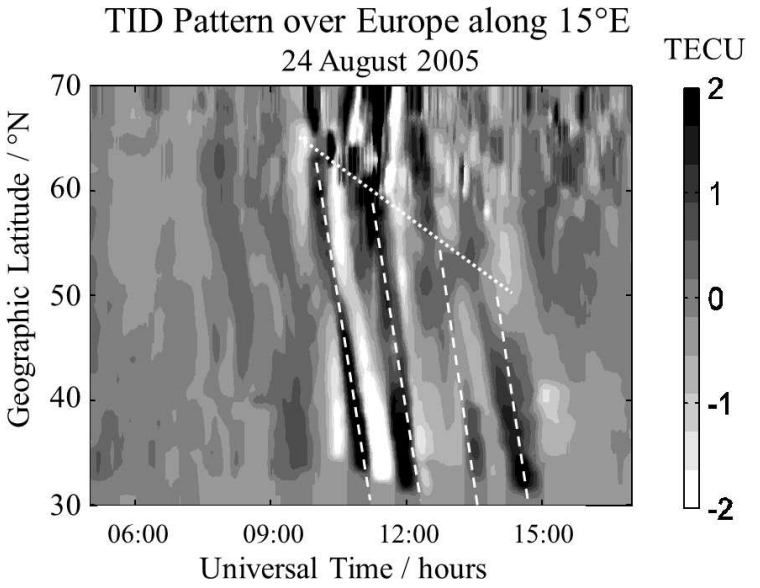

Fig. 5.21. Time-latitude plot of TEC perturbations for the 24 August 2005 around 15°E at daytime (Borries et al., 2009).

referred to as Ambiguity Resolution (AR). Whereas under quiet space weather conditions the search of the right integer number is usually successfully, the probability of a successful AR determination has been shown to drop to 78% during severe ionospheric storms (Wielgosz et al. 2005).

Besides large scale perturbations as discussed in the previous section, also medium scale TIDs may impact RTK systems. As shown by Lejeune et al. (2012), ionospheric positioning error during the occurrence of MSTIDs can reach about 25 cm for a 25 km baseline.

Because ionospheric large and medium scale perturbations are generated predominantly at high latitudes, GNSS applications are impacted in particular at high latitudes. Measurements of ionospheric disturbances and positioning network performance during geomagnetic activity in Norway have shown that the Northern part of the network is frequently disturbed, even during minor space weather events (e.g. Jacobsen and Schaefer, 2012).

5.6.6 Small scale irregularities - scintillations

Due to severe space weather impact on L-band signals of GNSS, tremendous international efforts are under way to measure and model ionospheric irregularities and resulting scintillation effects at radio signals. GNSS measurements

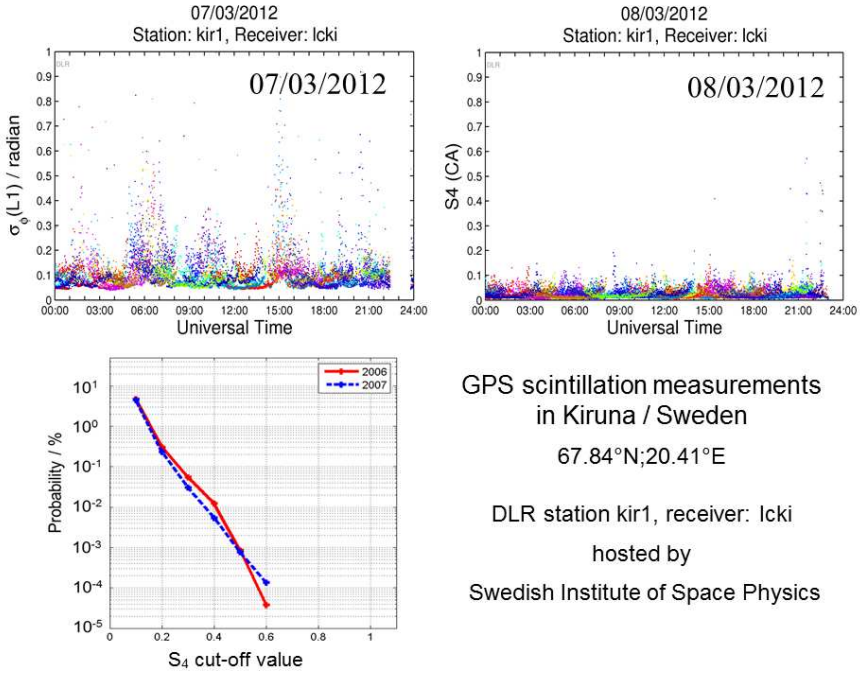

Fig. 5.22. Scintillation measurements in Kiruna, Sweden (67.8°N; 20.4°E) on March 7, 2012 (upper panels). Whereas the phase noise activity index σ_ϕ (left) indicates enhancement due to an ionospheric storm, the signal strength index S_4 (right) doesnt show remarkable activity at this high latitude station (actual information at http://www.swaciweb.dlr.de). Probability statistics for exceeding a selected cut-off value of the scintillation index S_4 in Kiruna under low solar activity conditions in the years 2006 and 2007 (lower panel).

essentially help to collect representative data sets for comprehensive theoretical and empirical data analysis. Whereas the US Airforce is establishing the low latitude SCINDA (SCINtillation and Decision Aid) ground station network (Carrano and Groves, 2006), the European Space Agency (ESA) is supporting the global deployment of scintillation receivers within the PRIS and MONITOR projects (Beniguel et al., 2009, Prieto-Cerdeira and Beniguel, 2011).

Based on a better understanding of the physics of the ionospheric plasma, forecast tools shall be developed to forecast onset of scintillation activity three to six hours in advance. A first step in this direction was the launch of the Communication / Navigation Outage Forecast System (C/NOFS) satellite of the US Air Force Research Lab in 2008 (De La Beaujardire et al., 2004). The estimation of the scintillation probability up to several hours in advance is an important issue to enhance the reliability of GNSS.

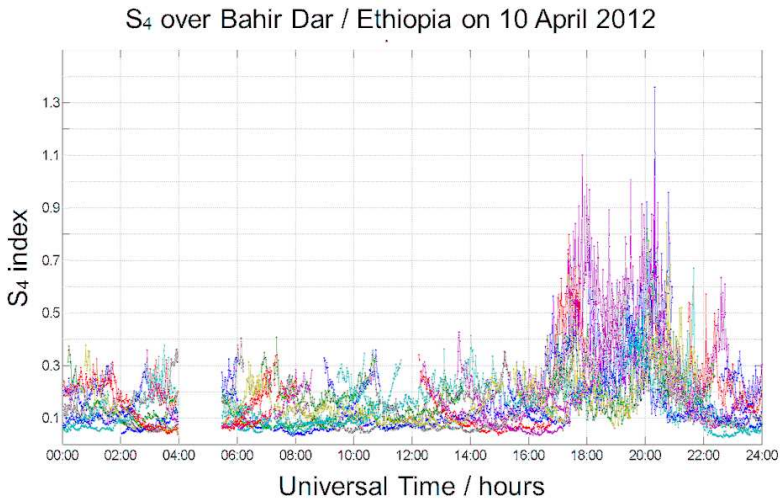

Fig. 5.23. S_4 scintillation measurements at Bahir Dar, Ethiopia (11.6°N; 37.4°E) on 11 April 2012 made on all available satellites (color marked). Onset of enhanced activity starts after sunset.

Because current GNSS such as GPS, GLONASS or Galileo operate in the L-band around 1.2 - 1.5 GHz, ionospheric scintillations have a strong impact on the functionality of these systems we rely on in our daily life. Long-term studies on scintillations have shown a strong dependence on solar activity and geophysical conditions such as location, season and daytime. As already pointed out in section 5.4.1.2, scintillations can primary be observed at high and low latitudes where they are generated by different physical processes. Scintillation effects observed at a high latitude station are shown in Fig. 5.22.

The observation results shown in Fig. 5.22 indicating that phase scintillations are much more pronounced than signal strength fluctuations, are typical for high latitudes.

This indicates a predominance of refractive index fluctuations δn versus diffraction or scattering effects at high latitudes. The latter appear primarily at low latitudes in the evening hours after sunset as considered in section 5.4.1.2. Such a behavior is confirmed in Fig. 5.23 where scintillation measurements from Bahir Dar /Ethiopia are presented. At the low latitude station at the Bahir Dar University a strong enhancement of signal strength fluctuations is observed immediately after sunset probably related to the Rayleigh plasma instability. The enhanced S_4 activity lasts typically a few hours un-

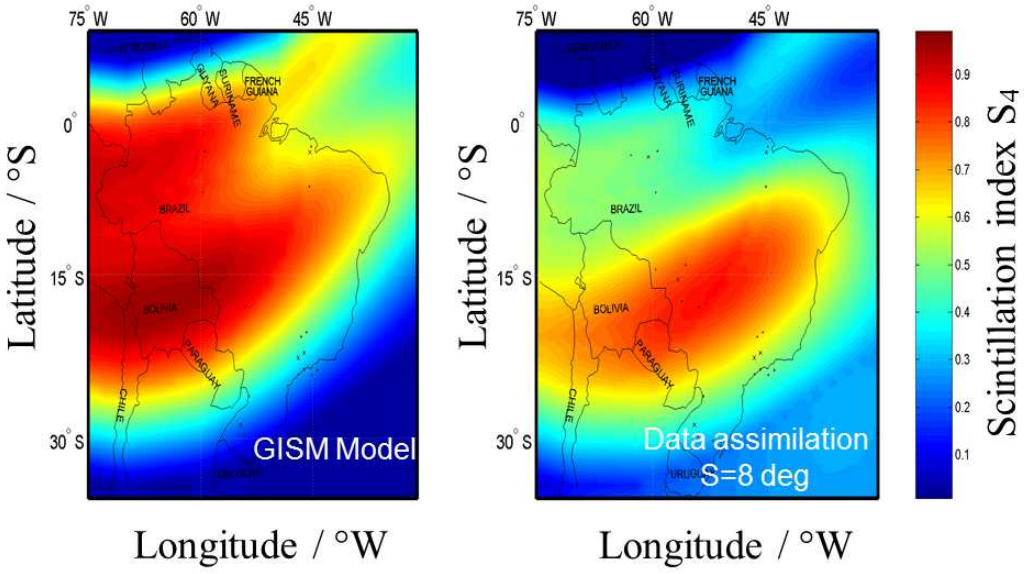

Fig. 5.24. S_4 scintillation map generated by the GISM model for January 11, 2002, at 00:30 UT, solar radio flux F10.7=150, background electron density model: NeQuick. (left panel) compared with a more realistic map generated by assimilating measured scintillation data into the GISM background model (right panel).

til midnight. Besides the scintillation strength or fading depth (more than a factor of 10 in amplitude at severe events possible in L-band) the occurrence probability is of major interest in GNSS measurement practice. To give an example, the occurrence probabilities of S_4 values which are higher than the cut-off value at x-axis are shown in Fig. 5.22. for the low solar activity years 2006/07 at the high latitude station Kiruna. Hereafter, the probability to observe severe impacts with $S_4 \geq 0.6$ under low solar activity conditions at Kiruna is of the order of less than 10^{-6}. In practical applications single station information is helpful but usually not sufficient. So it would be quiet useful to have regional or global scintillation maps available which provide scintillation information over a selected area at a given time under specific geophysical as well as space weather conditions.

Such maps can principally be generated by scintillation models such as the WBMOD (Secan et al., 1997) and GISM (Beniguel and Hamel, 2011) after feeding them with required input parameters, e. g. concerning the ionization level and solar activity.

A regional S_4 scintillation map computed for specific geophysical and solar activity conditions from GISM is shown in Fig. 5.24 (left panel). To improve the empirical and climatology model of S_4 activity, observation data can be

merged to the model. Because ionospheric models provide climatologic information, actual measurements may considerably deviate from the model. When constructing the scintillation maps, the correction is provided by the measurements. The more measurements are available, the higher is the spatial resolution of the maps. Fig. 5.24 shows the result for a large area (Brazil). Data from the following 6 stations have been provided by INPE/Brazil for January 10-18, 2002: Manaus, São Luís, Cuiabá, São José dos Campos, Cachoeira Paulista, Sáo Martinho da Serra. Assimilating these actual scintillation data into the GISM model, the resulting scintillation map is adapted to the real conditions. The assimilation procedure is the same as used for routinely generating TEC maps in DLR as shown already in Fig. 5.11 (Jakowski et al., 2011b).

Although ionospheric scintillations are due to small scale irregularities it is believed that the medium scale mapping reflects medium to large scale geophysical conditions that support the generation or maintenance of small scale irregularities in the mapping area. It is believed that the data assisted map gives more realistic information on the scintillation activity over the selected area at a concrete time. This may help users at sites where practically no measurements of scintillation activity are available.

Radio scintillations due to small scale ionospheric irregularities impact in particular the availability of GNSS signals e.g. for positioning, navigation and time transfer (PNT) services.

Today many technologies rely on GPS timing signals, mobile phone operations, banking, the internet and even the control power grids. Hence, any signal failure could cause serious problems in complex infrastructures. As already discussed, GNSS signals are vulnerable to space weather events and related ionospheric processes. If the required accuracy of timing is about 100 ns or less, ionospheric delay is not crucial in a dual frequency system. However, severe scintillations may cause loss of lock of GNSS signals (e.g. Kintner and Ledvina, 2005) thus reducing the availability of GNSS services. Whereas in SBAS systems extrem horizontal gradients of TEC are more dangerous than availability problems due to loss of lock, GNSS based time services rely on the availability and continuity of the GNSS signals. A loss of GNSS signals would disrupt a timing service with unpredictable consequences in a complex infrastructure.

5.7 Conclusions

It has been shown that there is a strong relationship between ionosphere and radio wave propagation. The initial utilization of radio waves for telecommunication was closely related to the discovery of the ionosphere. Systematic

studies of radio wave propagation have shown that the ionospheric behavior impacts or even enables radio wave propagation in many applications. On the other hand, radio waves are the most effective tool to probe the plasma of the global ionosphere with high accuracy and resolution in near real time. Both aspects have been discussed in particular for L-band signals used in the Global Navigation Satellite Systems such as GPS, GLONASS and Galileo. It has been shown that various types of ionospheric impact on radio wave propagation may degrade the performance of different user segments and systems. Ground and space based transionospheric GNSS measurements essentially contribute to monitor, model, understand and forecast the ionospheric behavior and to quantify the vulnerability of radio systems utilized in telecommunication, navigation and remote sensing. The permanent upgrading of GNSS ground station networks and the launch of new satellite missions like COSMIC-II will further contribute to the three dimensional modeling of the electron density distribution and forecast in near real time in the upcoming years. These capabilities will help to determine the full spectrum of space weather threats for the modern society and to develop adequate mitigation techniques.

Appendix I: Authors and editors

David Boteler
Natural Resources Canada
7 Observatory Crescent
Ottawa ON K1A 0Y3 , Canada
e: David.Boteler@NRCan-RNCan.gc.ca

Frances Bagenal (editor)
LASP - University of Colorado
392 UCB
Duane Room 153
Boulder, CO 80309-0392
email: Frances.Bagenal@colorado.edu

Norbert Jakowski
German Aerospace Center
Institute of Communications and Navigation
Kalkhorstweg 53
D-17235 Neustrelitz, Germany
email: norbert.jakowski@dlr.de

Karel Schrijver (editor)
Solar and Astrophysics Laboratory
Lockheed Martin STAR Labs
3251 Hanover Street, Bldg. 252
Palo Alto, CA 94304-1191
email: schryver@lmsal.com

Jan Sojka (editor)
Center for Atmospheric and Space Sciences
Utah State University
4405 Old Main Hill
Logan, UT 84322-4405
email: sojka@cc.usu.edu

Kent Tobiska
Space Environment Technologies
1676 Palisades Dr.,
Pacific Palisades, CA 90272 ...
email: ktobiska@spacenvironment.net

List of Illustrations

List of Tables

Bibliography

Adam, A., Pracser, E., & Wesztergom, V.: 2012, Acta Geod. Geoph. Hung. 47, 377, doi:10.1556/AGeod.47.2012.4.1

Afraimovich, E.L., Altynsev, A. T., Grechnev, V. V., & Leonovich, L. A.: 2002, Annals of Geophysics, doi:10.4401/ag-3480

Albertson, V.D., Kappenman, J.G., Mohan, N., & Skarbakka, G.A.: 1981, IEEE Trans. on Power App. & Sys. 100, 594

Albertson, V.D. & Thorson, J.M.: 1974, IEEE Trans. Power App. & Sys. 93, 1025

Albertson, V.D., Thorson, J.M., Clayton, R.E., & Tripathy, S.C.: 1973, IEEE Trans. Power App. & Sys. 471

Albertson, V.D., Thorson, J.M., & Miske, S.A.: 1974, IEEE Trans. Power App. & Sys. 93, 1031

Alfonsi, L., De Franceschi, G., Romano, V., Bourdillon, A., & M., Le Huy: 2011) GPS scintillations and TEC gradients at equatorial latitudes on April 2006, Advances in Space Research 47, 17501757

Allen, J., Krank, L., Sauer, H., & Reiff, P.: 1989, EOS 70, 1479

Amin, M.: 2005, *Powering the 21st Century: We can – and must – modernize the grid*, Today's Engineer: Mar 2005. http://www.todaysengineer.org/2005/Mar/grid.asp

Anderson, C.W., Lanzerotti, L.J., & Maclennan, C.G.: 1974, Bell Syst. Tech. J. 53, 1817

Appleton, E. V.: 1947

Baker, D.: 2000, IEEE Transactions on Plasma Science 28, 6

Baker, D.N.: 2009, Space Weather 7, S02003, doi:doi:10.1029/2009SW0004

Baker, D.N., Li, X., Pulkkinen, A., Ngwira, C.M., Mays, M.L., Galvin, A.B., & Simunac, K.D.C.: 2013, Space Weather 11, 585591, doi:doi:10.1002/swe.20097

Barclay, L.W.: 2003, *Propagation of Radio Waves, 2nd Edition*, The Institution of Electrical Engineers, London, UK, ISBN 085296 102 2

Barnes, P.R. & Van Dyke, J.W.: 1990, IEEE Power Eng. Review 10, 3

Baron, M.J. & Hunsuker, R.D.: 1973, Journal of Geophysical Research 78, 74517460

Bastian, T.: 2010, in C.J. Schrijver and G.L. Siscoe (Eds.), *Heliophysics: Space Storms and Radiation: Causes and Effects*, Cambridge university Press

Bedingfield, K.L., Leach, R.D., & Alexander, M.B.: 1996a, *Spacecraft System Failures and Anomalies Attributed to the Natural Space Environment, NASA Reference Publication 1390*, Marshall Space Flight Center, Alabama 35812

Bedingfield, K. L., Leach, R.D., & Alexander, M.B.: 1996b, NASA Reference Publication 1390

Beland, J. & Small, K.: 2004, in I. A. Eaglis (Ed.), *Effects of Space Weather on Technology Infrastructure*, Kluwer Acad. Publ., Dordrecht, Netherlands, p. 287

Belehaki, A., Cander, L., Zolesi, B., Bremer, J., Juren, C., Stanislawska, I., Dialetis, M., & Hatzopoulos, M.: 2006, Space Weather 4 (S12002), doi:10.1029/2006SW000270

Belov, A., Dorman, L., Iucci, N., Kryakunova, O., & Ptitsyna, N.: 2004, in *Effects of Space Weather on Technology Infrastructure*, Kluwer Academic Publishers, p. 147

Béniguel, Y., Adam, J.-P., Jakowski, N., Noack, T., Wilken, V., Valette, J.-J., Cueto, M., Bourdillon, A., Lassudrie-Duchesne, P., & Arbesser-Rastburg, B.: 2009, Radio Sci. 44, doi:10.1029/2008RS004090

Béniguel, Y. & Hamel, P.: 2011, Journal of Space Weather and Space Climate, doi:10.1051/swsc/2011004

Berg, J.: 2008, *Broadcasting On The Short Waves, 1945 To Today*, McFarland, NY

Berg Insight: 2009, *295 million GPS Handsets Sold in 2010; 940 million Expected in 2015; April 19, 2011*, http://www.gpsbusinessnews.com/tags/Berg%20Insight/, accessed April 20, 2012

Berkowitz, B.: 2011, *Extreme weather batters the insurance industry; February 09, 2011*, http://www.reuters.com/article/2011/02/09/us-insurance-climate-idUSTRE7182XG20110209?pageNumber=1, accessed May 4, 2012

Bilitza, D.: 2001, Radio Science 36, nr. 2, 261

Bilitza, D., Rawer, K., Bossy, L., & Gulyaeva, T.: 1993, Adv. Space Res. 13(3), 3

Billig, G., Feltens, J., Pallaschke, S., Smeds, B., & Volpp, H.-J: 2003, *Cluster AGC Fluctuations Working Group Final Report*, ESA Technical Note CL-COM-RP-1001-TOS, 22 December 2003

Blais, G. & Metsa, P.: 1993, in J. Hruska, M.A. Shea, D.F. Smart, and G. Heckman (Eds.), *Proc. Solar-Terrestrial Predictions Workshop, Ottawa, May 18-22, 1992; Vol. 1*, p. 108

Bolduc, L.: 2002, Journal of Atmospheric and Solar-Terrestrial Physics 64, 16, 1793

Borries, C., Jakowski, J., & Wilken, V.: 2009, Annales Geophysicae 27, 1605

Boston.com: 2012, *Computer glitch hits Brazils biggest airline; March 02, 2012*, http://articles.boston.com/2012-03-02/news/31117691_1_computer-glitch-check-in-system-airports, Accessed April 15, 2012

Boteler, D.H: 1994, IEEE Trans. Power Delivery 9, 50

Boteler, D.H: 2001a, Natural Hazards 23, 101

Boteler, D.H.: 2001b, AGU, Washington, p. 347

Boteler, D.H.: 2014, J. Space Weather and Space Climate, in press

Boteler, D.H. & Jansen van Beek, G.: 1999, Geophys. Res. Lett. 26, 577

Boteler, D.H. & Pirjola, R.J.: 1998, IEEE Trans. Power Delivery 13, 1303

Boteler, D.H., Pirjola, R.J., & Nevanlinna, H.: 1998, Advances in Space Research 22, 17

Bottollier-Depois, J.F., Chau, Q., Bouisset, P., Kerlau, G., Plawinski, L., & Lebaron-Jacobs, L.: 2000, Radiation Research 153, 526

Bowman, B.R. & Storz, M.F.: 2003, in J. LaFontaine (Ed.), *Astrodynamics 2003, 116 of Advances in Astronautical Sciences*, Univelt Inc., San Diego, AAS- 03-625

Bowman, B.R., Tobiska, W.K., Marcos, F.A., Huang, C.Y., Lin, C.S., & Burke, W.J.: 2008a, in *AIAA/AAS Astrodynamics Specialist Conference*, AIAA 2008-6438

Bowman, B.R., Tobiska, W.K., Marcos, F.A., & Valladares, C.: 2008b, JASTP 70, 774

Bozoki, B. & et al. (Working group K-11, IEEE power system relaying committee): 1996, IEEE Trans. Power Delivery 11, 725

Brekke, P., Chaloupy, M., Fleck, B., Haugan, S.V., van Overbeek, T., & Schweitzer, H.: 2004, in I.A. Daglis (Ed.), *Effects of space weather on technology infrastructure*, Kluwer Academic Publishers, p. 109

Brewitt-Taylor, C.R. & Weaver, J.T.: 1976, Geophys. J. R. Astr. Soc. 47, 375

Bruyninx, C., Baire, Q., Legrand, J., & Roosbeek, F.: 2011, *The EUREF Permanent Network (EPN): Recent Developments and Key Issues*, Presented at EUREF 2011 symposium, Chisinau, Republic of Moldova, May 25-28 2011

Budden, K.G.: 1985, *The Propagation of Radio Waves: the theory of radio waves of low power in the ionosphere and magnetosphere*, Cambridge University Press, Cambridge, ISBN 0 521 25461 2

Canfield, R.C., Hudson, H.S., & McKenzie, D.E.: 1999, Vol. 26, 627630

Careless, J: 2010, *Whatever Happened to Shortwave Radio?; 03.08.10*, http://www.rwonline.com/article/whatever-happened-to-shortwave-radio/2842, Accessed on April 19, 2012

Careless, J.: 2011, *Changes Continue for Shortwave, 10.26.2011*, http://www.rwonline.com/article/changes-continue-for-shortwave/24684, accessed on April 15, 2012

Cargill, P.J.: 2001, in I.A. Daglis (Ed.), *Space Storms and Space Weather Hazards*, Kluwer, Dordrecht, p. 177

Carrano, C.S. & Groves, K.: 2006, Proceedings of the 2006 National Technical Meeting of The Institute of Navigation, Monterey, CA, January 2006, p. 1036

CBS News: 2012, *Satellite problems ground Nunavut flights; October 6, 2011*, http://www.cbc.ca/news/technology/story/2011/10/06/north-satellite-phone- outage.html?cmp=rss, accessed April 15, 2012

Center, National Geophysical Data: 2007a, http://goes.ngdc.noaa.gov/data/plots/

Center, National Geophysical Data: 2007b, *Ap-Kp data from http://www.ngdc.noaa.gov/stp/GEOMAG/kp_ap.html*

Cerruti, A.P., Kintner, P.M., Gary, D.E., Lanzerotti, L.J., de Paula, E.R., & Vo, H.B.: 2006, Space Weather 4 (S10006), doi:10.1029/2006SW000254

Chapman, S.: 1931, Proc. Phys. Soc. 43, 1047

Charbonneau, P.: 2010, in C.J. Schrijver and G.L. Siscoe (Eds.), *Heliophysics: Evolving solar activity and the climates of space and earth*, Cambridge University Press; United Kingdom, p. 141

Chin, J.: 2005, J. of Astron. Astrophys. 5, 110

Cho, M. & Nozaki, Y.: 2005, J. Spacecr. Rockets. 42, N. 4, 740

Ciraolo, L., Spalla, P., & Beni, P.: 1994, Proceedings BSS94, Univ. of Wales, Aberystwyth, p. 21

Clark, S: 2010, *Galaxy 15 'zombiesat' still alive after expected off date; ,September 15, 2010*, http://www.spaceflightnow.com/news/n1009/15galaxy15/, accessed April 21, 2012

Cohen, E.A.: 1984, Radio Science 19, 769777

Colak, T. & Qahwaji, R.: 2007, Springer, p. 316, http://spaceweather.inf.brad.ac.uk/journals/wsc11_tc_rq.pdf, accessed April 20, 2012

Congress: 2003, *What is space weather and who should forecast it?: hearing before the Subcommittee on Environment, Technology, and Standards, Committee on Science, House of Representatives, One Hundred Eighth Congress, first session, October 30, 2003, Volume 4*, http://www.solarstorms.org/CongressSW.html, accessed, April 23, 2012.

Connors, M., Rostoker, G., Sofko, G., McPherron, R.L., & Henderson, M.G.: 2003, Annales Geophysicae 21, 493

Cucchi, G. & Ponder, J.: 1991, *Summary of March 13, 1989 geomagnetic storm effects*, presented at the Dallas Transmission & Distribution Conference, Sept. 26

Czeck, P., Huynh, H., & Dutil, A: 1992, in B. Damsky (Ed.), *Geomagnetically Induced Currents Conference, November 8-10, 1989, San Francisco*, Electric Power Research Institute, EPRI-TR-100450, p. 19

Daniell, R.E., Brown, L.D., Anderson, D.N., Fox, M.W., Doherty, P.H., Decker, D.T., Sojka, J.J., & Schunk, R.W.: 1995, Radio Sci. 30, 1499

Davidson, W.F.: 1940, Edison Electric Institute Bulletin 8, 365

Davies, K.: 1980, Space Science Reviews 25, 357

Davies, K.: 1990, *The ionospheric radio*, Peter Peregrinus Ltd, London. ISBN 0-86341-186-X

De La Beaujardière, O. & et al.: 2004, J. Atmos. Sol. Terr. Phys. 66, 15731591, doi:10.1016/j.jastp.2004.07.030

De Shelding, P.: 2011, *Electrostatic discharge crippled Galaxy 15 Intelsat says; January 13, 2011*, http://www.spacenews.com/satellite_telecom/110113-electrostatic-discharge- galaxy15.html, accessed April 15, 2012

Department of Energy: 2005, *Gridworks*, Office of Electricity and Energy Reliability: http://www.energetics.com/gridworks/index.html

Doherty, P.H.: 2011, *Space Weather Effects on GPS and WAAS; August 5, 2011*, http://www.bc.edu/research/isr/spaceweathereffect.html, accessed April 15, 2012

Dong, X., Liu, Y., & Kappenman, J.G.: 2001, Proc. IEEE 2001 Winter Meeting, Columbus, OH 318–322

Dorman, L. I. & et al.: 2005, Annales Geophysicae 23, 3009

Dow, J.M., Neilan, R.E., & Rizos, C.: 2009, Journal of Geodesy 83, Issue 3-4, 191

Duncan, G.: 2010, *Use a cellphone? Join the rest of mankind!*, http://www.digitaltrends.com/mobile/two-thirds-of-all-humans-use-a-cell-phone/, accessed May 2, 2012

Eaton Corporation: 2011, *Blackout Tracker: 2011 Annual Report*, http://powerquality.eaton.com/info/GenOutput.asp?Quest_user_id=657593&-leadG_Q_QRequired=False&menu=, April 20, 2012

Electromagnetic Pulse Commission: 2008, *Report of the Commission to Assess the Threat to the United States from Electromagnetic Pulse (EMP) Attack*

Elovaara, J., Lindblad, P., Viljanen, A., Mäkinen, T., Pirjola, R., Larsson, S., & Kielen, B.: 1992, *Geomagnetically induced currents in the Nordic power system and their effects on equipment, control, protection and operation*, pres. CIGRE Colloquim, 30 Aug - 5 Sept.

Energy Information Agency (EIA): 2006, *Electric Power Annual with data for 2005; EIA/DOE: revised 09.11.2006*, http://www.eia.doe.gov/cneaf/electricity/epa/epa_sum.html

Erinmez, A., Kappenman, J. G., & Radasky, W. A.

Falconer, D.A.: 2001, JGR 106, No. A11, 25,185

Farthing, W.H., Brown, J.P., & Bryant, W.C.: 1982, *NASA Tech Memo 83908, March 1982*, NASA

Fennell, J. F. & et al.: 2000, IEEE Trans. On Plasma Physics 28, 2029

Ferguson, I. J. & Odwar, H. D.: 1997, *Review of conductivity soundings in Canada, vol 3, Geomagnetic Hazard Assessment, Phase II*, Geological Survey of Canada, Open File No. 3420

Fernberg, P.A., Samson, C., Boteler, D.H., Trichtchenko, L., & Larocca, P: 2007, Annales Geophysicae 25, no. 1, 207

Ferris, D. L.: 2001, *Ph.D. thesis*, Masters Thesis, Department of Aeronautics and Astronautics, Massachusetts Institute of Technology

Ferster, W.: 2005, July 7, *Satellite industry revenue jumps 6 percent in 2003*, Space News

Fiori, R.A.D., Boteler, D.H., & Gillies, D.M.: 2014, Space Weather 12, 76

Fjeldbo, G.A., Kliore, J., & Eshleman, V.R.: 1971, Astronomical Journal 76, 123

Foerster, M. & Jakowski, N.: 2000, Surveys in Geophysics 21, 47

Forbes, T.: 2010, in C.J. Schrijver and G.L. Siscoe (Eds.), *Heliophysics: Space storms and radiation- causes and effects*, Cambridge University Press; United Kingdom, p. 159

Force, Task: 2004, *Final Report on the August 14, 2003 Blackout in the United States and Canada: Causes and Recommendations, U.S.-Canada Power System Outage Task Force*, https://reports.energy.gov/

Fukao, S., Yokoyama, T., Tayama, T., Yamamoto, M., Maruyama, T., & Saito, S.: 2006, Ann. Geophysicae 24, 1411

Fuller-Rowell, T. & Schrijver, C. J.: 2009, in C.J. Schrijver and G.L. Siscoe (Eds.), *Heliophysics: Plasma Physics of the Local Cosmos*, Cambridge university Press

Fuller-Rowell, T. & Solomon, S.C.: 2010, in C.J. Schrijver and G.L. Siscoe (Eds.), *Heliophysics: Space Storms and Radiation: Causes and Effects*, Cambridge university Press

Futron: 2002, July 10, *Satellite Insurance Rates on the Rise - Market correction or overreaction?*

Gallagher, P.T., Moon, Y.-J., & Wang, H.: 2002, Solar Phys. 209, 171

Garcia-Rigo, A., Hernandez-Pajares, M., Juan, J.M., & Sanz, J.: 2007, Advances in Space Research 39, ...

Gattens, P.R.: 1989, IEEE Power Engineering Review 19–20

Gaunt, C.T. & Coetzee, G.: 2007, in *Power Tech, 2007, IEEE Lausanne*, 807812

Gilbert, J.L.: 2005, Space Weather 3, S04A03, doi:10.1029/2004SW000120

Girgis, R. & Vedante, K.: 2013, in *Proc. IEEE Power & Energy Society General Meeting, Vancouver*

GMDTF: 2012, *Geomagnetic Disturbance Task Force Interim Report*, North American Electricity Reliability Corporation, Atlanta, GA

Gopalswamy, N., Aguilar-Rodriguez, E., Yashiro, S., Nunes, S., Kaiser, M.L., & Howard, R.A.: 2005, JGR 110, A12S07, doi:10.1029/2005JA011158

Hajj, G.A. & Romans, L.J.: 1998, Radio Sci. 33, 175

Hamachi-LaCommare, K. & Eto, J.: 2004, *Understanding the Cost of Power Interruptions to U.S. Electricity Consumers*, http://certs.lbl.gov/pdf/55718.pdf, accessed April 21, 2012

Hannah, E.: 2004, *Cosmic ray detectors for integrated circuit chips*, US Patent 7,309,866; http://patft.uspto.gov/netacgi/nph-Parser?Sect1=PTO1&Sect2=HITOFF&d=PALL&p=1&u=%2Fnetahtml%2-FPTO%2Fsrchnum.htm&r=1&f=G&l=50&s1=7,309,-866.PN.&OS=PN/7,309,866&RS=PN/7,309,866. Accessed April 15, 2012

Hecht, H. & Hecht, M.: 1986, *Reliability Prediction for Spacecraft*, Rome Air Development Center, Griffiss Air Force Base, New York, RADC-TR-85-229

Heise, S., Jakowski, N., Wehrenpfennig, A., Reigber, Ch., & Lühr, H.: 2002, Geophysical Research Letters 29, No. 14, doi:10.1029/2002GL014738

Held, G.: 2002, *Understanding Data Communications*, New Riders Publishing, NY, Sixth Edition, Chapter 7

Hernández-Pajares, M., Juan, J.M., & Sanz, J.: 1999, J. Atmos. Sol.-Terr. Phys. 61, 1237

Hernández-Pajares, M., Juan, J.M., & Sanz, J.: 2006, J. Geophys. Res. 111, A07S11, doi:10.1029/2005JA011474

Hernández-Pajares, M., Juan, J.M., Sanz, J., & Orús, R.: 2007, Journal Geophys. Res. 112, B08417, doi:10.1029/2006JB004707

Ho, M. C., Manucci, A. J., Lindquister, U. J., Pi, X., & Tsurutani, T. T.: 1996, Geophys. Res. Lett. 23, 3219

Hoque, M.M. & Jakowski, N.: 2006, Journal of Geodesy, doi:10.1007/s00190-006-0106-0

Hoque, M.M. & Jakowski, N.: 2008, Radio Sci. 43, RS5008, doi:10.1029/2007RS003817

Hoque, M.M. & Jakowski, N.: 2010, Adv. Space Res. 46, 162, doi:10.1016/j.asr.2010.02.013

Hoque, M.M. & Jakowski, N.: 2011a, Radio Sci. 46, No. RS0D06, doi:10.1029/2010RS004583

Hoque, M.M. & Jakowski, N.: 2011b, Radio Sci. 46, RS6015, doi:10.1029/2011RS004807

Hoque, M.M. & Jakowski, N.: 2012, Annales Geophysicae 30, 787, doi:10.5194/angeo-30-797-2012

Hoyos, S.E., Evans, H.D.R., & Daly, E.: 2004, IEEE Trans. Nucl. Sci. 51, 2927

Hudson, H.S.: 2010, in C.J. Schrijver and G.L. Siscoe (Eds.), *Heliophysics: Space storms and radiation- causes and effects*, (Cambridge University Press; United Kingdom, p. 123

Hunsucker, R.D.: 1991, Physics and Chemistry in Space 22, Planetology, Springer-Verlag Berlin Heidelberg 1991, ISBN 3-540-5346-7

Idaho National Laboratory: 2005, *Reevaluation of Station Blackout Risk at Nuclear Power Plants–Analysis of Station Blackout Risk*, http://www.nrc.gov/reading-rm/doc- collections/nuregs/contract/cr6890/, accessed April 20, 2012

International Cable Protection Committee (ICPC): 2009, *Fishing and Submarine Cables Working Together*, http://cil.nus.edu.sg/wp/wp-content/uploads/2009/10/ICPC-Fishing-Booklet- 090223.pdf, Accessed on April 18, 2012

ISO 14222: 2013, *Space environment (natural and artificial) Earth upper atmosphere*, International Standards Organization, Geneva

ISO 16290: 2012, *Definition of the Technology Readiness Levels (TRL) and their criteria of assessment*, International Standards Organization, Geneva

ISO 16457: 2014, *Space systems Space environment (natural and artificial) The Earths ionosphere model: international reference ionosphere (IRI) model and extensions to the plasmasphere*, International Standards Organization, Geneva

Jacobsen, K.S. & Schaefer, S.: 2012, J. Space Weather Space Clim. 2, A13, doi:10.1051/swsc/2012013

Jakowski, N.: 1996, in H. Kohl, R. Rüster, and K. Schlegel (Eds.), *Modern Ionospheric Science*, EGS, Katlenburg-Lindau, ProduServ GmbH Verlagsservice, Berlin, p. 371

Jakowski, N.: 2005, GPS Solutions 8895, doi:10.1007/s10291-005-0137-7

Jakowski, N., Béniguel, Y., De Franceschi, G., Hernández-Pajares, M., Jacobsen, K.S., Stanislawska, I., Tomasik, L., Warnant, R., & Wautelet, G.: 2012, J. Space Weather Space Clim. 2 (A22), doi:10.1051/swsc/2012022

Jakowski, N., Bettac, H.D., Lazo, B., Palacio, L., & Lois, L.: 1983, Physica Solar-iterrestris 20, 110116

Jakowski, N., Fichtelmann, B., & Jungstand, A.: 1991, J. Atmos. Terr. Phys. 53, 1125

Jakowski, N., Hoque, M.M., & Mayer, C.: 2011a, J. Geod. 85(12), doi:10.1007/s00190-011-0455-1

Jakowski, N., Mayer, C., Hoque, M.M., & Wilken, V.: 2011, Radio Sci. 46, RS0D18, doi:10.1029/2010RS004620

Jakowski, N., Mayer, C., Hoque, M.M., & Wilken, V.: 2011b, Radio Sci. 46, RS0D18, doi:10.1029/2010RS004620

Jakowski, N., Putz, E., & Spalla, P.: 1990, Ann. Geophysicae 8, 343

Jakowski, N., Schlueter, S., & Sardon, E.: 1999, J. Atmos. Solar-Terr. Phys. 61, 299

Jakowski, N., Stankov, S.M., Wilken, V., Borries, C., Altadill, D., Chum, J., Buresova, D., Boska, J., Sauli, P., Hruska, H., & Cander, L.: 2008, J. Atmos. Solar-Terr. Phys. 70, 836, doi:10.1016/j.jastp.2007.02.016

Jakowski, N., Wehrenpfennig, A., Heise, S., Reigber, Ch., Lühr, H., Grunwaldt, L., & Meehan, T.: 2002, Geophys. Res. Lett. 29, No. 10, doi:10.1029/2001GL014364

Jehle, M., Frey, O., Small, D., & Meier, E.: 2010, IEEE transactions on Geoscience and Remote Sensing 01/2010 48, 2460

Jose, P. D.: 1965, AJ 70(3), 193

JPL: 2012, April 20, *Ionospheric TEC Map*, http://iono.jpl.nasa.gov/latest_rti_global.html, accessed April 20, 2012

Kappenman, J.G., Space Weather S01004, doi:10.1029/2003SW000028

Kappenman, J.G., IEEE Power Engineering Review 5–

Kappenman, J.: 1997, EOS Transactions January 29, 37

Kappenman, J.G.: 2001, in I.A. Daglis (Ed.), *NATO Science Series*, Kluwer

Kappenman, J.G.: 2003, Space Weather 1, 1016, doi:doi:10.1029/2003SW000009

Kappenman, J.G.: 2010, *Geomagnetic Storms and Their Impacts on the U.S. Power Grid, Report no. Meta-R-319*, Metatech Corporation, submitted to Oak Ridge National Laboratory

Kappenman, J.: 2010, January, *Low-frequency protection concepts for the electric power grid: Geomagnetically Induced Current and E3 HEMP mitigation*

Kappenman, J.: 2012, *Impact of Severe Solar Flares, Nuclear EMP and Intentional EMI on Electric Grids, The Electric Infrastructure Security Summit, Third Annual World Summit, London*, http://www.eissummit.com/images/upload/conf/media/EIS_Kappenman_Part1.pdf; accessed April 20, 2012

Kappenman, J.G., Norr, S.R., Sweezy, G.A., Carlson, D.L., Albertson, V.D., Harder, J.E., & Damsky, B.L.: 1991, IEEE Trans. Power Delivery 6, 1271

Kappenman, G., J.: 2003a, Space Weather 1, 1011, doi:10.1029/2003SW000027

Kappenman, J. G., Space Weather 3

Kappenman, J. G.: 2003b, Space Weather 1, doi:10.1029/2003SW000009

Karn, R.: 2007, April 4, *Electrifying Change*, http://www.energybulletin.net/node/29104, accessed Apriul 15, 2012

Kedar, S., Hajj, G., Wilson, B., & Heflin, M.: 2003, Geophys. Res. Lett. 30 (16), 1829, doi:10.1029/2003 GL017639

Kintner, P.M. & Ledvina, B.M.: 2005, Adv. Space Res. 35, 788

Kirby, B.J., Kueck, J.D., & Poole, A.B.: 1988, *Evaluation of the Reliability for the Offsite Power Supply as a Contributor to the Risk of Nuclear Plants; ORNL/NRC/LTR-98/12*, http://www.consultkirby.com/files/NRC.pdf, accessed April 23, 2012

Kliore, A.J., Levy, G.S., Cain, D.L., Fjeldbo, G., & Rasool, I.: 1967, Science 158, 1683

Klobuchar, J.A.: 1987, IEEE Transactions on aerospace and electronic systems AES-23, No 3, 325331

Komjathy, A., Sparks, L., Mannucci, A.J., & Coster, A.: 2004, in *Proc. of ION GPS 2004, Long Beach, CA., Sept. 21-24*

Koons, H.C.: 2000, in *The Impact of the space environment on space systems; Proceedings of the 6th Spacecraft Charging Technology Conference*, Air Force Research Laboratory

Koons, H.C., Mazur, J.E., Selsnick, R.S., Blacke, J.B., Fennell, J.F., Roeder, J.L., & Anderson, P.C.: 1999, *The Impact of the Space Environment on Space Systems, Aerospace technical Report, TR-99(1670)-1, July 20, 1999*, Space and Missle Systems Center, Air Force Materials Command ,2430 E. El Segundo Boulevard, Los Angeles Air Force Base, CA, 90245

Kumar, S., Kishore, A., & Ramachandran, V.: 2007, Phys. Scr. 75, 258

L, Bolduc & Aubin, J.: 1978, Electr. Power Syst. Res. 1, 291

Lam, H.L., Boteler, D.H., & Trichtchenko, L.: 2002, Annales Geophysicae 20, 1073

Lanzerotti, L.J.: 2012, Space Weather 10, S02010

Lanzerotti, L.J.: 2014, Space Weather 12, doi:doi:10.1002/2014SW001076

Lanzerotti, L.J., Gary, D.E., Nita, G.M., Thomson, D.J., & Maclennan, C.G: 2005, Adv. in Space Research 36, No. 12, 2253

Lanzerotti, L.J. & Gregori, G.P., *Telluric Currents: the Natural Environment and Interactions with Man-made Systems*

Le, A.Q., Tiberius, C.C.J.M., Van der Marel, H., & Jakowski, N.: 2008, in *Observing our Changing Earth International Association of Geodesy Symposia, 133*, Springer Berlin Heidelberg, p. 759, ISBN 978-3-540-85425-8

Lean, J.L. & Woods, T.N.: 2010, in C.J. Schrijver and G.L. Siscoe (Eds.), *Heliophysics: Evolving Solar Activity and the Climates of Space and Earth*, Cambridge university Press

Lehtinen, M. & Pirjola, R.: 1985, Annales Geophysicae 3, 479

Lejeune, S., Wautelet, G., & Warnant, R.: 2012, GPS Solutions 16, 105116

Liu, C.-M., Liu, L.-G., & Pirjola, R.: 2009, IEEE Trans. Power Delivery 24(4), 2368, doi:10.1109/TPWRD.2009.2028490

Luo, M., Pullen, S., Dennis, J., Konno, H., Xie, G., Walter, T., Enge, P., Datta-Barua, S., & Dehel, T.: 2003, in *Proc. of ION GPS 2003, Portland, OR., Sept. 9-12*

Mack, E.: 2011, Oct. 6, *Major satellite outage affecting ISPs, ATMs and flights*, http://news.cnet.com/8301-1023_3-20116846-93/major-satellite-outage-affecting-isps-atms-flights/, accessed April 15, 2012

Maguire, T. & Woodford, D: 1990, *Geomagnetic induced current effect on SVC operation, CEA Report 316 T 745*

Marowits, R.: 2011, Oct. 6, *Satellite outage disrupts communications in Canadas North*, http://www.jocosarblog.org/jocosarblog/2011/10/satellite-outage-disrupts-communications-in-canadas-north.html, accessed April 15, 2012

Marshall, R. A., Dalzell, M., Waters, C. L., Goldthorpe, P., & Smith, E. A.: 2012, Space Weather 10, S08003, doi:10.1029/2012SW000806

Marshall, R. A., Gorniak, H., Van Der Walt, T., Waters, C. L., Sciffer, M. D., Miller, M., Dalzell, M., Daly, T., Pouferis, G., Hesse, G., & Wilkinson, P.: 2013, Space Weather 11, 6, doi:10.1029/2012SW000849

Marshall, R. A., Smith, E.A., Francis, M.J., Waters, C.L., & Sciffer, M.D.: 2011, Space Weather 9, S10004

Marti, L., Rezaei-Zare, A., & Boteler, D., IEEE Trans. Power Delivery", volume= 29, pages=802-807, year=2014

Marti, L., Rezaei-Zare, A., & Yan, A.: 2013, *Modelling considerations for the Hydro One real-time GMD management system, Proc. IEEE Power & Energy Society*

General Meeting, Vancouver

Martin, G.: 2012, Jan. 25, *SumbandilaSat beyond repair*, http://www.defenceweb.co.za/index.php?option=com_content&view=article&-id=22870:sumbandilasat-beyond-repair&catid=90:science-a-technology&Itemid=204, Accessed April 20, 2012

Mayer, C., Belabbas, B., Jakowski, N., Meurer, M., & Dunkel, W.: 2009, in *ION GNSS 2009, 22-25 Sep. 2009, Savannah, GA, USA*

Mayer, C. & Jakowski, N.: 2009, Ann. Geophys. 27, 1207

M.C., Kelley.: 1989, *The Earths Ionosphere, International Geophysics Series, Vol. 43*, Academic Press, Inc., San Diego, ISBN 0-12-404013-6

McCracken, K.G., Dreschoff, G.A.M., Zeller, E.J., Smart, D.F., & Shea, M.A.: 2001, J. Geophys. Res. 106 (A10), 21,585

McKay, A.J. & Whaler, K.A.: 2006, Geophys. J. Int. 167, 613

McPherron, R.L.: 2005, Surveys in Geophysics 26, 545

Mertens, C.J., Kress, B.T., Wiltberger, M., Blattnig, S.R., Slaba, T.S., Solomon, S.C., & Engel, M.: 2010, Space Weather 8, 3, doi:doi:10.1029/2009SW000487

Mertens, C.J., Kress, B.T., Wiltberger, M.J., Tobiska, W.K., Grajewski, B., & Xu, X.: 2012, in M. Nenoi (Ed.), *Current Topics in Ionizing Radiation Research*, ISBN: 978-953-51-0196-3, InTech

Mertens, C.J., Meier, M.M., Brown, S., Norman, R.B., & Xu, X.: 2013, Space Weather 11, 10, 603635, doi:doi:10.1002/swe.20100

Mertens, C.J., Tobiska, W.K., Bouwer, D., Kress, B.T., Wiltberger, M.J., Solomon, S.C., & Murray, J.J.: 2009, in *AIAA 2009-3633, 1st AIAA Atmospheric and Space Environments Conference, San Antonio, Texas*

Meyer, F., Bamler, R., Jakowski, N., & Fritz, Th.: 2006, IEEE Geoscience and Remote Sensing Letters 3, Nr. 4, 560

Molinski, T.S.: 2002, Journal of Atmospheric and Solar-Terrestrial Physics 64, 1765

Murtagh, W.: 2010, Sep. 8, *Space weather impacts on aviation systems*, http://www.easa.europa.eu/conferences/iascc/doc/Workshop%201%20Presentations/Workshop1_DAY%201/3_Murtagh_NOAA/Space%20Weather%20Impacts-%20on%20Aviation%20Systems.pdf, accessed April 15, 2012

National Academies Press: 2008, *Severe Space Weather EventsUnderstanding Societal and Economic Impacts Workshop Report, Committee on the Societal and Economic Impacts of Severe Space Weather Events: A Workshop, Space Studies Board, Division on Engineering and Physical Sciences, National Research Council, Washington, DC, ISBN: 0-309-12770-X*

National Academies Press: 2012a, *Solar and Space Physics: A Science for a Technological Society, Committee on a Decadal Strategy for Solar and Space Physics (Heliophysics); Space Studies Board; Aeronautics and Space Engineering Board; Division of Earth and Physical Sciences; National Research Council ISBN 978-0-309-16428-3*

National Academies Press: 2012b, *Terrorism and the Electric Power Delivery System, Committee on Enhancing the Robustness and Resilience of Future, Electrical Transmission and Distribution in the United States to Terrorist Attack, Board on Energy and Environmental Systems, Division on Engineering and Physical Sciences, National Research Council, Washington, DC, ISBN 978-0-309-11404-2*

National Academy of Sciences: 2008, *Severe Space Weather EventsUnderstanding Societal and Economic Impacts Workshop Report*, http://www.nap.edu/catalog.php?record_id=12507, accessed April 20, 2012

National Research Council Committee on the Societal and Economic Impacts of Severe Space Weather Events: 2008, *Severe space weather events? Understanding*

societal and economic impacts: A workshop report

National Space Weather Program Implementation Plan: 1997, *FCM-P31-1997, Washington, DC.*

National Space Weather Program Implementation Plan: 2000, *2nd Edition, FCM-P31-2000, Washington, DC.*

National Space Weather Program Report of the Assessment Committee for the National Space Weather Program: 2006, *FCM-R24-2006, Washington, DC.*

National Space Weather Program Strategic Plan: 1995, *FCM-P30-1995, Washington, DC.*

National Space Weather Program Strategic Plan: 2010, *FCM-P30-2010, Washington, DC.*

Nava, B., Coisson, P., & Radicella, S.M.: 2007, J. Atmos. Sol. Terr. Phys. 70(15), 18561862, doi:10.1016/j.jastp.2008.01.015

NERC: 2010, June, *High-Impact, Low-Frequency Event Risk to the North American Bulk Power System*, http://www.nerc.com/files/HILF.pdf, accessed April 20, 2012

New York Times: 1903, May 16a, *...*

New York Times: 1921, May 16b, *Sunspot credited with rail tieup*

New York Times: 1941, July 8, *Shortwave channels to Europe are affected*

New York Times: 1941, September 19, *Major baseball game disrupted*

New York Times: 1947, July 19, *Sunspots delay planes*

New York Times: 1950, August 20, 5

New York Times: 1950, February 21, 5

New York Times: 1957, April 18

New York Times: 1958, February 11, 62

Ngwira, C. M., Pulkkinen, A., Wilder, F. D., & Crowley, G.: 2013, Space Weather 11, 121

Nishioka, M., Saito, A., & Tsugawa, T.: 2008, J. of Geophys. Res. 113, A05301, doi:10.1029/2007JA012605

NOAA: 2001, Apr. 23, *Severe Space Weather Storms Affect GPS Meteorology Network*, http://www.esrl.noaa.gov/gsd/media/hotitems/2001/01Apr23.html, accessed April 15, 2012

NOAA: 2004, *Intense space weather storms: October 19 November 07, 2003. Service Assessment*

NOAA Magazine: 2007, Apr. 4, *Researchers find global positioning system is significantly impacted by powerful solar radio burst*

North American Electric Reliability Corporation: 2010, *High-Impact, Low-Frequency Event Risk to the North American Bulk Power System: A Jointly-Commissioned Summary Report of the North American Electric Reliability Corporation and the U.S. Department of Energy's November 2009 Workshop*

NPCC: 1989, *Procedures for Solar Magnetic Disturbances Which Affect Electric Power Systems; C-15*, https://www.npcc.org/Standards/Procedures/Forms/Public%20List.aspx, accessed April 20, 2012

Nunez, M., Fidalgo, R., Baena, M., & Morales, R.: 2005, Annales Geophysicae 23, 3129

Oak Ridge Laboratory: 2010, *Electromagnetic Pulse: Effects on the U.S. Power Grid*, http://www.ferc.gov/industries/electric/indus-act/reliability/cybersecurity/ferc_executive_summary.pdf, accessed April 20, 2012

Odenwald, S.F.: 1999, *The 23rd Cycle- Learning to live with an active star*, Westfield

Press, Boulder
Odenwald, S.F.: 2010, in C.J. Schrijver and G.L. Siscoe (Eds.), *Heliophysics: Space storms and radiation- causes and effects*, Cambridge University Press; United Kingdom, p. 15
Odenwald, S.F. & Green, J.L.: 2007, Space Weather 5 (S06002), doi:10.1029/2006SW000262
Odenwald, S.J., Green, J., & Taylor, W.: 2006, Adv. Sp. Res. 38
Oeschger, H., Siegenthaler, U., Schotterer, U., & Gugelmann, A.: 1975, Tellus 27(2), 168
OOSR, *On-Orbit Spacecraft Reliability', PRC Report R-1863, September 30, 1978 and Analysis of Spacecraft On-Orbit Anomalies and Lifetimes, PRC report R3579, February 10, 1983*
Parnell, B.-A.: 2012, Feb. 28, *Epic net outage in Africa as four undersea cables chopped*, http://www.theregister.co.uk/2012/02/28/east_africa_undersea_cables_cut/. Accessed on April 18, 2012
Patterson, T.: 2010, Oct. 15, *US Electricity Blackouts Skyrocketing*, http://www.cnn.com/2010/TECH/innovation/08/09/smart.grid/index.html, accessed April 20, 2012
Paxman, L. & Hyde, D.: 2011, Nov. 5, *HSBC systems crash affects millions across UK*, http://www.dailymail.co.uk/news/article-2057657/HSBC-customers-outraged-online-b, Accessed April 15, 2012
Penn, M.J. & Livingston, W.: 2006, IAU 273
Pesnell, W. D.: 2008, Solar Phys. 252, 209
Pirjola, R.: 2013, Advances in Applied Physics 1, 9
Pirjola, R., Kauristie, K., Lappalainen, H., & Viljanen, A.: 2005, Space Weather 3, S02A02
Pirjola, R. & Viljanen, A.: 1989, IEEE Trans. on Power Delivery 4, 1239
Powell, J.D. & Walter, T.: 2010, in *Proc. 16th Int. Flight Inspection Symp., Beijing, China, Flight Inspection Center of CAAC*
Price, A.T.: 1973, Phys. Earth and Planet. Int. 7, 227
Price, P.R.: 2002, IEEE Trans. Power Delivery 17, 1002
Prieto Cerdeira, R. & Beniguel, Y.: 2011, in *Ionospheric Effects Symposium, Alexandria VA.*
Prölss, G.W.: 1995, in H. Volland (Ed.), *Handbook of Atmospheric Electrodynamics, Vol. 2. CRC Press, Boca Raton*, 195248
Pulkkinen, A., Bernabeu, E., Eichner, J., Beggan, C., & Thomson, A. W. P.: 2012, Space Weather 10, doi:10.1029/2011SW000750
Pulkkinen, A., Hesse, M., Habib, S., Van der Zel, L., Damsky, B., Policelli, F., Fugate, D., Jacobs, W., & Creamer, E.: 2010, Natural Hazards 53, 333
Pulkkinen, A., Kuznetsova, M., Ridley, A., Raeder, J., Vapirev, A., Weimer, D., Weigel, R.S., Wiltberger, M., Millward, G., Rastätter, L., Hesse, M., Singer, H.J., & Chulaki, A.: 2011, Space weather 9, S02004
Pulkkinen, A., Lindahl, S., Viljanen, A., , & Porjola, R.: 2005, Space Weather 3 (S08C03)
Radio Netherlands: 2011, Aug. 9
Rawer, K.: 1993
Reinard, A., Henthorn, J., Komm, R., & Hill, F.: 2010, ApJL 710, L121
Reinisch, B.W., Huang, X., Galkin, I., Paznukhov, V., & Kozlov, A.: 2005, J. Atmos. and Solar-Terr. Phys. 67, 1054
Robbrecht, E., Berghmans, D., & van der Linden, R.A.M.: 2009, ApJ 691, 1222

Robertson, B. & Stoneking, E.: 2003, *Satellite GN and C Anomaly Trends, AAS Guidance and Control Conference; 5-9 Feb. 2003*, Breckenridge, CO; United States, Report Number AAS- 03-071

Rocken, C., Kuo, Y.-H., Schreiner, W., Hunt, D., Sokolovskiy, S., & McCormick, C.: 2000, Terrestrial, Atmosphere and Oceanic Science 11, 21

Saito, A., Fukao, S., & Miyazaki, S.: 1998, Geophysical Research Letters 25, 30793082

Santarini, M.: 2005, May 12, *Cosmic radiation comes to ASIC and SOC design*, http://www.edn.com/article/470298-Cosmic_radiation_comes_to_ASIC_and_SOC_design.php Accessed, April 15, 2012

Sardón, E., Rius, A., & Zarraoa, N.: 1994, Radio Sci. 29, 577

Schunk, R.W. & et al.: 2004, Radio Sci. 39, doi:RS1S02.doi.1029/2002RS002794

Schunk, R.W. & et al.: 2005, in J.M. Goodman (Ed.), *2005 Ionospheric Effects Symposium*, JMG Associates Ltd., p. 512

Secan, J.A., Bussey, R.M., Fremouw, E.J., & Basu, S.: 1997

Shortwave America: 2012, Jan. 23, *M9-class Long-Duration Solar X-ray Flare*, http://shortwaveamerica.blogspot.com/2012/01/m9-class-long-duration-solar-x-ray.html, accessed on April 12, 2012

Skone, S. & Coster, A.: 2008) Potential for issuing ionospheric warnings to Canadian users of marine DGPS, Space Weather 6, doi:10.1029/2007SW000336

Slothower, J.C. & Albertson, V.D.: 1967, J. Minn. Academy of Science 34, 94

Smith, A.M., Mitchell, C.N., Watson, R.J., Meggs, R.W., Kintner, P.M., Kauristie, K., & Honary, F.: 2008, Space Weather 6, S03D01, doi:10.1029/2007/SW000349

Solomon, S.C.: 2010, in C.J. Schrijver and G.L. Siscoe (Eds.), *Heliophysics: Evolving Solar Activity and the Climates of Space and Earth*, Cambridge university Press

Song, W.B.: 2010, Solar Phys. 261, 311

Space Weather Canada: 2011, *Geomagnetic Effects on Communications Cables*, http://www.spaceweather.gc.ca/se-cab-eng.php, accessed April 18, 2012

Stassinopoulos, E.G., Brucker, G.J., Adolphsen, J.N., & Barth, J.: 1996, J. Spacecraft and Rockets 33, 877

Sterling, A.C.: 2000, J. Atmosp. And Sol. Terr. Phys. 62, No. 16, 1427

Steward, G.A., Lobzin, V.V., Wilkinson, P.J., Cairns, I.H., & Robinson, P.A.: 2011, Space Weather 9 (S11004), doi:10.1029/2011SW000703

Stokes, D.E.: 1997

Storz, M.F., Bowman, B.R., Branson, J.I., Casali, S.J., & Tobiska, W.K.: 2005, Advances in Space Research 36, 24972505, doi:doi:10.1016/j.asr.2004.02.020

Telegeography: 2012, *Submarine Cable Map*, http://www.submarinecablemap.com/, Accessed May 4, 2012

Tezzaron Semiconductors: 2003, *Soft Errors in Electronic Memory*, http://www.tezzaron.com/about/papers/soft_errors_1_1_secure.pdf. Accessed, April 15, 2012

The Economist: 2009, Aug. 13, http://www.economist.com/node/14214847, accessed April 20, 2012

Thomson, A.W.P.: 2000, Geophys. Res. Lett. 27, 4049

Thomson, A.W.P., McKay, A.J., Clarke, E., & Reay, S.J.: 2005, Space Weather 3, S11002, doi:10.1029/2005SW000156

Thomson, A. W. P., Dawson, E. B., & Reay, S. J.: 2011, Space Weather 9, S10001, doi:10.1029/2011SW000696

Tobiska, W.K.: 2008, Space Weather 6, S06001, 67, doi:doi:10.1029/2008SW000410

Tobiska, W.K.: 2009, Space Weather 7, S10003, 67, doi:doi:10.1029/2009SW000510

Tobiska, W.K., Bouwer, S.D., & Bowman, B.R.: 2008, JASTP 803–819

Tobiska, W.K., Crowley, G., Oh, S.J., & Guhathakurta, M.: 2010, Space Weather 8, S10006, doi:doi:10.1029/2010SW000619

Tobiska, W.K., Gersey, B., Wilkins, R., Mertens, C., Atwell, W., & Bailey, J.: 2014, Space Weather 12, doi:doi:10.1002/2013SW001015

Tobiska, W.K., Knipp, D., Burke, W.J., Bouwer, D., Bailey, J., Odstrcil, D., Hagan, M.P., Gannon, J., & Bowman, B.R.: 2013, Space Weather 11, 490508, doi:doi:10.1002/swe.20094

Torta, J. M., Serrano, L., Regué, J. R., & Sánchez, A. M.: 2012, Space Weather 10, S06002

Townsend, L.W.: 2003, IEEE Trans. Nucl. Sci. 50, 2307

Tribble, A.: 2010, in C.J. Schrijver and G.L. Siscoe (Eds.), *Heliophysics: Space storms and radiation- causes and effects*, Cambridge University Press; United Kingdom, p. 381

Trichtchenko, L. & Boteler, D.H.: 2002, Annales Geophysicae 20, 1063

Trichtchenko, L. & Boteler, D.H.: 2004, IEEE Trans. Plasma Science 32, 1459

Trichtchenko, L. & Boteler, D.H.: 2007, in *Proc. Seventh Int. Symp. on Electromagnetic Compatibility and Electromagnetic Ecology*, p. 265

Trichtchenko, L., Zhukov, A., Van der Linden, R., Stankov, S.M., Jakowski, N., Stanislawska, I., Juchnikowski, G., Wilkinson, P., Patterson, G., & Thomson, A.W.P.: 2007, Space Weather 5

Tripathi, R. & Mishra, A.P.: 2005, *Properties of halo CMEs in relation to large CMEs*, 29th International Cosmic Ray Conference, Prune, http://dpnc.unige.ch/ams/ams_beta/ICRC/ICRC-05/PAPERS/SH14/ind-tripathi-R-abs1-sh14-poster.pdf, accessed April 15, 2012

Trivedi, N. B., Vitorello, I., Kabata, W., Dutra, S.L.G., Padilha, A.L., Bologna, M.S., de Padua, M.B., Soares, A.P., Luz, G.S., Pinto, F., Pirjola, R., & Viljanen, A.: 2007, Space Weather 5, S04004

Tsai, H.F. & Liu, J.Y.: 1999, Journal of Geophysical Research 104 (A6), 1265712668

Tsugawa, T., Saito, A., & Otsuka, Y.: 2004, Journal of Geophysical Research 109, 111

Tsurutani, B.T.: 2001, in I.A. Daglis (Ed.), *Space Storms and Space Weather Hazards*, Kluwer, Dordrecht, p. 103

Turnbull, K.L., Wild, J.A., Honary, F., Thomson, A.W.P., & McKay, A.J.: 2009, Ann. Geophys. 27, 3421

Uberoi, C.: 2011, Space Weather 9, S08005, doi:doi:10.1029/ 2011SW000686

Vampola, A.L.: 1987, J. Electrostatics 20, 21

Vasyliunas, V.: 2009, in C.J. Schrijver and G.L. Siscoe (Eds.), *Heliophysics: Plasma Physics of the Local Cosmos*, Cambridge university Press

Viljanen, A.: 1997, Geophys. Res. Lett. 24, 631

Viljanen, A., Amm, O., & Pirjola, R., J. Geophys. Res: Space Physics 104, A12, 28059

Viljanen, A. & Pirjola, R.: 1994, Surveys in Geophysics 15, 383

Wahlund, J.E., Wedlin, L.J., Carrozi, T., Eriksson, A.I., Holback, B., Andersson, L., & Laakso, H.: 1999, Feb. 22, *Analysis of Freja Charging Events: Statistical Occurrence of Charging Events*, WP 130 technical Note (SPEE-WP130-TN)

Wang, H., Spirock, T.J., Qui, J., Haisheng, J., Yurchyshyn, V., Moon, Y.-J., Denker, C., & Goode, P.R.: 2002, ApJ 576, 497

Wannamaker, P.E., Stodt, J.A., & Rijo, L.: 1987, Geophys. J. R. Astr. Soc. 88, 277

Watari, S., Kunitake, M., Kitamura, K., Hori, T., Kikuchi, T., Shiokawa, K., Nishitani, N., Kataoka, R., Kamide, Y., Aso, T., Watanabe, Y., & Tsuneta, Y.: 2009, Space Weather S03002, doi:10.1029/2008SW000417

Waugh, R.: 2012, Jan. 25, *Biggest solar storm since 2003 pummels atmosphere, forcing planes to divert from northern routes*, http://www.dailymail.co.uk/sciencetech/article-2091586/Solar-radiation-storm-Flights-diverted-Earths-atmosphere pummeled.html#ixzz1rjThzvhb, accessed April 15, 2012

Weaver, J.T.: 1994, *Mathematical methods for geo-electromagnetic induction*, Research Studies Press, Taunton, England

Whalling, R.A. & Khan, A.H.: 1991, IEEE Trans. Power Delivery 6

Wielgosz, P., Kashani, I., & Grejner-Brzezinska, D.: 2005, presented at ION Annual Meeting, Cambridge, MA, June 27-29

Wik, M., Pirjola, R., Lundstedt, H., Viljanen, A., Wintoft, P., & Pulkkinen, A.: 2009, Annals of Geophysics 27, 1775

Wilkinson, D.: 1994, Jour. Spacecraft and Rockets 31, 160

Wilkinson, D.C. & Allen, J.: 1997, *Satellite Anomaly Data Base*

Wilson, B.D. & Mannucci, A.J.: 1993, Proc. Inst. Navig. GPS 93, 1343

Wintoft, P.: 2005, Ann. Geophys. 23, 1949

Wrenn, G. L., Rodgers, D.J., & Ryden, K.A.: 2002, Annales Geophysicae 20, 953

Xihuanet: 2011, Feb. 16, *Solar flare affects shortwave radio communications in southern China*, http://news.xinhuanet.com/english2010/china/2011-02/16/c_13733621.htm, accessed on April 12, 2012

Xinhuanet: 2005, Jan. 21, *Solar storm interrupts China's short-wave radio transmission*, http://news.xinhuanet.com/english/2005-01/21/content_2491819.htm, Accessed on April 12, 2012

Xu, Z.W., Wu, Q.J., & Wu, Z.S.: 2008, IEEE Transactions on . . . 56 , No. 7, . . .

Yunck, T.P., Lindal, F., & Liu, C.H.: 1988, IEEE Cat. No.88CH2675-7 251–258

Zheng, K., Boteler, D. H., Pirjola, R., Liu, L. G., Becker, R., Marti, L., Boutilier, S., & Guillon, S.: 2014, IEEE Trans. Power Delivery 29, 890

Zheng, K., Trichtchenko, L., Pirjola, R., & Liu, L.-G.: 2013, IEEE Trans. Power Delivery 28, 1183